INVESTIGATING THE EFFECTS OF ANIMAL VENOMS IN OVARIAN CANCER

By

Charlotte Alice Akers

Canterbury Christ Church University

Thesis Submitted

For the Degree of MSc by Research

Year: 2019

TABLE OF CONTENTS

Chapter Four: Venom Assays

Chapter Five: Discussion

ABSTRACT

Objectives: Ovarian Cancer is considered the most lethal gynaecological disease with over 9 million women dying annually on a global scale. Current standards of care which consists of debulking surgery and adjuvant chemotherapy are proving to be inadequate due to chemoresistance whilst targeted-therapies available are limited. This prompts research into identifying the therapeutic potential of animal venoms in relation to ovarian cancer.

Materials and Methods: Using a 50% threshold, the ability of crude venom from *Parabuthus transvaalicus (*Transvaalicus thick-tailed scorpion), *Heterometrus madraspatensis* (Madras forest scorpion) and *Heterometrus mysorensis* to inhibit SK-OV-3 cell metabolism was analysed using dose response assays. Furthermore, fractioned venoms *Naja nigricollis*_r11 (Black-necked spitting cobra) and *Pandinus cavimanus*_r28 (Tanzanian red clawed scorpion) were also investigated for their inhibitory effects on the cell line.

Results: Crude *Parabuthus transvaalicus* venom at a concentration of 200µg/ml inhibited 44.55% of SK-OV-3 cell metabolism. *Heterometrus madraspatensis* and *Heterometrus mysorensis* venom at a concentration of 500µg/ml inhibited 0.78% and 2.35% of cell metabolism respectively. Fractioned venom *Pandinus cavimanus*_r28 at a concentration of 15.63µg/ml inhibited 2.54% of cell metabolism whilst *Naja nigricollis*_r11 venom fraction produced an LD50 of 37.23µg/ml.

Conclusion: *Parabuthus transvaalicus*, *Heterometrus madraspatensis*, *Heterometrus mysorensis* and *Pandinus cavimanus_r28* at the specified concentrations did not reach the inhibition threshold of 50% in regards to the SK-OV-3 cell line and were therefore not investigated further. The *Naja nigricollis*_r11 fraction exceeded the 50% threshold thus identifying as a positive hit and warrants further analysis.

ACKNOWLEDGEMENTS

Throughout this project I have received a great deal of support and assistance. I would first like to thank my MSc supervisor, Dr Carol Trim for her continued encouragement and expert advice throughout the project. No matter how small my query on the project was, you always made yourself available to help and steer me in the right direction.

I would also like to thank Danielle McCullough, Emily Knight, Alice Tirnoveanu and Dr Cornelia Wilson for their constant help within the laboratory, explaining and demonstrating how various experiments should be carried out, as well as using their expertise and experience in suggesting alternative experiments which would benefit my project. Not to mention their continuous help when it came to some of the most basic mathematics, thank you for dealing with my most simple moments. Your passion for science and hard-work is inspiring.

I would also like to acknowledge Steve Trim and Venomtech Ltd. His industry experience helped in shaping my project and without his sheer generosity, this investigation would not have been possible. You provided me with the fundamental equipment needed to complete this venture.

In addition, I would like to thank my parents, grandparents and uncle for their wise advice. You are always there for me and support me in everything I do. Thank you for constantly encouraging me to be the best person I can be.

Furthermore, many thanks to my good friend Melissa who was always prepared to spend long nights in the library with me to keep me company. Finally, I would like to thank my partner Will for your love and support. You were always happy to distract me when my mind needed a rest from research and to not mention the endless, freshly cooked meals after a long day in the lab.

ABBREVIATIONS

Abbreviation	Full name
4-AP	4-Aminopyridine
A.cpi	*Agkistrodon contortrix pictigaster*
AA	Alkylating Agents
ATP	Adenosine Triphosphate
Ca^{2+}	Calcium Ion
Cl^{-}	Chloride Ion
CTX III	Cardiotoxin III
DMEM	Dulbecco's Modified Eagles Medium
DMSO	Dimethyl Sulfoxide
DR	Dose Response
EGFR	Epidermal Growth Factor Receptor
EPA	Eicosapentaenoic Acid
ERK	Extracellular Signal Regulated Kinase
FCS	Foetal Calf Serum
FDA	U.S Food and Drug Association
FIGO	The International Federation of Gynaecology and Obstetrics
GDP	Guanosine Diphosphate
GRB2	Growth Factor Receptor Binding Protein 2
GTP	Guanosine Triphosphate
H.ben	*Heterometrus bengalensis* Koch
H.lao	*Heterometrus laoticus*
H.mad	*Heterometrus madraspatensis*
H.mye	*Heterometrus mysorensis*
HGEOC	High-Grade Endometrioid Ovarian Cancer
HGSOC	High-Grade Serous Ovarian Cancer
HPLC	High Pressure Liquid Chromatography
HRR	Homologous Recombination Repair
HS-1	Heteroscorpine-1
IC	Inhibitory Concentration
IDS	Interval Debulking Surgery
IHC	Immunohistochemistry
IMS	Industrial Methylated Spirit
K^{+}	Potassium Ion
LAAO	L-Amino Acid Oxidases
LCNs	Long Chain Neurotoxins
LD	Lethal Dose
LGEOC	Low-Grade Endometrioid Ovarian Cancer
LGSBT	Low-Grade Serous Borderline Tumours
LGSOC	Low-Grade Serous Ovarian Cancer
LOF	Loss of Function
MALDI-TOF	Matrix-Assisted Laser Desorption/Ionisation-Time of Flight
MEK	MAPK ERK Kinase
MFI	Mean Fluorescence Intensity
MOS	Median Overall Survival
MS	Mass Spectrometry
N.nig	*Naja nigricollis*

Na^+	Sodium Ion
NCD's	Non-Communicable Diseases
OC	Ovarian Cancer
P.cav	*Pandinus cavimanus*
P.reg	*Poecilotheria regalis*
PARP	Poly-ADP-Ribose Polymerase
PBS	Phosphate Buffered Saline
PFS	Progression Free Survival
PLA_2	Phospholipases A_2
R.jun	*Rhopalurus junceus*
RTK's	Receptor Tyrosine Kinases
SHC	Src Homology and Collagen
SNCs	Short Chain Neurotoxins
SOS1	Sons of Sevenless 1
TNM	Tumour, Node, Metastasis
Trypsin	Trypsin-Ethylene Diamine Tetra Acetic Acid
TTVGCC	T-Type Voltage-Gated Calcium Channel
VEGFR	Vascular Endothelial Growth Factor Receptor
VGPS	Voltage-Gated Potassium Channel
WHO	World Health Organisation
Z'	Z Prime

INVESTIGATING THE EFFECTS OF ANIMAL VENOMS IN OVARIAN CANCER

CHAPTER ONE: LITERATURE REVIEW

1.1. Introduction

Research currently shows that non-communicable diseases (NCD's) are the leading causes of death worldwide. According to the World Health Organisation (WHO) Global Health Observatory Data, NCD's amount to around 36 million deaths annually. Diseases in this category include cardiovascular disease, chronic lung disease, diabetes and cancer (Kim & Oh, 2013).

Of these diseases, cancer has been ranked as the leading cause of death and a major obstacle with regards to increasing life expectancy on a global scale. Factors including growth in populations and individuals living longer contribute to the increase in incidence and mortality of cancer as well as growth in established risk factors such as obesity, physical inactivity and smoking (Bray, *et al*., 2018).

GLOBOCAN and The International Agency for Research on Cancer have shown that in 2018 alone there were over 18 million new cases of cancer and over 9 million deaths globally (Ferlay, *et al*., 2018). Relating this to previously published data, GLOBOCAN in 2012 estimated that there were 14.1 million new cases of cancer and 8.2 million deaths on a global scale (Torre, *et al.*, 2015); this is an increase of 28.6% and 9.8% respectively. Although relatively more advanced treatments are employed in the battle against cancer, these statistics still highlight areas of treatment ineffectiveness.

One cancer of great concern to the female population is ovarian cancer (OC). On an annual scale, OC will affect around 239,000 individuals and cause 152,000 deaths worldwide (Reid, *et al*., 2017). Alternatively, in the UK alone there are around 7,000 new cases diagnosed and 4,000 deaths each year making it the sixth most common cancer in association with the female populace (Cancer Research UK, 2018). Unfortunately, due to the elusive, non-specific symptoms, especially early on, women are diagnosed at a much later stage making the disease harder to treat (Ebell, *et al*., 2016).

Non-targeted treatments for OC include surgery and chemotherapy. Although such treatments have improved over the years, they are becoming increasingly ineffective with more women dying due to drug resistance diseases (Bookman, *et al.*, 2009). Furthermore, non-targeted treatments tend to have more side effects for patients including hair loss and muscular ache

effecting a patient's quality of life (Hsu, *et al*., 2017). This ensures a need for more research into the area of targeted, novel therapies. Targeted-therapies are of popular choice in research due to their specificity in pursuing cancerous-cells increasing treatment effectiveness for certain patients. Such therapies include antiangiogenic agents, poly-ADP-ribose polymerase (PARP) inhibitors and targeting of the epidermal growth factor receptor (EGFR) (Coward, *et al.*, 2015).

When considering the side effects and poor outcomes of certain treatments associated with OC, the development of alternative treatments is imperative for the survival of individuals with the disease. One such area of research that is currently being explored is the development of novel treatments utilising animal venoms (Moridikia, *et al*., 2018). Venoms contain a cocktail of varying proteins and peptides which target physiological processes within the body; these include cell proliferation, migration, invasion and apoptotic activity which are considered as hallmarks of cancer (Chaisakul, *et al.*, 2016). It is therefore possible to isolate proteins and peptides within the cocktail to target certain cellular processes which influence the survival of tumorogenesis (Tan, *et al.*, 2018).

In this review, the cellular processes associated with OC, the current therapies available and new alternative targets for treatment will be highlighted. Contemporary research and advances made through the utility of anticancer properties in venom will also be discussed.

1.2. Ovarian Cancer: Classification and Mechanisms

It is not as straightforward to identify OC as a single homogenous disease as it was once regarded. Instead, considerations over the years have acknowledged a breakdown of the disease identifying and categorising types of OC, establishing a staging classification and asserting a grading system thus inaugurating a heterogeneous disease (Wang, *et al.*, 2005). Developments such as those stated above have assisted in the deeper understanding of the disease ultimately aiding in the optimisation of treatment plans which is paramount for survival (Javadi, *et al.*, 2016).

1.2.1. Staging Classification

OC can be divided and subdivided into several stages. Staging describes the location of the primary-tumour, the size and if the tumour has spread which can ameliorate the prognosis of the disease (Forstner, *et al.*, 2016). There are two leading staging classifications currently utilised; the number staging system developed by The International Federation of Gynaecology and Obstetrics (FIGO) as illustrated in Table 1.1 (Mutch & Prat, 2014), as well as the tumour,

node and metastasis (TNM) staging system developed by the American Joint Committee on Cancer and the Union for International Cancer Control (Union for International Cancer Control, 2017). Amendments over the years have ensured their effectiveness. The TNM staging system is now on its eighth-edition whilst the FIGO staging classification, originally constructed in 1988, was revised in 2013 (Shepherd, 1989). Revisions included the realisation that cancer of the ovary, fallopian tube and peritoneum are of similar nature and should be considered mutually; furthermore, stage IC was divided into 3 sub-stages for additional specificity (Sartorius, *et al.*, 2018). Such modifications offer explicit guidance on personalised management of the disease (Kandukuri & Rao, 2015).

Table 1.1. The now revised 2013 accepted staging of OC as developed by The International Federation of Gynaecology and Obstetrics (FIGO). Table adapted from (FIGO, 2015) source.

STAGE OF OC	DESCRIPTION
Stage I	Tumour isolated to ovaries or fallopian tube(s) and has not spread
IA	Tumour is located in one ovary or fallopian tube; confined to the inside of said ovary or fallopian tube. Tumour not detected on the surface of ovary or fallopian tube and no malignant cells found in peritoneal washings
IB	Tumour is located in both ovaries or fallopian tubes; tumour not detected on the surface of ovaries or fallopian tubes and no malignant cells found in peritoneal washings
IC • **IC1** • **IC2** • **IC3**	Tumour located in one or both ovaries or fallopian tubes, with any of the following; • Ruptured capsule during surgery • Capsule ruptured before surgery or tumour on ovary or fallopian tube surface • Malignant cells in peritoneal washings
Stage II	Tumour involves one or both ovaries or fallopian tubes and has spread to pelvis region
IIA	Extension and/or implants on uterus and/or fallopian tubes and/or ovaries
IIB	Extension to other regions near the pelvis
Stage III	Tumour involves one or both ovaries or fallopian tubes, pelvis region and/or the retroperitoneal lymph nodes
IIIA1 • **IIIA1(i)** • **IIIA1(ii)**	Positive retroperitoneal lymph nodes only (cytologically or histologically proven) • Metastasis up to 10mm in greatest dimension • Metastasis more than 10mm in greatest dimension
IIIA2	Microscopic extrapelvic peritoneal involvement with or without positive retroperitoneal lymph nodes
IIIB	Tumour less than 2cm in the greatest dimension visible outside pelvis and retroperitoneal lymph nodes and may or may not contain cancerous-cells
IIIC	Tumour is more than 2cm in the greatest dimension visible outside pelvis and retroperitoneal lymph nodes. May also be on the outside of liver or spleen
Stage IV	Cancer has spread beyond the pelvis and to other organs
IVA	Cancer-cells are identified in the fluid around the lungs
IVB	Cancer spread and identified inside spleen, liver, lungs and bones

1.2.2. Type and Molecular Characteristics

There are 3 common cell types whereby OC can start from as illustrated in Figure 1.1. Epithelial cells, which form the surface layers of the ovaries, account for 90% of all OC (Israelsson, *et al.*, 2017). Stromal cells, which make up the core of the ovaries, and germ cells, which develop into eggs, both contribute to 5% each of OC's as stated in Table 1.2 (Phyoe-Battaglia, *et al*., 2018, Park, *et al*., 2015). Epithelial-OC is the most common with 75% of women being diagnosed at much later stages in the disease, consequently having a fatal impact on the effectiveness of treatment and survival.

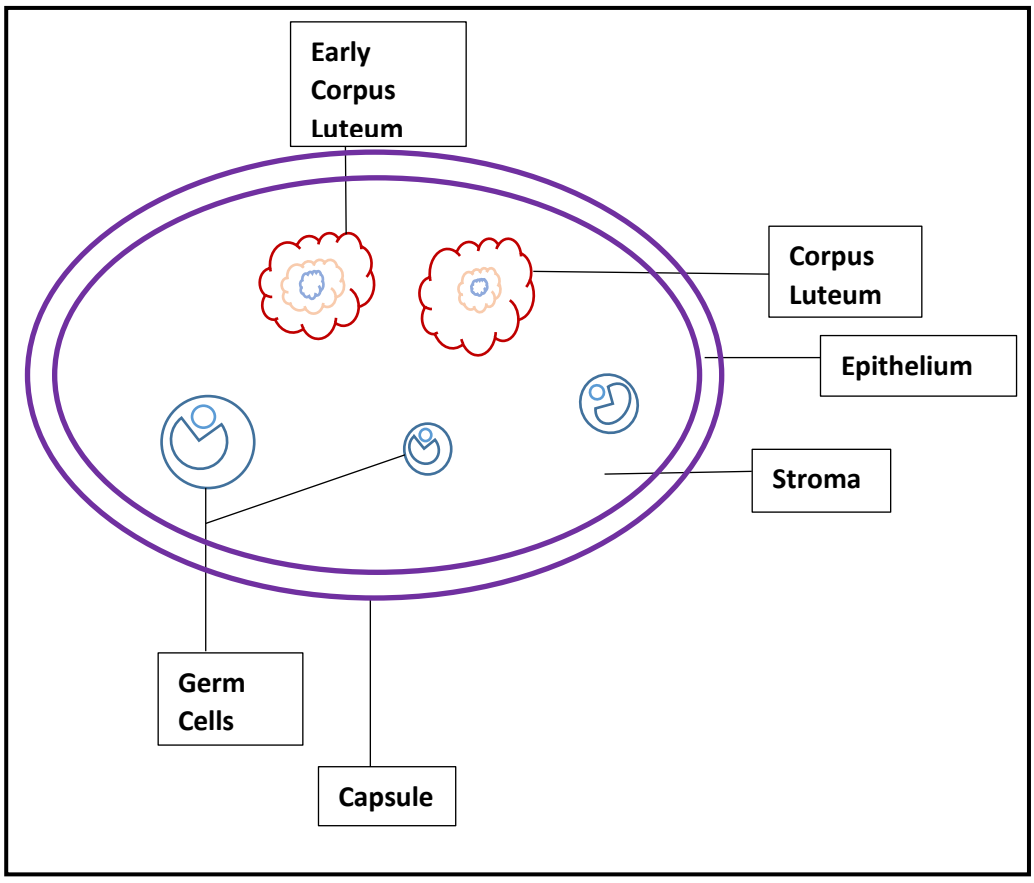

Figure 1.1. Diagram illustrating an ovary cell and the components which contribute to the formation of OC. This includes the epithelium, the stroma and germ cells.

Table 1.2. The frequency and types of OC associated with the epithelium, germ cells and the stroma (Cancer Research UK, 2018).

	Epithelial Cells	**Germ Cells**	**Stroma**
Frequency	90%	5%	5%
Types	Serous Mucinous Endometroid Clear cell	Mature Teratomas Immature Teratomas Dysgerminomas Yolk Sac Tumours Choriocarcinomas	Granulosa cell Thecoma Fibroma Sertoli-Leydig

Epithelial-OC is now sub-divided into serous (high-grade or low-grade), endometrioid, clear-cell and mucinous histotypes (Cheng, *et al*., 2005, Koshiyama, *et al*., 2017). Instead of considering them as one disease, each histotype is its own distinct disease differing in molecular characteristics, ways of metastasising and treatment plan. Further categorisations using various molecular and histopathological studies have now distinguished two types of epithelial-OC. Type I, accounting for 5-10% of deaths, includes low-grade endometrioid-OC (LGEOC), clear cell-OC, mucinous-OC and low-grade serous-OC (LGSOC). Type II on the other hand, accounting for 90% of deaths, includes high-grade serous-OC (HGSOC) and high-grade endometrioid-OC (HGEOC) (Garziera, *et al.*, 2018).

Extensive research has identified key mutations associated with molecular characteristics which permits the recognition of the aforementioned subtypes and this is clarified in Table 1.3. Somatic mutations in the tumour suppressor gene TP53 for example, are a major indication of type II OC. The Cancer Genome Atlas, for instance, analysed the DNA sequence of exons from coding genes of 316 HGSOC's and established that 96% of these tumours had a mutation in the TP53 gene (The Cancer Genome Atlas Research Network, 2011). Similarly, Cole *et al* 2016, using immunohistochemistry (IHC) and massively parallel sequencing, identified the TP53 gene was mutated in 94% of HGSOC's (Cole, *et al.*, 2016).

In addition to this research, Yaginuma and Westphal 1992, using immunoprecipitation and the monoclonal antibody PAb421 (raised to wild-type p53), identified that the p53 protein was not detectable in the Caov-3 and SK-OV-3 (an established HGSOC) cell lines which express the TP53 gene. This suggests that these cell lines are mutated through a loss-of-function (LOF) of the TP53 gene as there was no production of the p53 protein. As this protein is responsible for regulating cell division and preventing uncontrolled proliferation, the LOF to the gene prevents the production of the protein and thus control, allowing for the unrestrained proliferation of tumour-cells (Yaginuma & Westphal, 1992).

Alternatively, type I OC's are usually associated with mutations in KRAS, PIK3CA, PTEN or BRAF (Kurman & Shih, 2010). Singer *et al* 2003, analysed the KRAS gene and its downstream mediator BRAF, at codon 599 for BRAF and codons 12 and 13 for KRAS in LGSOC's and low-grade serous borderline tumours (LGSBT); results showed that mutations in the selected codons of either BRAF or KRAS transpired in 68% of LGSOC's and 61% of LGSBT. On the other hand, of the 72 HGSOC's analysed, no mutations were found in BRAF or KRAS highlighting their mutation specificity for type I LGSOC (Singer, *et al*., 2003). Similarly, McConechy *et al* 2014, using select exon capture sequencing on a panel of genes, identified that PTEN mutations were found in 67% of LGEOC (McConechy, *et al.*, 2014), whilst Kolasa *et al* 2006, using single-strand conformation polymorphism and sequencing, found that PTEN and KRAS mutations occurred in 80% of the LGEOC (Kolasa, *et al.*, 2006). This emphasises the association of mutations to specific cancer subtypes aiding with identification.

Table 1.3. The types of mutations which can be identified in particular types of OC; ● indicates that the mutation is present and ○ indicates that the mutation is not present.

		TP53 Mutation	**KRAS Mutation**	**BRAF Mutation**	**ARID1A Mutation**	**PIK3CA Mutation**	**PTEN LOH**	**B Catenin Mutation**
Type I Ovarian Cancer	**LGEOC**	○	○	○	●	●	●	●
	Clear Cell	○	○	○	●	●	○	○
	Mucinous	○	●	○	○	○	○	○
	LGSOC	○	●	●	○	○	○	○
Type II Ovarian Cancer	**HGSOC**	●	○	○	○	○	○	○
	HGEOC	●	○	○	○	○	○	○

Similarly, EGFR has known to be overexpressed in epithelial-OC and occurs in all histological subtypes providing an association to poor prognosis and decreased therapeutic responsiveness (Li, *et al.*, 2016). Wang *et al* 2016, using immunohistological staining and statistical analysis of 242 patients with epithelial-OC, found that there was a significant correlation between the level of EGFR (in tumour-cells and tumour stroma) with clinical stage (p values=0.005 and 0.008 respectively) and distant metastasis (p value<0.001 for both) (Wang, *et al.*, 2016).

In regards to the various types of OC and the differing stages and grades, treatment plans have become more tailored to the individual's cancer. However, as previously touched upon, cancer treatments are still proving to be inadequate regardless of such breakthroughs in disease specificities and this is down to a lack of advancements within the sector of targeted-therapies

for OC. Novel treatment strategies are essential in order to improve such negative statistics related to OC. Therefore, identifying and capitalising upon the various molecular-targets associated with cancer survival is crucial. This will assist in the development of better treatment strategies for OC patients and thus improve the outcome.

1.3. Potential Molecular-Targets in Ovarian Cancer

Molecular-targets are specific molecules which are involved in the growth and progression of cancer; they are therefore key elements which need to be addressed in the investigation into improving the survival of OC through precision medicine (Ke & Shen, 2017). Approaching this may involve identifying specific proteins involved in cancer progression which are distinctively present or overexpressed in cancer-cells. LOF or mutation of other particular proteins which play a crucial role in cancer development may also be identified (Abdelmoez, *et al.*, 2017). If a compelling molecular-target is established, research into developing therapies which impair the cancerous function of the specific molecules can be employed, ultimately selecting tumour-cells, inducing apoptosis and impeding progression (Itamochi, 2010).

One molecular-target of interest in OC is EGFR. This receptor is a part of the ErbB family of structurally related proteins, Her1 (EGFR), Her2 (ErbB2), Her3 (ErbB3) and Her4 (ErbB4) which are part of a larger family of receptor tyrosine kinases (RTK's). They are a collection of high-affinity cell surface receptors with a preciseness for growth factors, cytokines and hormones (McCullough & Trim, 2015). Each member of the family encompasses an intracellular juxtamembrane and large extracellular region, a tyrosine kinase and transmembrane domain and a carboxyterminal tail illustrated in Figure 1.2 (Ferguson, 2008). The regulation of the ErbB family is dependent on various ligands (known as growth factors) which can bind to the receptors distributed on the cell surface membrane as clarified in Table 1.4 (Yarden & Sliwkowski, 2001).

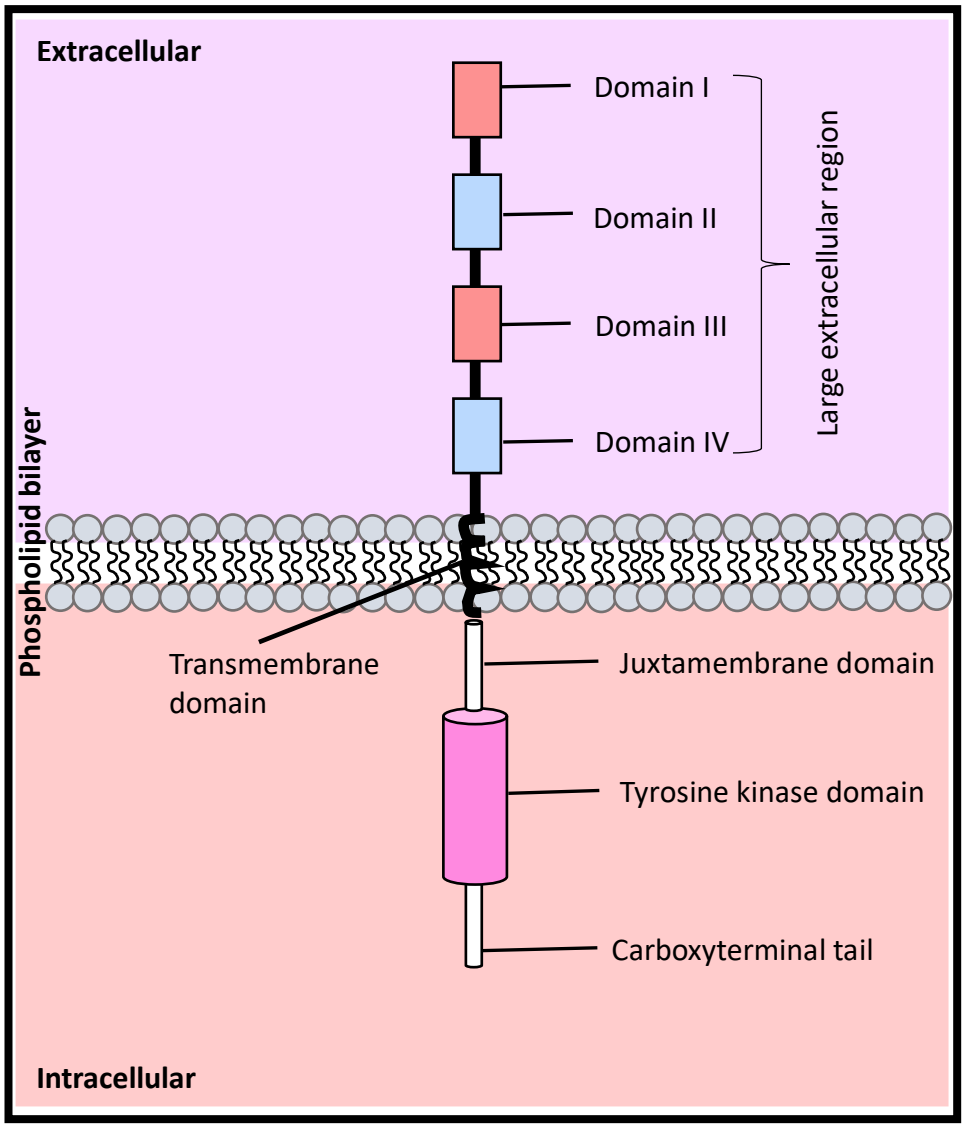

Figure 1.2. Diagram representing the structure of a typical RTK, in particular EGFR. The large extracellular region consists of 4 domains. Domains I and III are known as leucine rich domains which display a β-helical fold whilst domains II and IV contain cysteine rich motifs thus known as cysteine rich domains. Domain III is responsible for ligand binding (Ferguson, 2008). The transmembrane domain is hydrophobic and spans across the cell membrane. The juxtamembrane domain is located just inside the cell membrane followed by the protein kinase domain which plays an important role in the regulation of cell proliferation and differentiation (Voldborg, et al., 1997). Finally, the carboxyterminal tail plays a crucial role in the regulation of enzyme activity of the tyrosine kinase domain (Gajiwala, 2013).

Table 1.4. The ligand interactions in the EGF family of receptors; ● indicates interaction and ○ indicates there is no interaction (Yarden & Sliwkowski, 2001). High affinity ligands bind to the receptor 10- to 100-fold more than low affinity ligands (Freed, *et al*., 2017); as they all activate EGFR these ligands are known as EGFR agonists. Neuregulins are ligands which bind HER3 and HER4.

		Receptor Type			
	Ligand	**EGFR**	**HER2**	**HER3**	**HER4**
High Affinity Ligands	EGF	●	○	○	○
	TGF-α	●	○	○	○
	BTC	●	○	○	●
	HB-EGF	●	○	○	●
Low Affinity Ligands	EREG	●	○	○	●
	EPGN	●	○	○	○
	AREG	●	○	○	○
Neuregulins	NRG1	○	○	●	●
	NRG2	○	○	●	●
	NRG3	○	○	○	●
	NRG4	○	○	○	●

The incessant mutation and overexpression of EGFR is evident in various cancers including lung, breast, glioblastoma and OC (Sigismund, *et al*., 2017). The receptor is associated with signalling pathways, including Ras-Raf-MAPK pathway (Molina & Adjei, 2006), the Jak/STAT pathway (O'Shea, *et al.*, 2015) and PI3K/AKT/mTOR pathway (Porta, *et al.*, 2014) all of which are involved in cell division, survival and growth of cancer-cells as illustrated in Figure 1.3.

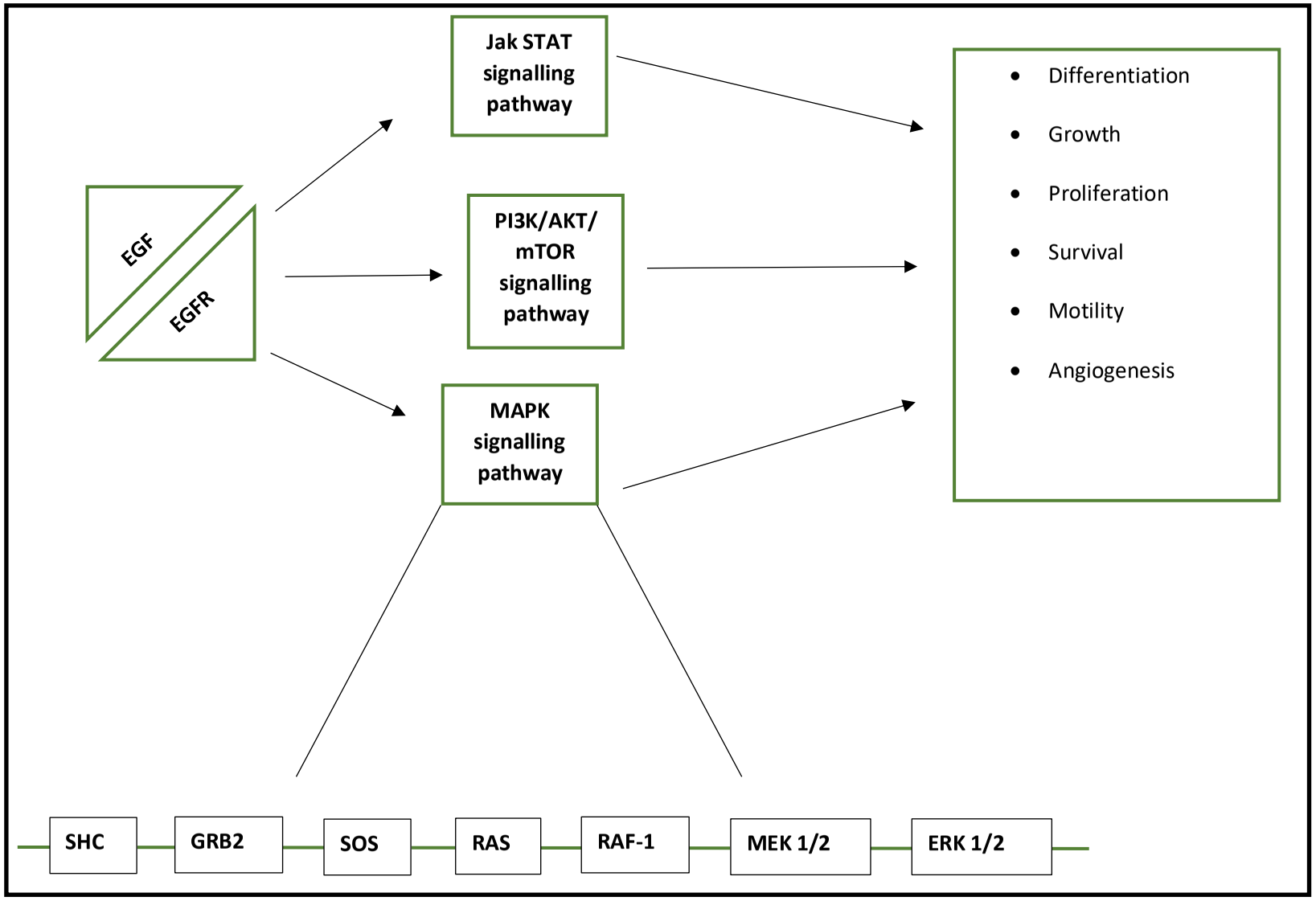
Jak STAT signalling pathway
PI3K/AKT/ mTOR signalling pathway
MAPK signalling pathway
EGF
EGFR
Differentiation
Growth
Proliferation
Survival
Motility
Angiogenesis
SHC
GRB2
SOS
RAS
RAF-1
MEK 1/2
ERK 1/2

Figure 1.3. Simple diagram illustrating the interaction between EGFR and subsequent initiation of signalling pathways. Ligand binding to EGFR contributes to the exposure of the dimer interface of the receptor and activation of the cytoplasmic domains. During this interaction, phosphorylation of tyrosine residues from adenosine triphosphate (ATP) occurs with the aid of a kinase enzyme. As a result, either homo-dimerisation or hetero-dimerisation ensues which ultimately inaugurates downstream signalling pathways associated with EGFR activation (Zhu, *et al.*, 2019). Jak/STAT, PI3K/AKT/mTOR and MAPK signalling pathways are initiated when EGFR is activated. This diagram also illustrates the MAPK signalling pathway in more depth through exemplifying the interactions involved in the pathway, which ultimately result in the physiological processes stated. When EGF binds to EGFR, Y1068 and Y1086 tyrosine residues bind directly to Growth Factor Receptor Binding Protein 2 (GRB2). Once bound, Src Homology and Collagen (SHC) is phosphorylated allowing itself to become a binding site for GRB2. Following this, the two SH3 domains on GRB2 bind to Sons of Sevenless 1 (SOS1) through the proline rich carboxyltail. SOS1 then activates RAS by instigating the exchange of guanosine diphosphate (GDP) to guanosine triphosphate (GTP). Through doing this, RAS can then interact with RAF1 which consequently activates MAPK ERK Kinase (MEK) 1/2 through the phosphorylation of serine residues at 217 and 221. MEK 1/2 can then activate Extracellular Signal-Regulated Kinase (ERK) 1/2 through phosphorylating the thr-glu-tyr motif in ERK 1/2 which can then phosphorylate various substrates to induce a biological response such as angiogenesis (Wee & Wang, 2017).

It is important to establish that EGFR is not solely identifiable in cancerous-cells but are expressed on normal cells, predominantly of epithelial origin. Expression levels can range from 40,000 to 100,000 receptors per cell (Harding & Burtness, 2005). To put overexpression of the receptor into perspective, some cancer-cells have been established to express $2x10^6$ receptors per cell, this is at least twenty times greater than normal cells (Milenic, *et al*., 2008). The amplified expression of the receptor on the cell allows for heightened activation thus increasing the stimulation of cell signalling pathways associated with certain hallmarks of cancer.

Nielsen *et al* 2004, using IHC, demonstrated that EGFR was overexpressed in 62% of 783 epithelial-OC patients (Nielsen, *et al.*, 2004). In addition to this, Milenic *et al* 2008, compared the overexpression of EGFR in various cell lines, including SK-OV-3, to the A431 cell line (EGFR expression level of $2x10^6$ receptors per cell). The percentage of cells positive for EGFR and the mean fluorescence intensity (MFI) of EGFR expression was measured using flow-cytometric techniques. Results indicated that 99.7% of SK-OV-3 cells were positive for EGFR, whereas 95.4% of A431 cells were positive. Additionally, the level of EGFR expression for A431 cells had an MFI result of 1480.5 in comparison to 452.9 for SK-OV-3 cells. Although this seems like a dramatic decrease, SK-OV-3 cells had the second highest level of expression (Milenic, *et al.*, 2008). This demonstrates that there are more cells that contain the receptor in SK-OV-3 compared to A431, whereas there are more receptors per cell in A431 in comparison to SK-OV-3. Ultimately, these

results highlight that SK-OV-3 expresses an excessive level of EGFR demonstrating a compelling molecular-target when considering precision medicine.

In addition to EGFR, vascular endothelial growth factor receptor (VEGFR) has shown to be overexpressed in SK-OV-3 cells also (as mentioned in Section 1.4.2) (Spannuth, *et al.*, 2009). This receptor regulates the process of angiogenesis (formation of new blood vessels), a critical process in the growth of cancer as well as invasion and metastasis (Benedito, *et al.*, 2012). For its dominant role in the progression of cancer whilst proving to aid in the poor prognosis of OC, this receptor is another molecular-mark that therapies can target to impair tumour-cells.

Targets which cause tumorogenesis are clearly an excellent focus, however, identifying molecular mechanisms familiar in cancerous and normal cells can be exploited in the degradation of tumours. PARP is a protein found in most cells with the role of repairing single-stranded DNA breaks through the utilisation of the base excision repair pathways *(Morales, et al.*, 2016). Through inhibiting PARP's, the mechanism of repairing single-stranded DNA breaks is impaired which eventually leads to cell death (Lin & Kraus, 2017). Cells also use the homologous recombination repair (HRR) mechanism, which involves the BRCA1 and 2 genes, to repair double-stranded DNA breaks; this means cells with a working HRR mechanism and healthy BRCA genes are less susceptible to the effects of PARP inhibitors (Roy, *et al.*, 2012). However, cells with faulty BRCA genes, as witnessed in HGSOC (Neff, *et al*., 2017), impair the ability of double-stranded DNA breaks being corrected and are therefore more vulnerable to the effects of PARP inhibitors, making cell death more imminent (Chandna, 2019).

Considering the examples outlined here, molecular-markers must have a strong ascendancy with the hallmarks of cancer (Hanahan & Weinberg, 2011) and therefore able tumorogenesis in some form. Such mutations are usually specific to not only the form of cancer but the histotypes associated with those forms. Due to the specificity, this makes the molecular-targets distinct and thus lays the foundations for research into precision medicines which has resulted in the successful development of targeted-treatments (Section 1.4.2). Unfortunately, OC remains as the most lethal gynaecologic malignancy (Du, *et al.*, 2015), however, continuing to establish molecular-marks and exploring unprecedented routes of treatments will surely improve the outcomes for OC patients in the near future.

1.4. Contemporary Treatments in Ovarian Cancer

Symptoms associated with OC include pain and pressure in the pelvis, back pain and change in bowel habits (National Health Service , 2017). Ambiguous symptoms such as these are commonly misdiagnosed for irritable bowel syndrome, menstruation and dyspepsia. By extension only 25% of women will be diagnosed at stages I and II whilst 75% are diagnosed at stages III and IV, by which point the cancer has spread (Ebell, *et al.*, 2016). This explains why over 239,000 women are diagnosed worldwide annually with OC (Reid, *et al.*, 2017) and accounts for approximately 5% of cancer related deaths among women; greater than any other gynaecological disease (American Cancer Society , 2019). With this in mind, the progression and development of therapies utilised in the treatment of OC are imperative for survival.

1.4.1. Non-Targeted Therapies

Non-targeted therapies do not specifically target cancer-cells and their genomic modifications, instead such therapies work by ostracising cells in the body that grow and divide quickly (Athauda, *et al*., 2019). Unfortunately, with lack of specificity, healthy cells may also be attacked consequently increasing the number and severity of side effects (Kayl & Meyers, 2006). This is not said to discredit the impact non-targeted therapies have had over the decades, nonetheless, progression in medicine is required to overcome barriers such as resistance.

Existing non-targeted therapies commonly used in the process of treating OC include surgery and chemotherapy (Eisenkop & Spirtos, 2001). The current standard of care includes initial debulking surgery and adjuvant platinum/taxane based chemotherapy (Lheureux, *et al.*, 2015).

1.4.1.a. Surgery

Surgery is an important first-line intervention in the early treatment of OC (Meigs, 1934). It is initially utilised to remove and stage the cancer; this is achieved through an omentectomy, sampling of the pelvic region and peritoneal or abdominal washings. Research suggests there is a direct association between cytoreductive surgery and prognosis (McGuire III & Markman, 2003, Iura, *et al*., 2018). Surgery is commonly used as a singular therapy in stage I OC whilst all efforts are made to sustain fertility (Schorge, *et al*., 2018). Adjuvant chemotherapy is also not necessary for this stage, instead an active surveillance programme is operated involving regular clinical reviews and examinations including abdomen and pelvic sonography; this ensures optimal survival and maintains a reoccurrence rate of 15-25% (Ray-Coquard, *et al.*, 2018).

Surgery which salvages reproductive capability is highly unlikely with regards to advanced stage OC as both ovaries and/or fallopian tubes are involved. Instead a total-abdominal-hysterectomy and bilateral-salpingo-oophoectomy are performed; this involves the removal of both ovaries and fallopian tubes as well as the womb and cervix (Katz, *et al.*, 2019).

As alluded to, surgical debulking followed by platinum-based chemotherapy is the primary standard of care for advanced OC. However, some researchers have investigated the potential benefits of neoadjuvant chemotherapy as well as interval debulking surgery (IDS) *(Schorge, et al.*, 2010). Kehoe *et al* 2015, in a phase 3 trial undertaken in 87 hospitals in the UK and New Zealand, randomly assigned stage III and IV OC patients to either primary surgery followed by 6 cycles of adjuvant chemotherapy or 3 cycles of chemotherapy, IDS, followed by 3 more chemotherapy cycles. Results showed that the median overall survival (MOS) was 24.1 months compared to 22.6 months in favour of the primary chemotherapy with IDS. Furthermore, 24% (primary surgery) compared to 14% (primary chemotherapy with IDS) of women died within 28 days of surgery (p-value=0.0007) (Kehoe, *et al.*, 2015). These results were emphasised further in similar research carried out by Vergote *et al* 2010, establishing the benefits of neoadjuvant chemotherapy and IDS (Vergote, *et al*., 2010). Subsequent to these studies, Meyer *et al* 2016, indicated that there was an increase in the use of neoadjuvant chemotherapy from 16%, starting in 2003 to 2010, to 24%, during 2011-2012 for stage III OC, whilst stage IV OC saw an increase from 41% to 62% respectively (Meyer, *et al.*, 2016). Such research highlights why progression and development in medicine is obligatory.

1.4.1.b. Chemotherapy

Chemotherapy is a common treatment used across a range of cancers and has made huge progressions with goals of curing, controlling or palliating the disease (Chabner & Roberts Jr, 2005). Using cytotoxic drugs which circulate in the bloodstream, rapidly dividing cells such as cancer-cells are attacked through the prevention of DNA replication (Frezza, *et al.*, 2017). It has been suggested that OC was one of the first tumours to be treated by means of chemotherapy with the use of single alkylating agents (AA). This was considered as the optimal treatment plan for OC up until the mid-1970's with median survival among recipients ranging from 17 to 20 months (BMJ, 1991). However, as documented in Table 1.5, there have been multiple advancements in the field of chemotherapy over the decades ultimately leading to the optimal treatment plan of platinum/taxane based chemotherapy used today (Katsumata, *et al.*, 2013).

A common theme however, which can be attributed to the multiple progressions in chemotherapy regimens, is in fact chemoresistance; this is when the cancer-cells become unaffected by the cytotoxic drugs used in chemotherapy and thus continue to thrive. Chemoresistance is a huge challenge in the therapeutics community and is a huge impediment to the long-term success of treatment (Asare-Werehene, *et al*., 2019). Unfortunately, due to chemoresistance, as many as 70-80% of OC patients will succumb to the disease as there are no alternative treatment options (Granados, *et al.*, 2015). A few brief examples of this are demonstrated in Table 1.5. Young *et al* 1978, initially found that combining AA in the treatment of OC increased MOS by 12 months in advanced stage OC patients compared to monotherapy (p-value=0.02) (Young, *et al*., 1978). However, this therapy regimen was quickly reviewed when chemoresistance to AA increased; this instigated the eventual research by Neijt *et al* 1984, into the combination of cisplatin with cyclophosphamide, which significantly improved the MOS (p-value=0.002) (Neijt, *et al.*, 1984). Once more, cyclophosphamide, as an AA, proved to become more ineffective, this prompted further research into alternative therapies. This resulted in Piccart *et al* 2000, and Neijt *et al* 2000, publishing research on the significant benefits of combining paclitaxel with either cisplatin or carboplatin with an increase in MOS of 9.8 months and an average of 81.4 months respectively (Piccart, *et al.*, 2000, Neijt, *et al*., 2000).

Table 1.5. Primary research published from 1978 to 2013 representing key advancements made in the development of therapies for OC ultimately progressing to the optimal treatment regimen available today.

Author	Title	Method	Results	Reference
Young *et al* 1978	*Advanced ovarian adenocarcinoma. A prospective clinical trial of melphalan (L-PAM) versus combination chemotherapy.*	80 patients with advanced stage OC treated with either four-drug-combination (4A) of hexamethylmelamine, cyclophosphamide, methotrexate and 5-fluorourcil or single alkylating drug melphalan (1A).	Patients treated with 4A were associated with significantly higher overall response rate compared to those treated with 1A (75% and 54% respectively), more complete remissions (33% vs 16% accordingly) and longer median survival (29 months vs 17 months) (p-value<0.02)	(Young, et al., 1978)
Young *et al* 1979	*cis-Dichlorodiammineplatinum(II) for the treatment of advanced ovarian cancer.*	Used cisplatin to treat 29 patients with advanced stage OC and resistance to alkylating agents.	Results showed 29% of patients responded positively to the treatment	(Young, et al., 1979)
Lambert and Berry 1985	*High dose cisplatin compared with high dose cyclophosphamide in the management of advanced epithelial ovarian cancer (FIGO stages III and IV): report from the North Thames Cooperative Group.*	Compared the treatment of cisplatin with cyclophosphamide in 86 patients with stage III or IV OC.	Treatment with cisplatin significantly improved median survival time in comparison to cyclophosphamide (19 months vs 12 months respectively) and longer median duration of clinical response (18 months vs 8 months accordingly)	(Lambert & Berry, 1985)

Neijt *et al* 1984	*Randomised trial comparing two combination chemotherapy regimens (Hexa-CAF vs CHAP-5) in advanced ovarian carcinoma.*	Compared the combination of hexamethylmelamine, cyclophosphamide, methotrexate and 5-fluoroucil (Hex-CAF) with combination of cyclophosphamide, hexamethylmelamine altered with doxorubicin and cisplatin (CHAP-5) in 186 advanced staged OC patients.	CHAP-5 significantly improved complete remissions (p-value<0.004), longer overall survival and progression free survival (PFS) (p-value<0.002) and better overall response (p-value=0.0001).	(Neijt, et al., 1984)
Omura *et al* 1986	*A randomized trial of cyclophosphamide and doxorubicin with or without cisplatin in advanced ovarian carcinoma. A gynaecologic oncology group study.*	Stage III and IV OC patients subject to either cyclophosphamide and doxorubicin (CA-120 women) or cyclophosphamide, doxorubicin and cisplatin (CAP-107 women).	Complete response rate for CA was 26% vs 51% for CAP (p-value<0.0001), median survival being 19.7 vs 15.7 months in favour of CAP	(Omura, et al., 1986)
Piccart *et al* 2000	*Randomized intergroup trial of cisplatin-paclitaxel versus cisplatin-cyclophosphamide in women with advanced epithelial ovarian cancer: three-year results.*	680 patients with stage IIb to IV OC were treated with either cisplatin and paclitaxel or cisplatin and cyclophosphamide.	Overall response rate was 59% vs 45% in favour of paclitaxel group. Complete clinical remission rates were 41% vs 27% in favour of paclitaxel again. Longer progression free survival was also witnessed in the paclitaxel group (median 15.5 months vs 11.5 months; p-value=0.0005) and longer overall survival (median of 35.6 months vs 25.8 months; p-value=0.016)	(Piccart, et al., 2000)

Neijt *et al* 2000	*Exploratory phase III study of paclitaxel and cisplatin versus paclitaxel and carboplatin in advanced ovarian cancer.*	208 advanced stage OC patients subject to either paclitaxel with cisplatin or carboplatin.	Paclitaxel with carboplatin was associated with significantly less nausea and vomiting (p-value<0.01) and less peripheral neurotoxicity (p-value=0.04). However more granulocytopenia and thrombocytopenia (p-value<0.01)	(Neijt, et al., 2000)
Katsumata *et al* 2013	*Long-term results of dose-dense paclitaxel and carboplatin versus conventional paclitaxel and carboplatin for treatment of advanced epithelial ovarian, fallopian tube, or primary peritoneal cancer (JGOG 3016): a randomised, controlled, open-label trial.*	Compared conventional treatment of carboplatin 6mg/ml per min on day 1 and paclitaxel 180mg/m^2 on day 1 (312 OC stage II-IV women) with dose-dense treatment carboplatin 6mg/ml per min on day 1 and paclitaxel 80mg/m^2 on days 1,8 and 15 (319 OC stage II-IV women).	Median progression free survival was 28.2months vs 17.5 months and median overall survival was 100.5 months vs 62.2 months both in favour of the dose-dense treatment.	(Katsumata, et al., 2013)

Tumours can be intrinsically resistant preceding to chemotherapy (attributed to the existence of cancer stem cells) (Zheng, 2017) or the resistance can be acquired throughout treatment (attributed to genetic and epigenetic dysregulation of onco- and tumour suppressor genes) (Liu, *et al.*, 2012). Drug resistance is extremely complex due to its multi-factorial phenomenon; factors contributing to resistance include accelerated drug-efflux, alterations in drug target, DNA methylation and evasion of apoptosis (Pan, *et al.*, 2016). Another common cause of chemoresistance is drug-inactivation, commonly noted in OC patients in relation to platinum-based therapies. This mechanism involves glutathione (a powerful antioxidant found in all living organisms). Glutathione forms conjugates with platinum-based drugs, such as cisplatin or carboplatin, and inactivates the cytotoxic effects of the drug through inhibiting oxidative stress which would have the potential to damage RNA and DNA of the tumour-cells which is evident in SK-OV-3 (Mistry, *et al*., 1991). Furthermore, when the platinum-based drugs covalently link to

glutathione, a substrate for ATP-binding-cassette-transporter proteins is produced resulting in drug-efflux, another form or chemoresistance (Wilson, *et al*., 2006).

Treatment failure is having a huge impact on the success and survival of OC. Reviewing the previous topics discussed regarding non-targeted therapy, it is clear that a lack of specificity with the use of a 'one-size-fits-all' therapeutic approach, chemoresistance is increasing. Using non-targeted therapies is resulting in transient responses diminishing survival of the disease, especially if progression in drug development is not made. This is why there is an enormous requirement for research to delve into targeted-therapies which will improve the effectiveness of treatment, increase the number of women who survive the disease and overcome chemoresistance.

1.4.2. Targeted Therapies

Alternative to non-selective therapeutics, targeted-therapies prevent tumorigenesis through identifying and restraining specific molecular-targets. These include transduction pathways, specific proteins related to cancer progression, or through the stimulation of the immune system aiding in the delivery of cytotoxic drugs (Perez-Herrero & Fernandez-Medarde, 2015). Such treatments can prevent the growth, progression and spread of cancer-cells. Oncogenes, tumour-suppressor genes and the completion of the human genome sequence have assisted in the understanding of the foundations of cancer initiation and progression, which can be capitalised upon to research beneficial targets in the battle against cancer (Jones, *et al.*, 2016). Precision medicine isolates and centres treatment on the specific abnormalities of cancer-cells and therefore aims to reduce the number and severity of side effects associated with the general treatments commonly administered today (Hait, 2009).

Cancer occurs when there is a substantial change in the cells genetic identity which modifies the cells molecular programming preventing healthy functioning. It is the distinctive molecular changes initiating cancer development which researchers are interested in as this molecular-marker can act as the target for potential therapies (Wilson, *et al.*, 2018).

Targeted-therapies are not a new concept, however, there has been a dramatic peak of interest in the subject over the years. From a literature search on PubMed using the inputs of 'cancer-' or 'ovarian cancer- AND targeted therapies' the surge in publications from 1977 until now is evident as illustrated in Figures 1.4 and 1.5 (National Center for Biotechnology Information, 2019). However, what is also apparent from both figures is publications decreased from 2017 to present by 73% and 2016 to present by 75% respectively. Although this is not a direct

representation for the development of new targeted-therapies, it does suggest interest in the topic could be wane. While there are targeted-therapies available, they are limited to certain sub-types of cancer, meaning many individuals will not be eligible for the precision medicine available; this alone is a convincing reason as to why research needs to continue to find such unique markers within cancer to develop more direct treatments.

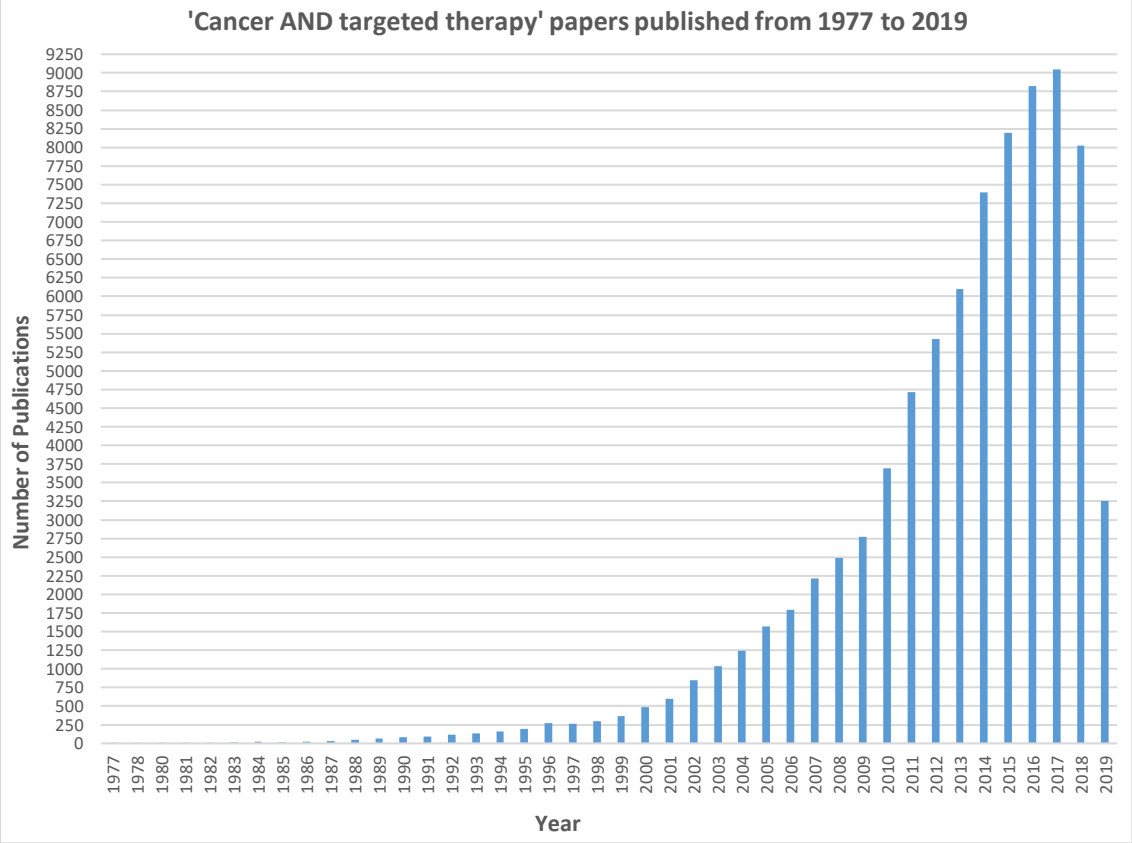

Figure 1.4. Cancer and targeted therapy publication rate. The number of articles deposited in PubMed per year from 1977 to 2019. Data collected using search input 'cancer AND targeted therapies'.

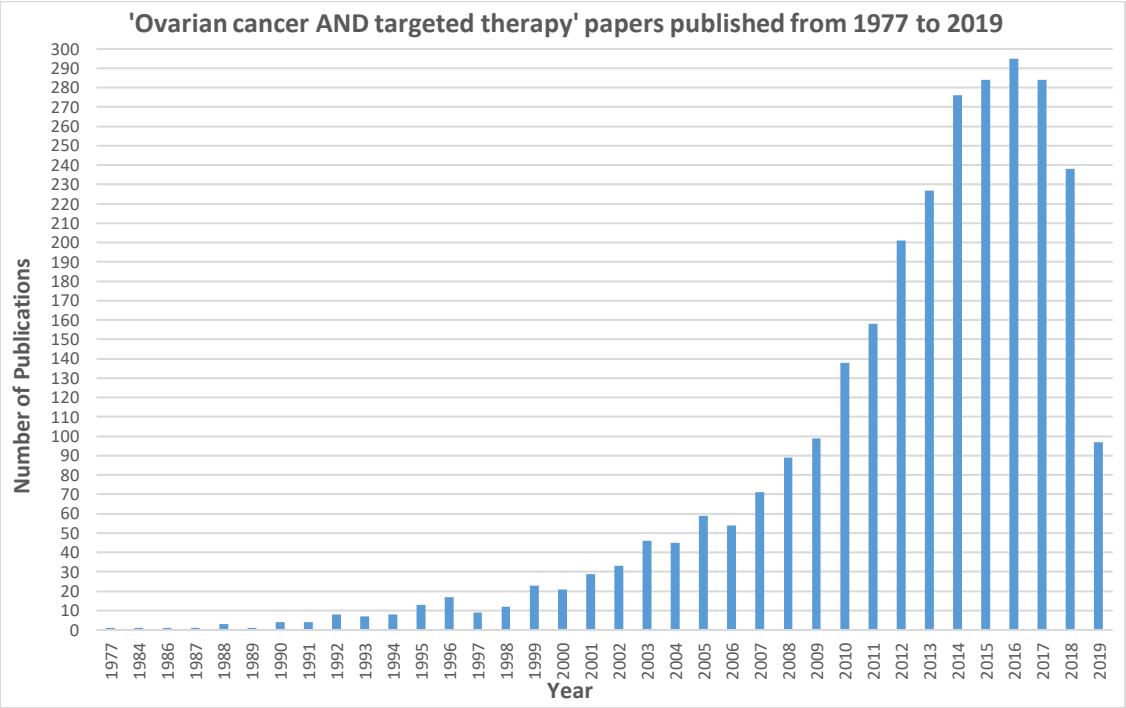

Figure 1.5. Ovarian cancer and targeted therapy publication rate. The number of articles deposited in PubMed per year from 1977 to 2019. Data collected using search input 'ovarian cancer AND targeted therapies'.

Trastuzumab (Herceptin) is a targeted-therapy developed through the identification of some breast-cancers distinctively overexpressing the HER2 protein involved in extensive cell proliferation (Risi, *et al*., 2018). Dr D.Salmon identified the amplification of the HER2/neu gene in 30% of the 189 primary human breast-cancers investigated with an amplification of 2- to 20-fold (Slamon, *et al.*, 1987). This was supported by Dr W.Gullick, however, with the use of immunohistological staining and Western Blotting, Dr Gullick established that the HER2 protein was also overexpressed in 33% of the HER2 gene emphasised breast-cancers (Gullick, *et al.,* 1987). In agreement, it was established that HER2 was in fact a worthy target in treating HER2 positive breast-cancer. Through this important research, Dr Ullrich and Dr Shepard at Genentech developed an antibody which blocked the receptor activity of HER2; this drug was trastuzumab. Initial clinical trials started in 1992 with 15 women which expanded to 900 women by 1996 eventually leading to the fast-tracked approval by the U.S Food and Drug Administration (FDA) (Harries & Smith, 2002). Herceptin is now a mainstream treatment for patients with HER2 positive breast-cancer through research identifying a molecular-target creating a vulnerability for the cancer.

With respect to OC more specifically, one targeted-therapy approved by the National Institute of Health Care and Excellence is olaparib (Lynparza) (National Institure for Health and Care Excellence , 2016). This drug is used as a maintenance therapy for OC patients with platinum

sensitivity. Eligibility for this drug involves the cancer patient having a mutation in their BRCA1 or BRCA2 gene whilst also having had 3 or more courses of platinum based therapy *(Robson, et al.*, 2017). Olaparib inhibits the ability of PARP to repair single stranded DNA breaks (Morales, *et al.*, 2016) thus leading to cell death (Lin & Kraus, 2017). However, cells must have faulty BRCA genes to procure the full impact of the PARP inhibitor otherwise cells are less susceptible to the inhibitory effects and increases cells survival (as explored in Section 1.3). It is for this reason that patients receiving this treatment must have faulty BRCA genes (Chandna, 2019).

Numerous studies have illustrated the benefits of using olaparib as a maintenance drug for advanced, platinum sensitive OC. Ledermann *et al* 2012, carried out a randomised, double-blinded phase 2 study with 265 OC patients. 136 patients were assigned to 400mg of olaparib twice daily whilst 129 were assigned a placebo. Results showed that median PFS was 8.4 months vs 4.8 months respectively (Ledermann, et al., 2012). This is supported by Oza *et al* 2015, who compared olaparib, paclitaxel and carboplatin with paclitaxel and carboplatin alone; results showed PFS was significantly higher in the group treated with olaparib (median 12.2 months vs 9.6 months respectively; p-value=0.0012) (Oza, *et al.*, 2015).

For precision medicines to be developed, a target within the cancer must be identified and exploited which does limit the number of patients who will benefit from the potential drug. This is why it is important to not look at certain cancers as a singular disease but instead study the individual histotypes and their unique targets. For OC, PARP and VEGF inhibitors are the precision medicines currently available; however, these are limited to those with faulty BRCA genes or high expression levels of VEGF-A (Goel & Mercurio, 2013). As previously mentioned, EGFR is expressed in up to 90% of certain OC histotypes (Wilken, *et al.*, 2012) while also overexpressed in the SK-OV-3 cell line; with its crucial role in cell proliferation, migration and invasion, the receptor becomes a compelling target to explore for potential inhibitors in OC patients who overexpress EGFR (Wang, *et al*., 2016). Research has highlighted a positive result in targeting this receptor for the likes of non-small cell lung-cancer and pancreatic-cancer with gefitinib (Hirsch, *et al.*, 2018) and erlotinib (Wang, *et al.*, 2015). Unfortunately, these results are not yet mirrored for OC. However, further investigations need to be aroused into finding alternative, unorthodox therapies which have the potential to target unique marks such as EGFR. One route into novel, targeted-therapies which needs to be explored deeper is the use of anticancer venom peptides.

1.5. Natural Sources and Venom Constituents; Their Potential in Drug Development

Throughout history, natural sources have been utilised to treat a number of diseases and infections since ancient times and in folklore (Dar, *et al*., 2017). The first records, written on clay tablets in cuneiform, are from Mesopotamia and date back to 2600 B.C. Such records evidenced the use of oils collected from *Cupressus sempervirens* and *Commiphora myrrha* which were used to treat colds, coughs and bronchitis (Dias, *et al*., 2012). Moreover, Egyptian medicine recorded in the Ebers Papyrus from 1500 B.C documents 700 drugs primarily sourced from plants; these range from ointments, to pills and infusions (Cragg & Newman, 2005). Drawing back to the beginning of the 21st century, 11% of the 252 drugs considered as basic and essential by the World Health Organisation (WHO) were in fact from plant origin (World Health Organisation, 2020). It is therefore no surprise that natural sources remain a popular area of investigation in the drug discovery sector.

Anticancer activity is another area in which natural sources have played a significant role. Terrestrial plants, the marine environment, microbes and slime molds are some of the natural sources with anticancer activity (Desai, *et al*., 2008). Paclitaxel, known as Taxol, is a microtubule-stabilizing drug utilised in the treatment of numerous cancer including ovarian, breast, lung and pancreatic cancer (Zein, *et al.*, 2019). This plant alkaloid was first isolated from *Taxus brevifolia* (pacific yew) in 1971 and approved for medical use in 1993 (Weaver, 2014). In addition to terrestrial plant sources, the marine environment also contains anticancer potential. Ecteinascidin-743, also known as Yondelis, is an extract from the sea squirt *Ecteinascidia turbinata* and is used to treat advanced soft tissue sarcoma through inhibiting the transcription of protein-coding genes (Tumini, *et al.*, 2018). Ultimately, this is just a snapshot of the significance natural sources have had with respect to cancer therapeutics.

As previously articulated, the treatment options available for OC are not only limited but are subject to several side effects, poor clinical outcomes and have restricted long-term success due to chemoresistance (Kim, *et al.*, 2018). Investigations into finding alternative, novel and targeted-therapies has never been more applicable. Although a variety of targeted-therapies have been discovered and are used with varying successes for a variety of cancers (Section 1.4.2) there is still a shortage for OC making research in this field fundamental (Cortez, *et al*., 2018). Therefore, it has never been more relevant to explore the depths that natural sources have to offer which is why the anticancer activity of animal venoms is an essential step into finding alternative and novel therapeutics.

Venoms are a complex mixture of many biologically active compounds; proteins, peptides, enzymes and toxins contribute to the sophisticated cocktail (Williams, *et al.*, 2019). Not all venomous animals contain the exact same composition of elements in their venom and will vary according to species, age, sex and geographical location (Tasoulis & Isbister, 2017). In natural settings, venom is utilised to either defend or hunt, which is why the arrangement of compounds in venoms have been selected by evolution to most beneficially impact the animal in its preferred environment (Trim & Trim, 2013). Natural selection has highlighted the specificity that venom toxins have for molecular-targets to ensure a desirable effect is achieved on the predator or prey whilst optimising the species energy expenditure (Casewell, *et al.*, 2013). Such toxins can be classified depending on their specific biological effect; these include cytotoxins, neurotoxins, cardiotoxins and hemotoxins (Shanbhag, 2015). Depending upon their mode of action, it is possible to exploit certain venom components in the development of therapeutic agents.

Unfortunately, research into the potential venom has in the therapeutic community has been restricted, researchers lacked the applicable equipment and methods in analysing the minuscule amounts of venom secreted by animals in a laboratory setting. However, with huge advances in omics analysis as well as innovations in bioinformatics and computational biology, exploring the capabilities of venoms and their diversification has never been more accessible (Utkin, 2017). This has not only aided in the FDA approval of 6 venom-based drugs and 3 more venom derived peptides in clinical trials, but also the plethora of research investigating the anticancer properties of venom (Pennington, *et al*., 2018).

Song *et al* 2012, found that snake venom toxin from *Vipera lebetina turanica* (not yet identified) inhibited OC cell growth dose-dependently with an inhibitory concentration (IC50) of 4.5µg/ml in PA-1 cells and 6.5µg/ml in SK-OV-3 cells. Furthermore, apoptotic cell death was induced in these cell lines through inhibiting the NF-kB and STAT3 signal whilst also hindering P50 and P65 translocation to the nucleus. In addition to this, the snake venom toxin also increased the expression of pro-apoptotic proteins Bax and caspase-3 and downregulating the anti-apoptotic protein Bcl-2 (Song, *et al.*, 2012). Similarly, Chiu *et al* 2009, identified that the 60-amino-acid polypeptide residue cardiotoxin III (CTX III) isolated from *Naja naja atra* venom downregulated NF-kB in the human breast-cancer cell line MCF-7, which by extension inhibited proliferation and prompted apoptosis. Sub-G1 formation, PARP cleavage and phosphatidylserine externalisation established such results. This was achieved at an IC50 of 2µg/ml (Chiu, et al., 2009). Moreover, Su *et al* 2010, indicated CTX III inhibited the phosphorylation of EGFR which prevented the activation of the JAK/STAT and PI3K/AKT signalling pathways (mentioned in Section 1.3) ultimately stimulating apoptosis in human adenocarcinoma A549 cells (Su, *et al.*,

2010). However, CTX III is a cardiotoxin and is known to cause direct myocardial damage which can result in arrhythmias, bradycardia, tachycardia or hypotension; this means further investigations into the potential side effects this toxin could offer is required before drug development, as well as identifying the active anticancer constituent that is not cardiotoxic (Campbell & Cohall, 2017). As well as snake venom, scorpion venom also presents anticancer activity. Diaz-Garcia *et al* 2013, using an MTT assay identified venom from *Rhopalurus junceus* (*R.*jun) reduced cell viability significantly of epithelial cancer-cells at an IC50 ranging between 0.6-1mg/ml. Furthermore, this scorpion venom induced apoptosis in Hela cells through overexpression of p53 and Bax mRNA, increase in caspases 3, 8, and 9 and downregulation of bcl-2 mRNA (Diaz-Garcia, *et al.*, 2013)

Anticancer properties of venom are not only utilised for their direct effect on particular cancer-cells, but certain venom peptides can be utilised to aid in the detection of cancer. Recently, a novel imaging technique has been developed which employs the use of a synthesised form of scorpion venom which 'lights up' brain tumours, empowering neurosurgeons to identify malignant growths with greater superiority. Researchers from Cedars-Sinai led the phase 1 clinical trial involving glioma patients; Tozuleristide (BLZ-100), which is composed of a synthetic chlorotoxin peptide found in scorpion venom, was attached to infrared-fluorophore-indocyanine-green (fluorescent dye) and administered to 17 patients intravenously receiving doses between 3 and 30mg. Results showed tumour identification was significantly clearer using the Tozuleristide drug including both high-grade and low-grade gliomas; moreover, patients did not present serious adverse responses to the drug when monitored for 30 days after the trial (Patil, *et al.*, 2019).

Not all venoms will have anticancer properties nor will the same effect that occurred in one cell line necessarily be imitated in another cell line. Giovannini *et al* 2017, identified that the Vidatox-30-CH drug, derived from the *R.jun* scorpion venom induced proliferation in hepatocellular carcinoma cells significantly when rats were treated for 30 days in comparison to the control group of rats identified using immune-staining for Ki-67 (p-value=0.01) (Giovannini, *et al*., 2017). However, venom from this same scorpion did prove to reduce cell viability in epithelial cancer-cells, as previously mentioned, but did not affect hematopoietic tumour-cells *(Diaz-Garcia, et al.,* 2013) illustrating the varied outcomes possible when used in different combinations. Although cytotoxic abilities of venom present specificity which ultimately limits the number of cancer types which will benefit from the effects, it does highlight that the venom must be targeting explicit molecular mechanisms and pathways. This further demonstrates why utilising

venom as a novel, targeted-therapy would be beneficial considering its particularity for cancer progression mechanisms.

This snap-shot of research exemplified illustrates the vast prospective that venom has in a variety of cancers and the huge potential still unfilled. As documented, venom can interfere with cell signalling pathways imperative for cancer progression, as well downregulating and/or upregulating necessary proteins which initiate apoptosis and cancer-cell degradation. Moreover, significant peptides or proteins can be isolated and synthesised to be utilised synergistically alongside current treatments at lower doses increasing their effectiveness and limiting toxicity. It is however important to remember that cancer is a genetic disease with a unique amalgamation of genetic changes, therefore cancer-cells, even if they arise from the same area, will still vary significantly amongst each other. For this reason, venoms from the same species, even the same peptides, proteins or toxins will not automatically affect all cancer-cells the same way. Consequently, it is essential that researchers not only identify and isolate specific proteins with cytotoxic capabilities, but also find the optimal venom-to-cancer coalition. This will aid in developing a panel of specific venom proteins that target distinct cancer types and molecular mechanism, essentially supporting the developments of novel therapies combatting the life-altering disease.

1.6. Conclusion

OC contributes to the greatest number of deaths in regards to gynaecological diseases and is the sixth most common cancer in association with the UK female population. Non-targeted therapies that are currently employed and contribute to the optimal treatment plan are becoming increasingly ineffective. With 75% of OC cases being diagnosed at stages III and IV as well as chemoresistance preventing the long-term success of standard treatments, the hugely negative statistics associated with the disease comes as no surprise. With this in mind, it is imperative for the discipline of drug development to delve into research concerning alternative and unconventional therapies in order to overcome the barriers associated with successfully treating the disease. As established, the scientific literature available is abundant in investigations into the potential venoms have in a variety of diseases. Such research has allowed for the FDA approval of 6 venom-based drugs which have contributed to the management of cardiovascular diseases and chronic pain. Furthermore, contemporary investigations evident in the published literature have highlighted the number of successes occurring in the laboratory setting in relation to the anticancer properties of venom. Through the targeting of particular receptors as well as the upregulation and/or downregulation of certain proteins which are detrimental to the survival of cancer, the capability of certain venoms in relation to particular cancers are endless. As previously touched upon, the effects certain proteins and peptides have on one cancer will not necessarily be imitated in another type of cancer as well as among cancer histotypes which demonstrates the venoms specificity.

For such reasons, the following project of investigating the effects of animal venoms in OC has been employed to contribute to the unconventional, novel therapeutics community. OC is associated with incredibly negative statistics and the number of women surviving the disease is not decreasing. With the technology currently available and the grounding research establishing the huge benefits that animal venoms can have, this investigation carried out has the potential to improve those statistics and the hope in finding a valuable treatment for OC.

Using an assortment of crude and fractioned venoms at a range of doses utilising the resazurin assay, the cell viability of SK-OV-3 cells will be measured. This will aid in determining a profile of venoms at specific concentrations which have the ability to prevent SK-OV-3 cell metabolism. Furthermore, venoms which do not significantly affect cell viability can also be characterised into a profile and can be considered as redundant. Predominantly, the investigation can set the ground work for future perspectives. Venoms which are considered as hits can be easily identified and analysed further (i.e fractioned further to identify the specific proteins causing

the effect) whilst the venoms which are classed as redundant, in relation to SK-OV-3 cells, can be steered away from thus producing a groundwork in future investigations.

Overall, the aims of this project are to:

- Optimise the cell number of the SK-OV-3 cell line in the setting of a 96 well plate resazurin-based assay.
- Optimise the positive control in regards to the optimal SK-OV-3 cell number, whilst in the setting of a 96 well plate resazurin-based assay.
- Identify a number of crude and fractioned venoms that significantly reduce the cell metabolism of SK-OV-3 cells.

CHAPTER TWO – GENERAL MATERIALS AND METHODS

2.1. Cell Line, Culture and Maintenance

2.1.1. SK-OV-3 Cell Line

Throughout this study, the Human ovarian cancer cell line SK-OV-3 was used. The cell line was derived from the ovary epithelium of a 64-year-old Caucasian female suffering from HGSOC; this specific cell line also significantly overexpresses the EGFR (Paramee, *et al.*, 2018). The cell line was available from laboratory stocks which were originally sourced from the American Type Culture Collection (American Type Culture Collection, 2019). This cell line was authenticated by the European Collection of Authenticated Cell Culture using short tandem repeat profiling in March 2018 showing that the profiles match 100%.

2.1.2. Routine Cell Culture and Maintenance

All cell culture-based work was carried out under sterile conditions in a cell culture flow hood (MSC Advantage™ – Thermo Fisher, UK); 70% industrial methylated spirit (IMS) was used to sterilise equipment entering the flow hood and any substances applied to the cells were warmed before application.

SK-OV-3 cells were cultured as cohesive monolayers in both T25 ($25cm^3$) and T75 ($75cm^3$) cell culture flasks. Cells were maintained in Dulbecco's Modified Eagles Medium (DMEM) which was supplemented with 10% Foetal Calf Serum (FCS), 1% Penicillin Streptomycin and 1% L-Glutamine (collectively known as media) (Thermo Fisher, UK). All cells were routinely incubated at 37°C, 95% air and 5% CO_2 (HERAcell 150i, Thermo Fisher, UK).

Introduction of the first cryotube containing 1ml of SK-OV-3 cells was thawed at room temperature on the workbench before the contents were transferred to a T25 flask containing 5ml of media. Once cells had settled (approximately 5 hours) the media was changed due to the presence of dimethyl sulfoxide (DMSO) in the freezing media.

Sub-culturing occurred when cells were approximately 70% confluent and were usually split in a 1:2 or 1:3 ratio as recommended (ATCC, 2019). Media was removed from the flask and cells were washed with phosphate-buffered saline (PBS) twice. 0.05% trypsin-ethylene diamine tetra

acetic acid (trypsin-EDTA) was used to dissociate the cells; flasks were then returned to the incubator for a maximum of 10 min. Once cells had dislodged from the flask and depending on the cell split ratio, media was applied to the flask to collect the cells (pipetting up and down to reduce cell clumps) and appropriately aliquoted into new cell culture flasks containing fresh media. Depending upon the size of the cell culture flask used (T25 and T75 – Thermo Fisher, UK), volumes of media, PBS, trypsin-EDTA and DMSO/FCS varied; refer to Table 2.1 for clarification.

Table 2.1. Depending upon the size of flask used, varying volumes of standard contents applied to the cells varied. This included cell culture media aiding in cell growth, PBS to wash the cells, trypsin-EDTA to split the cells and DMSO/FCS used to freeze the cells.

Contents	**Flask Size**	
	T25 Flask	***T75 Flask***
Media	5ml	15ml
PBS	2ml	5ml
Trypsin-EDTA	0.2ml	0.5ml
DMSO/FCS	1ml	1.2ml

2.1.3. Freezing Stocks

SK-OV-3 cells were frozen down to ensure continuous stocks of the cell line were available. Once cells had reached 80% confluency (increased confluency to account for any cells lost during cryopreservation process), routine cell culture protocol was followed, however, the addition of 10% DMSO/90% FCS was used to collect the dislodged cells and transfer contents to sterile cryotubes (Thermo Fisher, UK). Stocks were frozen down in a 1:1 ratio (one flask to one cryotube). Cryotubes were slowly frozen, initially placed in the -20°C freezer for 20 min. before being transferred to the -80°C freezer (this is to ensure the cells were gradually frozen preventing ice crystal formation (Chaytor, *et al.*, 2012)). A number of stocks were also stored in liquid nitrogen for permanent storage.

2.2 Cell Viability Resazurin Assay

Resazurin, an oxidation-reduction indicator, was used to assess cell viability. This was utilised to evaluate the cell viability of SK-OV-3 cells when exposed to different animal venoms and at varying concentrations. Assays were executed over a 2-day period. Day 1 consisted of combining several flasks ready to be counted and plated into a 96 well plate (Thermo Fisher, UK). Day 2 the venom (Venomtech Ltd, UK) was prepared by diluting the stock with PBS for the desired working concentration before the application to the cells. Resazurin (Thermo Fisher, UK) was also prepared on day 2 by diluting the stock concentration with a known volume of media for the desired working concentration before the plate was analysed and the data collected.

2.2.1. Day One: Harvesting and Plating Generic Protocol

To harvest the cells, several T75 flasks at 80% confluency were combined to be counted. This procedure followed the standard protocol for sub-culturing as stated in Section 2.1.2 up until the incubation period in trypsin. After 10 min. in the incubator, 2ml of media was added into each flask and all contents were transferred and combined in a 15ml falcon tube (Thermo Fisher, UK). Cells were thoroughly pipetted up and down to disband any cellular clumps.

20µl of the combined cells, 12µl of PBS and 8µl of trypan blue were transferred to a 0.5ml Eppendorf tube (Thermo Fisher, UK), again pipetting up and down to certify the cells were evenly dispersed before counting. Following this, a haemocytometer (Fisher Scientific, UK) was cleaned using 70% IMS and prepared by placing a glass coverslip over the counting chambers. The haemocytometer has two counting chambers, both of which consist of 9 squares. Cell counting involved the 4 corner squares of 1 chamber only.

Once the haemocytometer was prepared, the cells were counted. This involved transferring 20µl of the contents in the Eppendorf tube into one side of the haemocytometer under the coverslip; through capillary action, the cells were drawn into the counting chamber ready to be counted. At this point, the cells in the falcon tube were stored at 4°C to prevent cells from settling whilst counting occurred. Using an inverted microscope (Leica, UK), cells were counted at 10x magnification. All cells inside the 4 corners were counted; the rule ‘top left in’ was utilised to ensure all cells were only counted once and to guarantee counts were consistent. Cells which were stained blue were not counted; this was an indication that the membrane was not intact and therefore cells were not viable. Once all cells were counted, the calculations exemplified in Figure 2.1 were used to determine if there were enough cells present to continue with the assay and by extension the volume per well required for the particular cell number desired.

Cell count calculation:

1. *Average number of cells*
   - Total number of cells counted / number of corners counted
2. *Cells per ml*
   - 2 x average number of cells x 10^4
3. *Total number of cells*
   - Cells per ml x total volume*
4. *Volume per well*
   - Cell number required / cells per ml

**total volume added to combine cells.*

Figure 2.1. The calculations utilised to find the cells per ml, total number of cells and the volume per well required.

Upon determining the volume per well required, the combined cells were collected from the fridge. Cells were pipetted up and down before being transferred to a 50ml reservoir (Thermo Fisher, UK), this ensured cells were evenly dispersed in the media before application to the 96 well plate. The required volume per well of cells was transferred to the 96 well plate according to the layout of the specific assay. The plate was then returned to the incubator overnight allowing the cells to adhere.

2.2.2. Day Two: Venom and Resazurin Application Generic Protocol

Day 2 of the assay consisted of first applying the required concentration and species of venom over a 2hour period, and then applying 160µM resazurin to the cells to determine the cell viability through measuring the fluorescence. Stock concentrations of venom were diluted with PBS whilst resazurin was diluted with media to make the required working concentrations.

After approximately 24 hours (and the cells adhering to the plate), the media from all wells was removed and discarded. Again, depending on the assay being performed, the media was replaced with 50µl of venom (to the positive wells) or 50µl of PBS (to the negative wells). Ensuing venom application, the plate was returned to the incubator for 2 hours.

During incubation time, the FLUOstar Omega Microplate reader (BMG Labtech, UK) was prepared and the working concentration of resazurin was made. To prepare the plate reader,

the protocol *'resazurin fluo bottom'* was selected and the temperature was set to 37°C. Parameters included an excitation of 544, emission of 590 and gain of 800 with a 90% target value. Formulating the resazurin involved diluting the stock concentration of 1.6mM to the working concentration of 160µM with a known volume of media. The volume of resazurin required was dependent on the number of wells in use.

Subsequent to the 2 hour incubation time, the PBS and venom was removed and replaced with 50µl of the 160µM resazurin. The fluorescence of the plate was then measured every 15 min. for 1 hour, followed by every 30 min. for the following 4 hours. The raw data was stored using the MARS Data Analysis Software (BMG Labtech, UK) and processed using Microsoft Excel 2016 or GraphPad Prism 5.

2.3. Resazurin Assay – Z Prime

The Z prime (Z') assay was utilised throughout the optimisation protocols in order to determine assay quality and robustness. This type of assay is commonly used in high-throughput screening to assess whether the response in a particular assay is great enough to permit further attention. The Z' assay produces a Z-factor which describes how well separated the positive and negative controls are through processing the means and standard deviations of the data; this helps to eliminate the likelihood of false positives and negatives in the results. A Z-factor between 0.5-1 represents an excellent assay as this indicates there is a large separation band between the positive and negative means exhibiting a difference in the controls. Below 0.5 suggests the assay is not robust and therefore does not pass due to a small or overlapping separation band. This type of assay was consequently used to ensure conclusions drawn from the optimisation assays were robust enough to continue with, as well as determining the optimal time point to which the plate should be analysed (Zhang, *et al.*, 1999).

The Z' assay was set up as described in Chapter 2.2 in regards to counting and plating cells on day 1, followed by venom and resazurin application on day 2 as well as data collection. The assay layout remained consistent throughout the project; the 96 well plate was divided into four quadrants. The positive controls (venom) were located opposite one another in the top left and bottom right quadrants of the plate. Likewise, the negative controls (PBS) were also positioned opposite one another in the bottom left and top right quadrants of the plate. This is done to eliminate the 'edge effect'.

After 2 hours of incubation in either venom or PBS, all contents were removed and replaced with 160µM resazurin. The fluorescence of the plate was then measured and data analysed as described in Section 2.2.2.

2.4. Resazurin Assay – Dose Response

Dose responses (DR's) were performed on the various venoms throughout the project to investigate lethal doses (LD). This assay was used throughout the optimisation process and during the introduction of test compounds.

Again, following the same protocol described in Chapter 2.2, the cells were plated on day 1 and left to adhere overnight whilst day 2 consisted of applying the venom and resazurin. In addition to day 2 and before venom application, a compound plate was set up to aid in the serial dilution of the venom and to simplify the transfer of venom to the test plate. Column 1 of the compound plate contained the highest concentration of venom, this was serially diluted by half across the plate in PBS. Positive and negative controls were allocated to columns 11 and 12 respectively.

Upon completing the compound plate, the media from the test plate was removed and replaced with 50µl of the corresponding contents in the compound plate. The test plate was then returned to the incubator for 2 hours as per standard protocol. Following this, all contents were removed from the plate and replaced with 160µM resazurin and analysed as outlined in Section 2.2.2.

CHAPTER THREE – OPTIMISATION OF RESAZURIN ASSAY

3.1. Aims

The following experiments were utilised to optimise the resazurin assay before the introduction of test compounds. First, the optimal cell density of SK-OV-3 cells was investigated to compare a variety of different cell densities and thus find the cell number which produced the maximum assay window. This window demonstrates the fold change between the positive and negative controls, thus the larger the window the greater the difference is between the controls. The optimal cell density should have a window high enough that it produces a measurable signal, nevertheless, overcrowding must be avoided. Following this, a DR was carried out on the crude *Naja nigricollis* (*N.nig*) venom to find the LD90 and thus solidify the positive control for the forthcoming test assays; this provides a baseline with which the results from test compounds can be compared and validated. Finally, Z' assays were implemented to calculate a Z-factor which measures assay quality and therefore determines the robustness of the assay before moving forward as explained in Section 2.3.

3.2 Background

Resazurin assays are a fluorometric assay which have the aptitude to determine the metabolic ability of active cells in a high throughput setting through the reduction of non-fluorescent resazurin to highly fluorescent resorufin. The higher the fluorescence, the more metabolically active cells present. Such assays are commonly used within drug discovery due to their high throughput capabilities, it is therefore important to optimise the assay ensuring its high sensitivity and prompt result production enabling a robust and reliable system (Kim & Jang, 2017). Furthermore, assays of this sort are commonly used to determine cell viability and the proliferation capacity in eukaryotic cells. Walzl *et al* 2014, utilised the resazurin assay to distinguish between cytotoxic and cytostatic compounds in several colonic cancer cell lines (Walzl, *et al.*, 2014) whilst Ricigliano *et al* 2017, using a resazurin assay, investigated the most effective third line of treatment for pancreatic adenocarcinoma patients (Ricigliano, *et al.*, 2017). Moreover, Czekanska 2011, assessed the effectiveness of resazurin assays for cell viability and cell proliferation investigation; it was determined that the assay utilises all features of an ideal and reliable test whilst it is sensitive, safe, non-toxic to cells and extremely cost effective

(Czekanska, 2011). Such examples validate the effectiveness of the resazurin assay in terms of investigating cell viability and establish it is a fitting assay for this investigation.

3.3 Methods

3.3.1. *Optimisation of SK-OV-3 Cell Number*

3.3.1.1. 100µg/ml *N.nig* Venom

3.3.1.1.1. Method

Amongst the literature, investigations involving the SK-OV-3 cell line and cell viability assays showed that a cell density ranging from 10^4 to 10^5 were used (Attar, *et al*., 2017, Chan, *et al*., 2003). It was the interest of this experiment to test a range of cell densities relevant to the literature available. 4 cell densities consisting of $2x10^5$, $1x10^5$, $5x10^4$ and $2.5x10^4$ number of cells were therefore explored.

100µg/ml *N.nig* venom (diluted from a stock concentration using PBS) was initially used as the positive control and PBS dedicated to the negative control. As illustrated in Table 3.1, the highest cell density was plated at the top with decreasing densities down the plate. Each cell number had 12 replicates which were divided into 6 positive, and 6 negative repeats. Following standard procedure explained in Section 2.2, cells were plated on day 1 whilst the venom and resazurin was applied on day 2. The fluorescence of the plate was then measured every 15 min. for 1 hour followed by every 30 min. for the following 4 hours.

Table 3.1. Plate layout for optimisation of cell number. Rows A, C, E and G were the positive controls and therefore had 50µl of the 100µg/ml *N.nig* venom applied. Rows B, D, F and H were the negative controls and therefore had 50µl of PBS applied.

	1	2	3	4	5	6	7	8	9	10	11	12
A	$2x10^5$	$2x10^5$	$2x10^5$	$2x10^5$	$2x10^5$	$2x10^5$						
B	$2x10^5$	$2x10^5$	$2x10^5$	$2x10^5$	$2x10^5$	$2x10^5$						
C	$1x10^5$	$1x10^5$	$1x10^5$	$1x10^5$	$1x10^5$	$1x10^5$						
D	$1x10^5$	$1x10^5$	$1x10^5$	$1x10^5$	$1x10^5$	$1x10^5$						
E	$5x10^4$	$5x10^4$	$5x10^4$	$5x10^4$	$5x10^4$	$5x10^4$						
F	$5x10^4$	$5x10^4$	$5x10^4$	$5x10^4$	$5x10^4$	$5x10^4$						
G	$2.5x10^4$	$2.5x10^4$	$2.5x10^4$	$2.5x10^4$	$2.5x10^4$	$2.5x10^4$						
H	$2.5x10^4$	$2.5x10^4$	$2.5x10^4$	$2.5x10^4$	$2.5x10^4$	$2.5x10^4$						

To analyse the data, an average of the fluorescence at each time point for the cell numbers including the positive and negative control were taken. A fold change at each time point was then calculated by dividing the average negative control by the average positive control. The graph of window (y-axis) against time point (x-axis) was then plotted for each cell number. As previously stated, the larger the window the greater the difference is between the positive and negative controls.

3.3.1.1.2. Results and Discussion

From the results, illustrated in Figure 3.1, it is clear that the 100µg/ml *N.nig* venom used did not prevent cell metabolism at the two highest cell densities ($2x10^5$ and $1x10^5$). This is evident as the window for both cell densities does not reach above 2 suggesting there is a small difference between the positive and negative control. The highest window is achieved by the smallest cell density of $2.5x10^4$ which reaches a window of 14 after 300 min. Unfortunately, the fold change produced by the cell numbers using 100µg/ml crude *N.nig* venom suggests a measurable signal would not be produced. Although $2.5x10^4$ produces the greatest window overtime, this is not achieved until 5 hours which is not an ideal length of time to read the plate. Due to such reasons, no cell density could be considered as 'optimal' and therefore the experiment needed repeating.

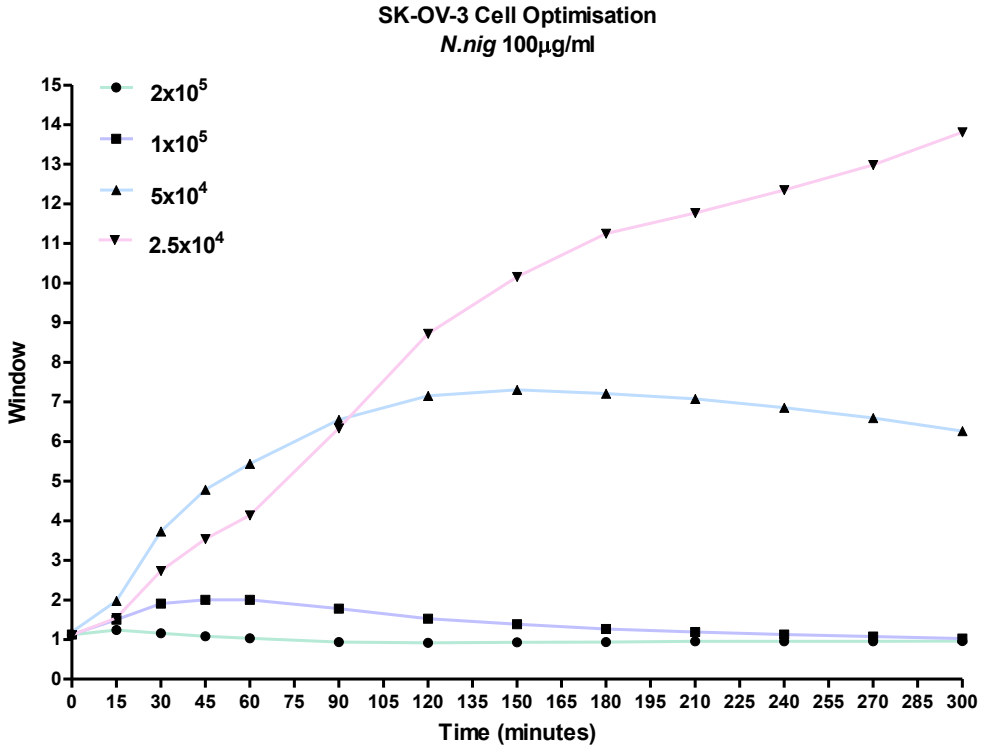

Figure 3.1. The processed data of the SK-OV-3 cell number optimisation assay using 100µg/ml *N.nig* venom (positive control) and PBS (negative control). The graph illustrates the fold change between the positive and negative control over a 5 hour period for the cell densities $2x10^5$, $1x10^5$, $5x10^4$ and $2.5x10^4$.

3.3.1.2. Investigating Higher Concentrations of Venom for the Positive Control – 200µg/ml and 500µg/ml *N.nig* Venom

3.3.1.2.1. Method

Following the previous results, the experiment was repeated with the same intention of finding the optimal cell density of SK-OV-3. As previously described, 100µg/ml *N.nig* venom did not prevent cell metabolism, therefore the concentration of venom used was increased by 2- and 5-fold to ensure cell metabolism across all cell densities were reduced. The same cell densities used in the previous assay were investigated as explained in Section 3.3.1.1. This time the plate was separated into 2 distinct sections, the left side dedicated to 200µg/ml and the right side dedicated to 500µg/ml *N.nig* venom.

As illustrated in Table 3.2, cell densities were plated from highest to lowest down the plate. Each cell density had 10 replicates (for each venom concentration) which were divided into 5 positive controls and 5 negative controls. Following standard procedure, cells were plated on day 1 whilst the venom and resazurin were applied on day 2. The fluorescence of the plate was then measured every 15 min. for 1 hour followed by every 30 min. for the following 4 hours.

Table 3.2. Plate layout for optimisation of cell number. Rows A, C, E and G were the positive controls and therefore had 50µl of either 200µg/ml *N.nig* venom or 500µg/ml *N.nig* venom applied. Rows B, D, F and H were the negative controls and therefore had 50µl of PBS applied. Columns 6 and 7 have been removed from the plate layout illustrated as they remained empty throughout the assay.

	200µg/ml					**500µg/ml**				
	1	2	3	4	5	8	9	10	11	12
A	$2x10^5$	$2x10^5$	$2x10^5$	$2x10^5$	$2x10^5$	$2x10^5$	$2x10^5$	$2x10^5$	$2x10^5$	$2x10^5$
B	$2x10^5$	$2x10^5$	$2x10^5$	$2x10^5$	$2x10^5$	$2x10^5$	$2x10^5$	$2x10^5$	$2x10^5$	$2x10^5$
C	$1x10^5$	$1x10^5$	$1x10^5$	$1x10^5$	$1x10^5$	$1x10^5$	$1x10^5$	$1x10^5$	$1x10^5$	$1x10^5$
D	$1x10^5$	$1x10^5$	$1x10^5$	$1x10^5$	$1x10^5$	$1x10^5$	$1x10^5$	$1x10^5$	$1x10^5$	$1x10^5$
E	$5x10^4$	$5x10^4$	$5x10^4$	$5x10^4$	$5x10^4$	$5x10^4$	$5x10^4$	$5x10^4$	$5x10^4$	$5x10^4$
F	$5x10^4$	$5x10^4$	$5x10^4$	$5x10^4$	$5x10^4$	$5x10^4$	$5x10^4$	$5x10^4$	$5x10^4$	$5x10^4$
G	$2.5x10^4$	$2.5x10^4$	$2.5x10^4$	$2.5x10^4$	$2.5x10^4$	$2.5x10^4$	$2.5x10^4$	$2.5x10^4$	$2.5x10^4$	$2.5x10^4$
H	$2.5x10^4$	$2.5x10^4$	$2.5x10^4$	$2.5x10^4$	$2.5x10^4$	$2.5x10^4$	$2.5x10^4$	$2.5x10^4$	$2.5x10^4$	$2.5x10^4$

500µg/ml:

Data was processed as described in the previous cell number optimisation assay. As illustrated in Figure 3.2, it is clear that the *N.nig* venom at a concentration of 500µg/ml reduced cell metabolism as the window between the positive and negative controls across all cell densities were marginally greater in comparison to the previous assay. $2x10^5$ achieved the greatest window of 28.44 at 60 min. before gradually decreasing. $1x10^5$ achieved a maximum window of 25.98 at 120 min before gradually decreasing, however, $1x10^5$ attained the greatest window until 210 min. $5x10^4$ and $2.5x10^4$ also have improved fold changes reaching a window in the high teens after 120 min. and 210 min. respectively, in addition $5x10^4$ after 240 min. achieved the greatest window.

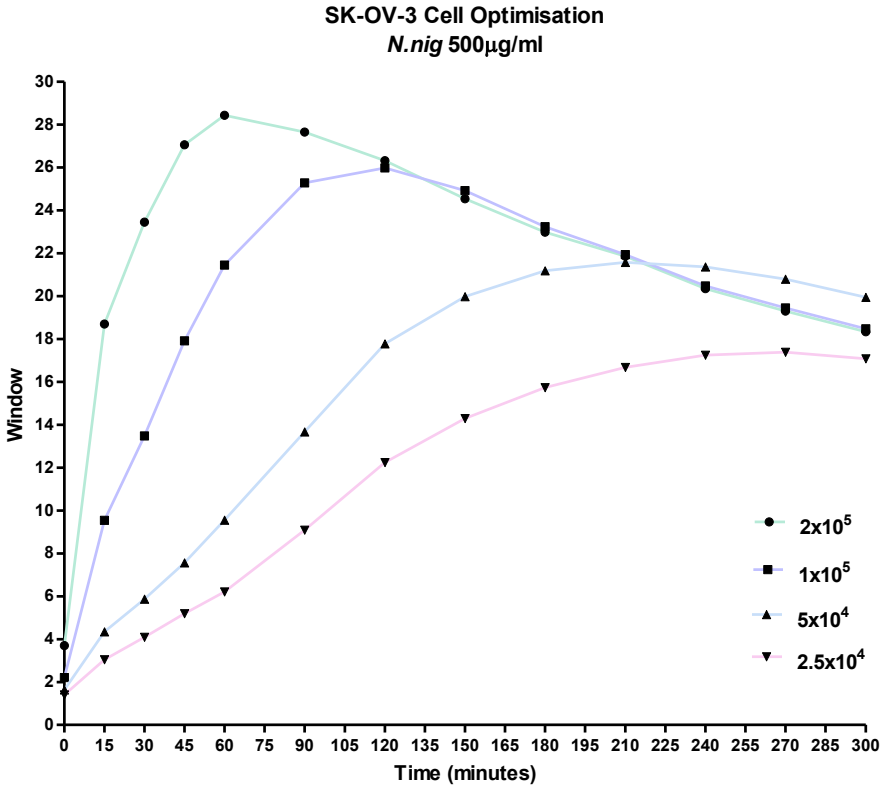

Figure 3.2. The processed data of the SK-OV-3 cell number optimisation assay using 500µg/ml *N.nig* venom (positive control) and PBS (negative control). The graph illustrates the fold change between the positive and negative control over a 5 hour period for the cell densities $2x10^5$, $1x10^5$, $5x10^4$ and $2.5x10^4$.

200µg/ml:

As illustrated in Figure 3.3, 200µg/ml *N.nig* venom also reduced cell metabolism across all cell densities. Parallel to the previous assay, the greatest window is achieved by $2x10^5$ reaching 27.88 after 90 min. before gradually decreasing for the duration of the assay. Once again, $1x10^5$ reaches a maximum window of 27.09 at 120 min. which is the greatest window at that time point. This cell density continues to have the greatest window until 240 min. whereby $5x10^4$ takes over. Both $5x10^4$ and $2.5x10^4$ achieve a more gradual increase in window overtime in a similar way when dosing the cells with 500µg/ml reaching maximum windows of 22.14 after 240 min. and 20.83 after 270 min. respectively.

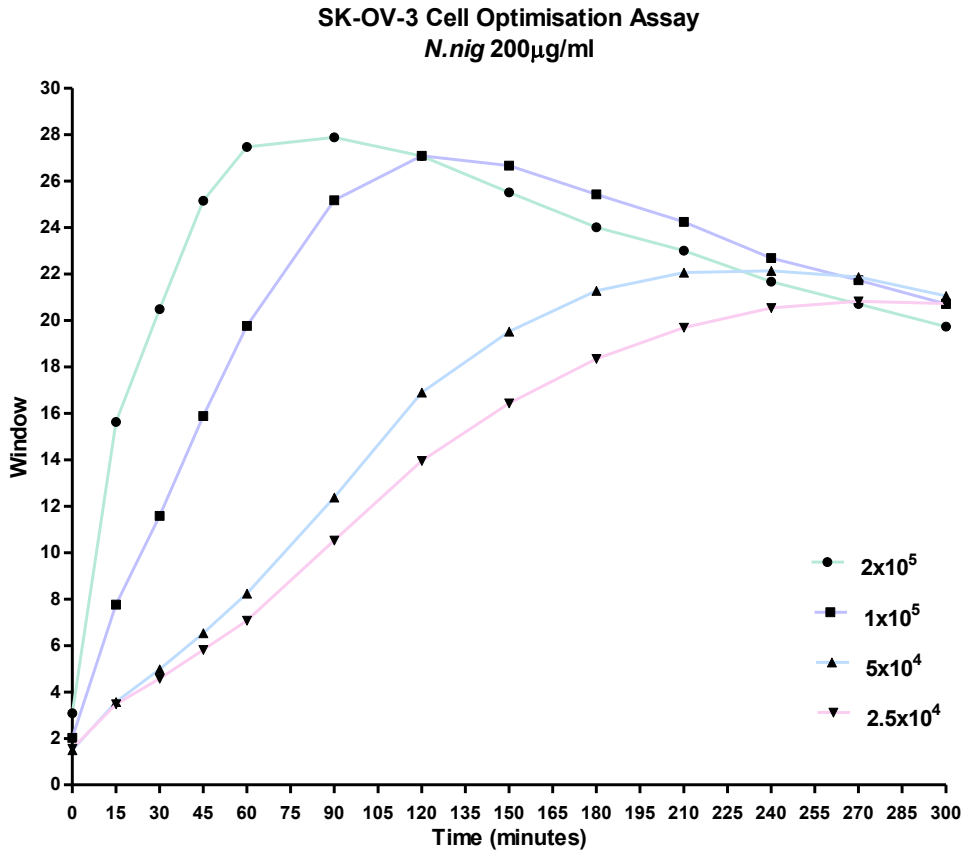

Figure 3.3. The processed data of the SK-OV-3 cell number optimisation assay using 200µg/ml *N.nig* venom (positive control) and PBS (negative control). The graph illustrates the fold change between the positive and negative control over a 5 hour period for the cell densities $2x10^5$, $1x10^5$, $5x10^4$ and $2.5x10^4$.

As mentioned, $2x10^5$ and $1x10^5$ number of cells presented the greatest fold changes over time, however, $1x10^5$ number of cells presented a more gradual increase in window whereas $2x10^5$ number of cells contributed a much sharper increase; this means subtle changes in the test assays could potentially be missed using the higher cell number due to the sharp increase. Furthermore, by using the cell density of $1x10^5$ relative to $2x10^5$ less flasks would be required to perform the assay and by extension a shorter time period of growth is required to prepare the cells. With the most compelling argument, it was decided that the optimal cell density to move forward with was $1x10^5$.

When considering the optimal cell density, the greatest window achieved, the time taken to reach that window, the venom concentration utilised and number of flasks required were considered. Firstly, both concentrations investigated in this assay reduced cell metabolism across all densities. As less venom from the stock concentration was required to make the working concentration of 200µg/ml, it was logical to focus on this concentration ensuring venom stocks were not wasted, therefore the fold change results associated with 200µg/ml were further analysed in deciding the optimal cell number. As explained, $2x10^5$ produced the greatest window relative to the other cell densities, however this window is achieved rather rapidly with a sharp increase in window in only 45-90 min. where the cell density peaks and gradually decreases. As there is such a rapid increase, subtle results produced in test assays could potentially be missed due to the sharp increase. On the other hand, $1x10^5$ represented a more gradual increase in window overtime and achieved the greatest window after 120 min. to 240 min. whereby $5x10^4$ seized the maximum window. As $1x10^5$ represents a more steady increase subtle changes in test assay are more likely to be witnessed, furthermore, using this cell number required the cultivation of less flasks which again prevents wasting materials. Although, as mentioned, $5x10^4$ attains the maximum window after 240 min. this is not an ideal time to read the plate whereas 120 min. is a more reasonable time to analyse the assay. In summary, with the reasons listed here the most compelling, optimal cell density is $1x10^5$ number of cells and was therefore utilised in subsequent assays. In regards to current research in association with SK-OV-3 and resazurin based assays, cell densities used range from $5x10^4$ to $4x10^5$ which are fitting with the optimal cell density identified here (Jiang, *et al*., 2009, Chan, *et al*., 2003).

3.3.2. Z' Assay for the Optimal Cell Number

3.3.2.1. Method

The Z' assay was utilised to generate a Z-factor for the previous optimal cell density assay to demonstrate the robustness of using $1x10^5$ cells in the subsequent assays. On day 1, $1x10^5$ cells were plated across all 96 wells on the plate. The following day the plate was divided into 4 quadrants as described in Section 2.3; 2 quadrants were dedicated to the positive control, 200µg/ml *N.nig* venom, whilst the other 2 quadrants were dedicated to the negative control, PBS. This layout is illustrated in Table 3.3. The plate was analysed following standard protocol (Section 2.2.2).

Table 3.3. Plate layout of the Z' assay used to test the robustness of the optimal SK-OV-3 cell number chosen, $1x10^5$. On day 1, $1x10^5$ cells were plated across all 96 wells. On day 2, the plate was split into four quadrants, two dedicated to the positive control and two dedicated to the negative control. Controls were located opposite each other. 50µl of 200µg/ml *N.nig* venom was applied to the positive wells and 50µl of PBS was applied to the negative wells.

	1	2	3	4	5	6	7	8	9	10	11	12
A	+	+	+	+	+	+	-	-	-	-	-	-
B	+	+	+	+	+	+	-	-	-	-	-	-
C	+	+	+	+	+	+	-	-	-	-	-	-
D	+	+	+	+	+	+	-	-	-	-	-	-
E	-	-	-	-	-	-	+	+	+	+	+	+
F	-	-	-	-	-	-	+	+	+	+	+	+
G	-	-	-	-	-	-	+	+	+	+	+	+
H	-	-	-	-	-	-	+	+	+	+	+	+

3.3.2.2. Results and Discussion

From the raw data collected, the fold change was processed first (as described in Section 3.3.1.1.1) to determine the window between the positive and negative controls and to also ensure this assay was in agreement with the previous optimal cell density assay. From Figure 3.4, it is clear that the results are consistent with those of the previous assay in Section 3.3.1.2.2. This agreement is displayed with the gradual increase in fold change overtime reaching a window of 26 after 120 min. whereby the fold change begins to steadily decrease.

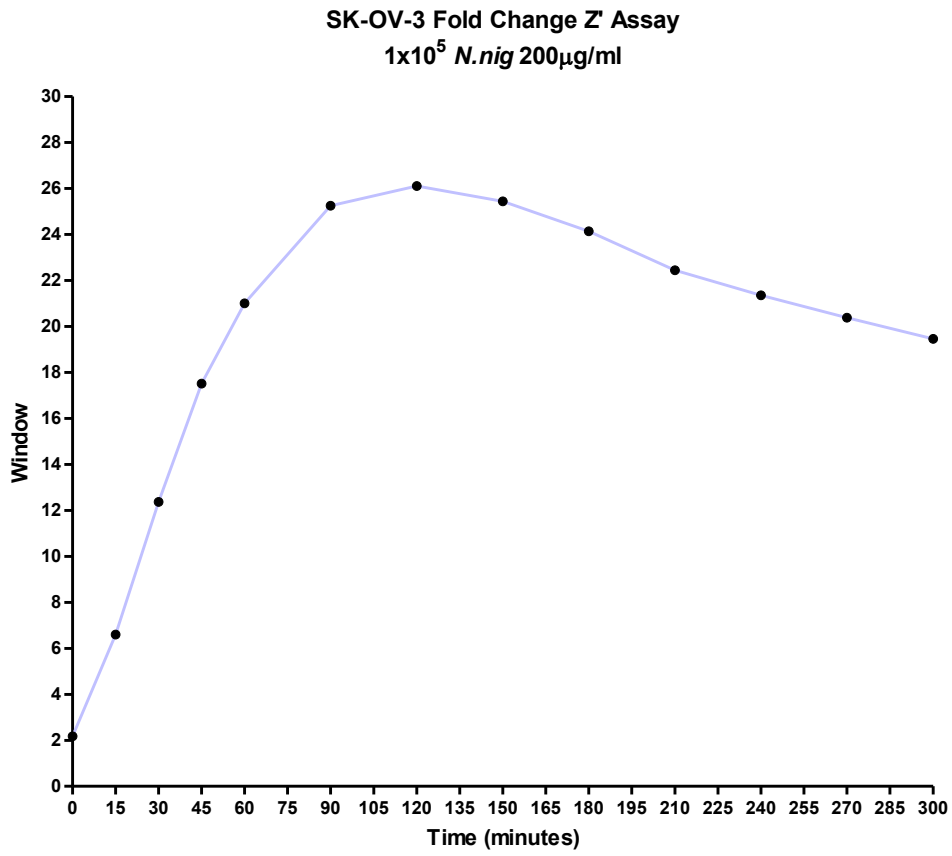

Figure 3.4. The processed data of the Z' Assay for the optimal SK-OV-3 cell number 1x10^5. The graph illustrates the fold change between the positive control (200µg/ml *N.nig* venom) and the negative control (PBS) over a 5 hour period.

Ensuing this, the Z-factor was calculated. The Z-factor is defined in terms of the means (µ) and standard deviations (σ) of the positive (p) and negative (n) controls and is calculated using the following equation:

$$Zfactor = 1 - \frac{3(\sigma p + \sigma n)}{|\mu p - \mu n|}$$

An average of the positive and negative controls were taken at each time point, thus a Z-factor at each time point was calculated. From this a graph of Z-factor (y-axis) against time (x-axis) was plotted as exemplified in Figure 3.5. As confirmed, a Z-factor between 0.5-1 indicates an excellent assay and is therefore considered as robust. A Z-factor below 0.5 (marginal assay) or 0 (poor assay) implies the assay is not robust (Doherty, et al., 2011). It is therefore promising to see at time point 0 min., the Z-factor is 0.52 as illustrated in Table A.1 in the appendix. The Z-factor continues to increase reaching highs of 0.96 after 150 min. This signifies an excellent assay and suggests the use of 1x10^5 number of cells is robust enough to move forward with. Such results can now be used as a ground work for future research when using the SK-OV-3 cell

number and venom-based compounds in the setting of a resazurin assay as the optimal cell density has been identified.

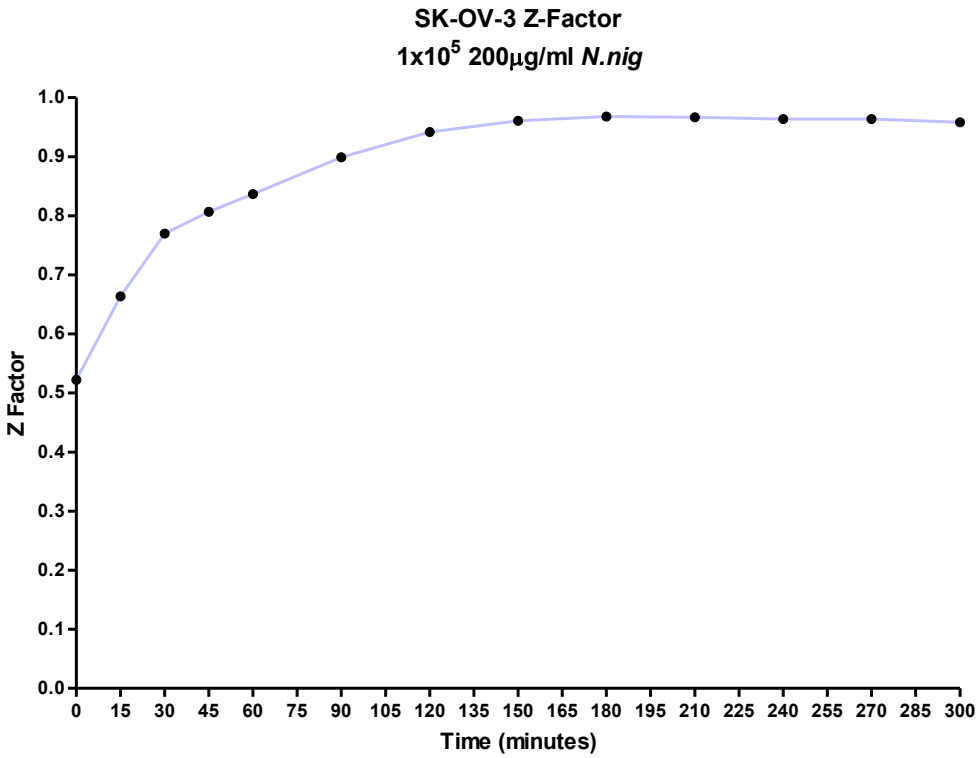

Figure 3.5. The processed data of the Z' Assay for the optimal SK-OV-3 cell number $1x10^5$. The graph illustrates the calculated Z-factor over a 5 hour period.

3.3.3. Dose Response of *N.nig* Venom

3.3.3.1. Method

A DR curve of the *N.nig* venom was produced with the purpose of finding the LD90 (dose required to kill 90% of the population) and thus solidify the positive control utilised for the subsequent assays involving the test compounds. Table 3.4 demonstrates the layout of the assay plate. $1x10^5$ number of SK-OV-3 cells were plated on day 1 and returned to the incubator overnight as per standard protocol established in Section 2.2.

Table 3.4. The layout of the assay plate required for the DR of the *N.nig* venom. Each column had 5 replicates of $1x10^5$ SK-OV-3 cells.

	1	2	3	4	5	6	7	8	9	10	11	12
A	$1x10^5$	$1x10^5$	$1x10^5$	$1x10^5$	$1x10^5$	$1x10^5$	$1x10^5$	$1x10^5$	$1x10^5$	$1x10^5$	$1x10^5$	$1x10^5$
B	$1x10^5$	$1x10^5$	$1x10^5$	$1x10^5$	$1x10^5$	$1x10^5$	$1x10^5$	$1x10^5$	$1x10^5$	$1x10^5$	$1x10^5$	$1x10^5$
C	$1x10^5$	$1x10^5$	$1x10^5$	$1x10^5$	$1x10^5$	$1x10^5$	$1x10^5$	$1x10^5$	$1x10^5$	$1x10^5$	$1x10^5$	$1x10^5$
D	$1x10^5$	$1x10^5$	$1x10^5$	$1x10^5$	$1x10^5$	$1x10^5$	$1x10^5$	$1x10^5$	$1x10^5$	$1x10^5$	$1x10^5$	$1x10^5$
E	$1x10^5$	$1x10^5$	$1x10^5$	$1x10^5$	$1x10^5$	$1x10^5$	$1x10^5$	$1x10^5$	$1x10^5$	$1x10^5$	$1x10^5$	$1x10^5$
F												
G												
H												

The following day a compound plate was constructed to serially dilute the crude *N.nig* venom before the application to the assay plate. To do this, 500µg/ml *N.nig* venom was applied to column 1, rows A,B and C. In columns 2 to 12, rows A,B and C, 120µl of PBS was applied as illustrated in Table 3.5.a. In order to serially dilute the venom by 1:2, 120µl of contents in column 1 were transferred to column 2 and thoroughly mixed. 120µl of the contents in column 2 were then transferred to column 3 and thoroughly mixed. This was repeated across the plate until column 11. A key has been constructed as shown in Table 3.5.b which specifies the concentration in each column after the serial dilution.

Table 3.5.a. A colour coded layout of the compound plate used to serial dilute the *N.nig* venom. Column 1 contained 240µl of 500µg/ml and columns 2 to 12 contained 120µl of PBS. The venom was then serially diluted by 1:2 across the plate until column 11; column 12 was dedicated to the negative control containing PBS only. Definitively, columns 1 to 10, and 12 (row a, b and c) contained a final volume of 120µl, whilst column 11 (row a, b and c) contained a final volume of 240µl.

	1	2	3	4	5	6	7	8	9	10	11	12
A												
B												
C												
D												
E												
F												
G												
H												

Table 3.5.b. A colour coded key corresponding to the concentration of *N.nig* venom in each column. Starting at 500µg/ml in column 1 and diluting by half each time reaching the lowest concentration of 0.488µg/ml in column 11. The negative control was PBS, therefore only PBS was allocated to column 12.

KEY	
	500.00µg/ml
	250.00µg/ml
	125.00µg/ml
	62.50µg/ml
	31.25µg/ml
	15.63µg/ml
	7.81µg/ml
	3.91µg/ml
	1.95µg/ml
	0.98µg/ml
	0.49µg/ml
	Cells and PBS only

Upon completing the compound plate, the media was removed from the assay plate and replaced with 50µl of the contents in the corresponding wells of the compound plate i.e. contents of column 1 of compound plate into column 1 of assay plate. As established in the key, column 12 was allocated as the negative control, therefore 50µl of PBS was applied to cells in the column. The assay plate was then returned to the incubator for 2 hours before the application of 160µM resazurin and the plate fluorescence was measured following standard procedure in Section 2.2.2.

The data was collated and processed to produce a DR curve; from this curve the LD90 of the *N.nig* could be deduced. A DR curve is a plot of the percent inhibition (y-axis) against the Log10 of the chemical concentration (x-axis). Firstly, an average of the fluorescence for each concentration across all time points was taken as well as the Log10 of the concentration. From this, the percentage of growth was calculated using the equation: $\%Growth = \left(\frac{F}{MF}\right) x\ 100$ whereby 'F' is the fluorescence of the concentration of interest (i.e. the average fluorescence at 500µg/ml) and 'MF' is the maximum fluorescence (i.e. the average of the negative control, PBS). Once the percentage of growth was calculated, the percentage of inhibition could be considered. This was done by using the equation: $\%Inhibition = 100 - \%Growth.$ The DR curve was then plotted with Log10 of the concentration on the x-axis and percent of inhibition on the y-axis with a line of best fit. From the y-axis, a horizontal straight line can be inserted from 90% inhibition to the line of best fit which can then be extended by a vertical line to the x-axis to find the Log10 of the concentration which causes 90% inhibition. Taking the exponential

of the Log10 concentration required to cause 90% inhibition then calculates the actual concentration of the *N.nig* venom in µg/ml.

3.3.3.2. Results and Discussion

Once the raw data was processed the graph, illustrated in Figure 3.6, was constructed as explained in the previous section. Using the line of best fit, the concentration required to inhibit 90% of cell metabolism was determined. In this case, at 90% inhibition, the log10 concentration of *N.nig* venom was 1.42, therefore $10^{1.42}$ resulted in 26.92μg/ml and is the calculated LD90. To test the robustness of this value and solidify the optimised positive control for the forthcoming venom assays, a Z-factor was analysed to statistically confirm the positive control.

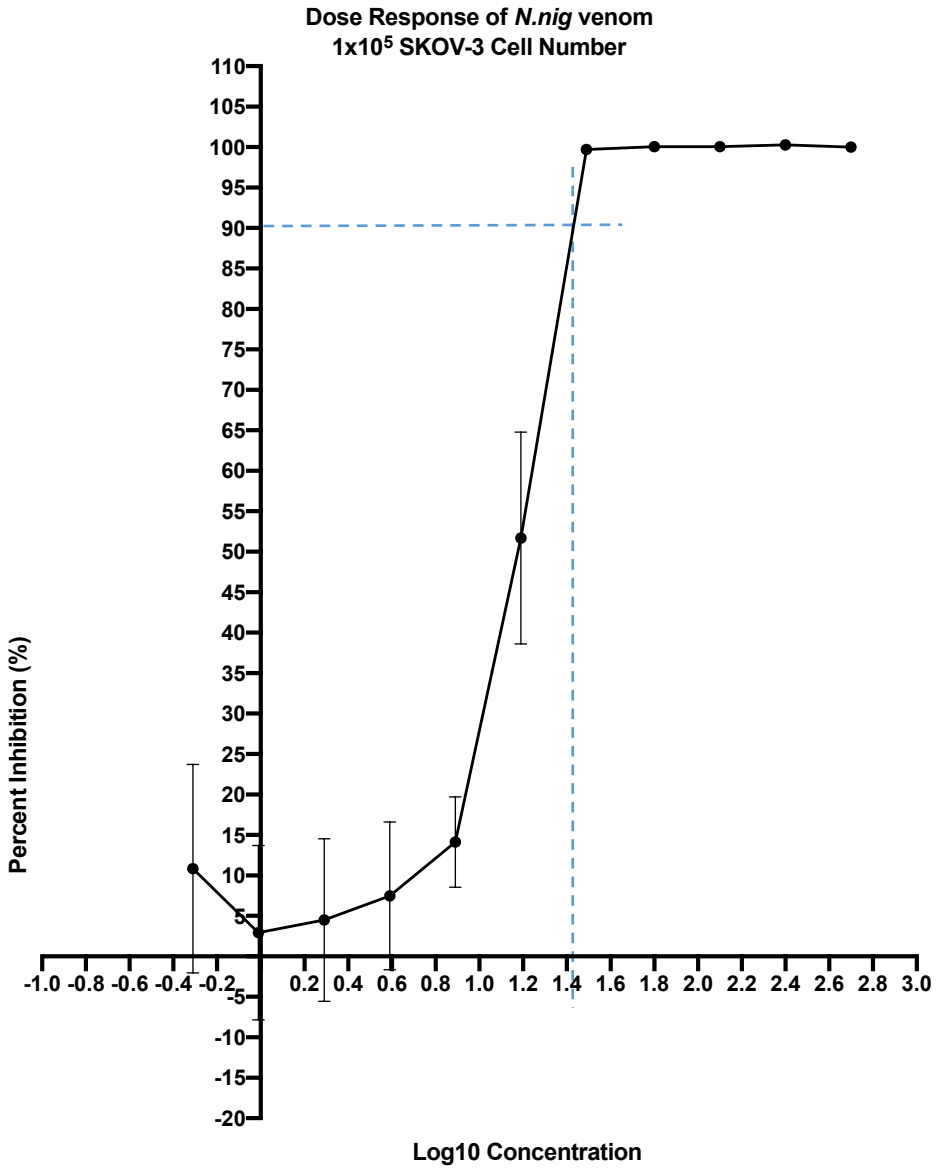

Figure 3.6. The DR curve produced for the *N.nig* venom to find the LD90. Raw data was processed and averaged over a 5 hour period.

Moreover, this experiment clarified a batch variation issue in relation to the first vial of *N.nig* crude venom used in Section 3.3.1.1. From the results of that experiment, it was clear that the *N.nig* venom at 100μg/ml did not reduce cell metabolism. This prompted the increase in venom concentration in the second cell density optimisation assay in Section 3.3.1.2 to 200μg/ml and 500μg/ml. This conceivably suggests that the initial batch of venom used was not as active as the subsequent batches. The most probable cause for this batch variation could be due to the number of freeze-thaw cycles. Morrison *et al* 1983, identified that 10 freeze-thaw cycles of *Tropidechis carinatus* (elapid) venom resulted in a loss of activity by 9% (Morrison, *et al.*, 1983) whilst Bloom *et al* 1998, acknowledged that *Chironex fleckeri* (box jellyfish) venom lost activity after 2 freeze-thaw cycles (Bloom, *et al.*, 1998).

To reiterate, results expressed here set the foundation for forthcoming assays in the present work carried out and for future investigation. Resazurin based assays utilising the SK-OV-3 cell line and investigating the cytotoxic effects of venom can ultimately refer to optimisation processes and results outlined here to obtain not only the optimal cell density but also the positive control.

3.3.4. Z' Assay for the LD90 of *N.nig* venom

3.3.4.1. Method

Similar to the previous Z' assay, the experiment was utilised to calculate the Z-factor and determine whether the LD90 of *N.nig* venom was robust enough to move forward with as the positive control. As per the standard protocol (Section 2.2.1), $1x10^5$ number of SK-OV-3 cells were plated across the 96 well plate on day 1 and returned to the incubator. On day 2, all contents from the wells were removed and the plate was divided into 4 quadrants; 2 dedicated to PBS only (negative control) and 2 dedicated to 26.92μg/ml *N.nig* venom as shown Table 3.6. Matching controls were diagonally opposite one another to avoid the edge effect. Once the controls were applied to the cells, the plate was returned to the incubator for 2 hours. Proceeding this, all contents were removed once again before the application of 160μM resazurin and the plate was analysed using the plate reader following standard protocol (Section 2.2.2).

Table 3.6. 1x10^5 number of cells were plated across the 96 well plate on day 1. The following day the controls were applied, 50μl of PBS as the negative control, and 50μl of 26.92μg/ml *N.nig* venom as the positive control.

	1	2	3	4	5	6	7	8	9	10	11	12
A	+	+	+	+	+	+	-	-	-	-	-	-
B	+	+	+	+	+	+	-	-	-	-	-	-
C	+	+	+	+	+	+	-	-	-	-	-	-
D	+	+	+	+	+	+	-	-	-	-	-	-
E	-	-	-	-	-	-	+	+	+	+	+	+
F	-	-	-	-	-	-	+	+	+	+	+	+
G	-	-	-	-	-	-	+	+	+	+	+	+
H	-	-	-	-	-	-	+	+	+	+	+	+

The fold change of the cell number was processed first to establish that there was a great enough window between the positive and negative control. Figure 3.7 demonstrates that the fold change followed a similar pattern to the previous assay in Section 3.3.2. There is a steady increase in window which reached highs of 19.9 after 120 min. before gradually decreasing.

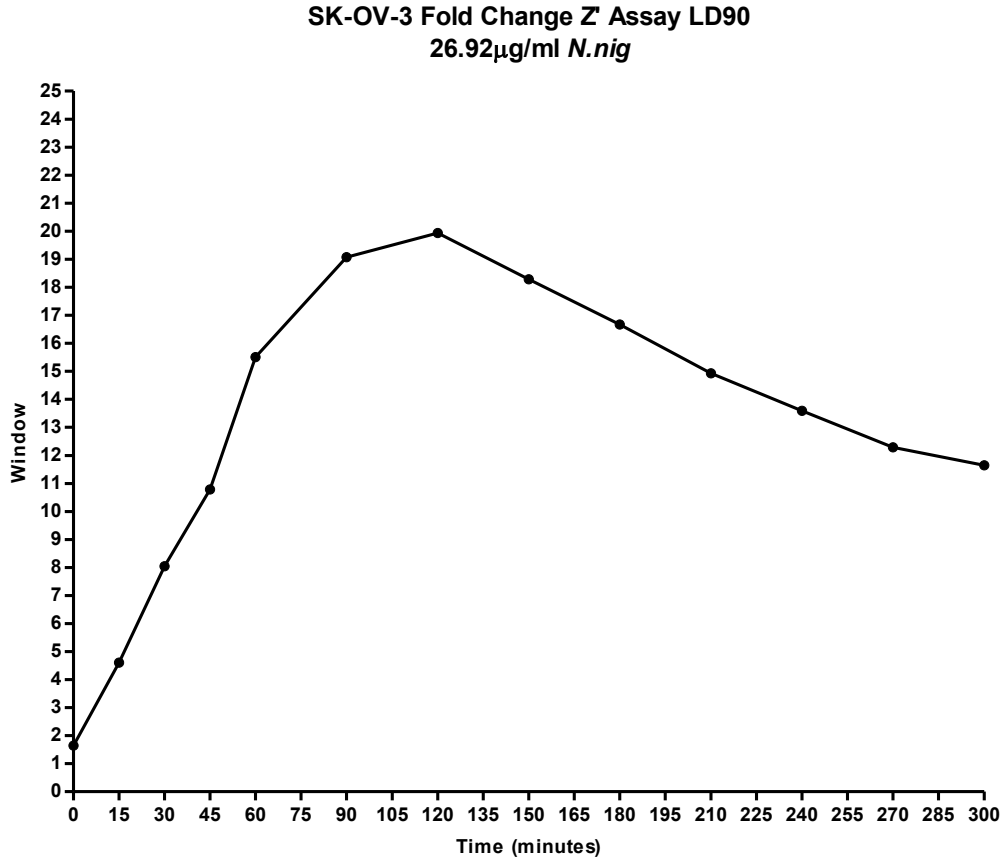

Figure 3.7. The processed data of the Z' assay 4.0 for the LD90 of *N.nig* crude venom. The graph illustrates the fold change between the positive control (26.92µg/ml *N.nig* venom) and the negative control (PBS) over a 5 hour period.

Following this, the Z-factor was calculated using the equation expressed in Section 3.3.2.2 and articulated in graphical form. Referring to Figure 3.8, it is clear that the LD90 selected as the positive control was robust; after 15 min. a Z-factor of 0.61 was achieved which continued to increase up until 0.91 at time point 120 min. before gradually decreasing. This indicates an excellent assay solidifying the positive control. In addition to this, the data also reveals that the optimal time to read the fluorescence of the plate is 120 min as this produced the greatest Z-factor.

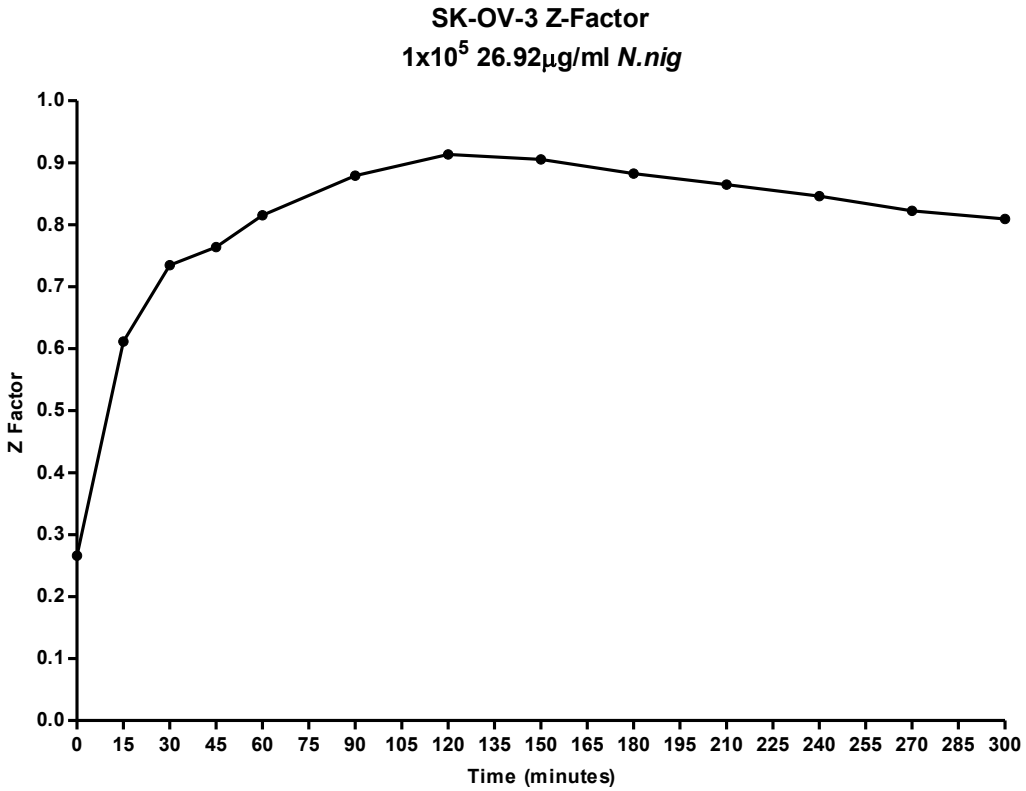

Figure 3.8. The processed data of the Z' assay for the LD90 of *N.nig* crude venom. The graph illustrates the calculated Z-factor over a 5 hour period.

Although the results here illustrate that the assay was robust, this was not the first Z' assay utilised, instead this was the fourth attempt. The Z-factor results of the first Z' assay is illustrated in Figure A.1 in the appendix. Results illustrate that over a 5 hour period, a Z-factor above 0.5 is not achieved rendering the assay as a poor assay and not robust. However, upon analysing the raw data illustrated in Figure A.2, the positive control demonstrated a great deal of variation. Due to this variation the calculated means of the positive and negative control were too similar reducing the separation window causing the positive and negative controls to overlap thus producing a low Z-factor score (GraphPad, 2010).

The Z' assay was repeated a second time, this time a full 96 well plate was used increasing the number of replicates (as opposed to Z' assay 1.0 which used 64 wells only). Furthermore, to overcome variation in the negative control, cells were pipetted up and down multiple times in the reservoir before being aliquoted into the wells; this was done to reduce cellular clumps. If cells were clumped together when plating occurred, there would be more than $1x10^5$ number of cells in the well therefore the surplus SK-OV-3 cells not inhibited by the venom can reduce resazurin thus explaining one cause of the variation. Although Z-factor results improved, as illustrated in Figure A.3, a Z-factor above 0.5 was only achieved between 30 and 90 min before returning to a poor assay. Investigating the raw data, illustrated in Figure A.4, there was still

variation within the negative control which by extension calculated means for the positive and negative control which were too similar thus resulting in a low Z-factor.

The Z' assay was carried out for a third attempt. This time the venom and resazurin were both pipetted up and down before application to the cells as well as pipetting the cells up and down. This was done to ensure the protein composition in the venom was evenly dispersed amongst the cells. This ensured inhibitory capabilities of the venom were evenly dispersed as well as certifying uniform levels of resazurin were applied to the cells allowing for similar reduction rates of resazurin to occur. The results of the Z-factor produced from the third assay are illustrated in Figure A.5. Over the 5 hour period, a Z-factor above 0 was not achieved, once again signifying the assay as poor and not robust. This time the raw data, exemplified in Figure A.6, demonstrated that there were 7 wells amongst the negative control which produced a great deal of variation suggesting less metabolism was occurring in these wells compared to the positive control. As the Z-factor is sensitive to the variability in the positive and negative control, a Z-factor above 0.5 was not achieved (Boveia, *et al*., 2009). A possibility as to why this occurred could be due to adhesion of the plate not being as strong resulting in cells being removed when discarding media and venom; however, this was ultimately unexplained during the time of the investigation, therefore a fourth Z' assay was carried which produced a Z-factor above 0.5 for the duration of the assay and therefore considering 26.92µg/ml as a robust positive control.

Alongside determining the Z-factor for the LD90 of *N.nig* venom (as established in Section 3.3.3), GraphPad Prism 5 was also utilised to statistically confirm the LD90 of the venom. Using nonlinear regression analysis, dose-response special of Find ECanything and setting the F constraint to 90%, the LD90 (ECF) was determined as 24.13µg/ml, as illustrated in Table A.2. Unfortunately, this was not done until after utilising test compounds, however the Z-factor produced identified that 26.92µg/ml *N.nig* venom was an acceptable and robust LD90. Therefore, to remain consistent throughout experiments, 26.92µg/ml *N.nig* was set as the positive control.

INVESTIGATING THE EFFECTS OF ANIMAL VENOMS IN OVARIAN CANCER

CHAPTER FOUR – OPTIMISED VENOM ASSAYS

4.1. Aims

After optimising the parameters for the resazurin assay, the test compounds were introduced. Such compounds included venoms from a variety of species both crude and fractioned using high pressure liquid chromatography (HPLC). Crude venom of *Parabuthus transvaalicus* (*P.tra – scorpion*), *Heterometrus madraspatensis* (*H.mad – scorpion*) and *Heterometrus mysorensis* (*H.mye - scoprion*) were exploited. Fractioned venom comprised of *N.nig*, *Agkistrodon contortrix pictigaster* (*A.cpi* – viper snake), *Poecilotheria regalis* (*P.reg* – spider) and *Pandinus cavimanus* (*P.cav* – scorpion). The venom was then utilised in the setting of a DR assay which determined if a certain venom significantly reduced SK-OV-3 cell metabolism and to what extent metabolism was reduced (in terms of percent inhibition). An arbitrary threshold was considered throughout the assays and employed to determine if the venom was of significance; if the venom inhibited 50% or more of cell metabolism, this would be considered as significant. Venoms of significance were then utilised further, this involved fractioning the venom to further analyse any significant proteins or peptides present which could then have the potential to be analysed further using mass spectrometry.

4.2 Background

A DR describes the way in which an organism responds to certain levels of exposure from a specific compound. In terms of drug development, a DR is an appropriate way of characterising 'hit' compounds which affect an organism in a desired way (Blass, 2015). Moreover, DR relationships are important in assessing the efficacy and potency of drugs, whilst also a useful tool for the interpretation of drug and receptor interactions (Campbell & Cohall, 2017). In terms of this project, the DR was utilised to identify which venoms inhibited cell metabolism of SK-OV-3 cells. Through dosing the cells with a serial dilution of the venom and developing the DR curve, it is possible to eliminate venoms which do not reduce cell metabolism and identify venoms which successfully inhibit the cell metabolism. As previously touched upon, in order to determine whether a venom was of significance, a threshold of 50% was established, otherwise known as the median lethal dose (LD50). This is the dose required to kill 50% of a population after a specified test duration. As the LD50 is utilised in pharmacology to indicate a substances acute toxicity, it was fitting to use this threshold to categorise significant venoms and their acute

toxicity (Ng, 2004). Furthermore, although arbitrary, the threshold indicates that there is more cell inhibition than metabolism therefore highlighting itself as a logical cut-off.

4.3 Methods

4.3.1. Dose Response of Crude *P.tra* Venom

Using crude *P.tra* venom, a DR was carried out to identify if the venom from this particular scorpion species had a significant effect on the cell metabolism of SK-OV-3 cells as well as detecting the LD50 of the venom.

Following standard procedure in Section 2.2.1, $1x10^5$ number of SK-OV-3 cells were plated on day 1 according to the plate layout established in Table 4.1. The plate was returned to the incubator overnight allowing cells to adhere. A compound plate was set up on the following day as demonstrated in Table 4.2 a-b; this was done to serially dilute the venom and simplify the application of venom to the test plate. Starting at a concentration of 200µg/ml, the venom was serially diluted by 1:2 as utilised in the previous assay illustrated in Section 3.3.3.1. Once the venom was appropriately diluted, the contents from the test plate were replaced by the corresponding contents in compound plate. The test plate was then returned to the incubator for 2 hours before replacing the contents with 160µM resazurin and analysing the plate.

Table 4.1. The layout of the assay plate for the DR of *P.tra* scorpion venom. Each column had 5 replicates of $1x10^5$ SK-OV-3 cells.

	1	2	3	4	5	6	7	8	9	10	11	12
A	$1x10^5$	$1x10^5$	$1x10^5$	$1x10^5$	$1x10^5$	$1x10^5$	$1x10^5$	$1x10^5$	$1x10^5$	$1x10^5$	$1x10^5$	$1x10^5$
B	$1x10^5$	$1x10^5$	$1x10^5$	$1x10^5$	$1x10^5$	$1x10^5$	$1x10^5$	$1x10^5$	$1x10^5$	$1x10^5$	$1x10^5$	$1x10^5$
C	$1x10^5$	$1x10^5$	$1x10^5$	$1x10^5$	$1x10^5$	$1x10^5$	$1x10^5$	$1x10^5$	$1x10^5$	$1x10^5$	$1x10^5$	$1x10^5$
D	$1x10^5$	$1x10^5$	$1x10^5$	$1x10^5$	$1x10^5$	$1x10^5$	$1x10^5$	$1x10^5$	$1x10^5$	$1x10^5$	$1x10^5$	$1x10^5$
E												
F												
G												
H												

Table 4.2.

a. A colour coded layout of the compound plate used to serially dilute the *P.tra* venom. Column 1 contained 240µl of 200µg/ml *P.tra* venom whilst column 2 to 10 contained 120µl of PBS. The venom was then serially diluted by 1:2 across the plate as explained in Section 3.3.3.1. Column 11 was dedicated to the positive control (26.92µg/ml *N.nig* crude venom) and column 12 was dedicated to the negative control (PBS). Definitively, columns 1 to 9, 11 and 12 (row a and b) contained a final volume of 120µl, whilst column 10 (row a and b) contained a final volume of 240µl.

	1	2	3	4	5	6	7	8	9	10	11	12
A												
B												
C												
D												
E												
F												
G												
H												

b. The colour coded key (to Table 4.2.a.) corresponding to the concentration of *P.tra* venom in each column. Starting at 200µg/ml in column 1 and diluting by half each time reaching the lowest concentration of 0.391µg/ml in column 10. The positive and negative control are situated in column 11 and 12.

KEY	
	200.00µg/ml
	100.00µg/ml
	50.00µg/ml
	25.00µg/ml
	12.50µg/ml
	6.25µg/ml
	3.13µg/ml
	1.56µg/ml
	0.78µg/ml
	0.39µg/ml
	N.nig 26.92µg/ml
	Cells and PBS only

Results for the DR were processed at time point 120 min. in accordance to the Z' assay results in Section 3.3.4.2. The data was processed as demonstrated in Section 3.3.3.1 and a graph of percent inhibition (y-axis) against Log10 of the concentration (x-axis) was constructed.

4.3.2. Dose Response of Crude *H.mad* and *H.mye* Venom

With a similar aim to the previous assay, a DR was utilised to identify if the crude venom from *H.mad* and *H.mye* significantly reduced cell metabolism of the SK-OV-3 cell line as well as determining the LD50. The results from the previous DR illustrated that the scorpion venom was not potent enough at 200μg/ml and therefore did not completely prevent cell metabolism of the SK-OV-3 cell line. Due to this, the highest venom concentrations of both *H.mad* and H.mye were increased to 500μg/ml; this was done in the hope that the previous results were not repeated and a 100% inhibition rate was reached.

Once again, cells were plated on day 1; $1x10^5$ number of SK-OV-3 cells were applied to the 96 well plate according to the plate layout in Table 4.3. The plate was then returned to the incubator overnight allowing the cells to adhere. Again, to set up the serial dilution and to simplify the application of venom to the test plate, a compound plate was employed. One compound plate was used to dilute both venoms; 2 rows were dedicated to *H.mad* and 2 rows were dedicated to *H.mye*. Both venoms started at a concentration of 500μg/ml which was serially diluted by 1:2 across the plate as represented in Table 4.4 a-b. When the compound plate was complete, the contents from the test plate were removed and replaced with the corresponding contents in the compound plate. The test plate was then returned to the incubator for 2 hours before applying the resazurin and analysing the plate as per Section 2.2.2.

Table 4.3. The plate layout for the DR of *H.mad* and *H.mye* venom. Rows A, B, C and D were dedicated to the *H.mad* venom whilst rows E, F, G and H were dedicated to the *H.mye* venom. Both venoms at each concentration had 4 replicates. The positive and negative controls were situated in columns 11 and 12 respectively.

	1	2	3	4	5	6	7	8	9	10	11	12
A	$1x10^5$	$1x10^5$	$1x10^5$	$1x10^5$	$1x10^5$	$1x10^5$	$1x10^5$	$1x10^5$	$1x10^5$	$1x10^5$	$1x10^5$	$1x10^5$
B	$1x10^5$	$1x10^5$	$1x10^5$	$1x10^5$	$1x10^5$	$1x10^5$	$1x10^5$	$1x10^5$	$1x10^5$	$1x10^5$	$1x10^5$	$1x10^5$
C	$1x10^5$	$1x10^5$	$1x10^5$	$1x10^5$	$1x10^5$	$1x10^5$	$1x10^5$	$1x10^5$	$1x10^5$	$1x10^5$	$1x10^5$	$1x10^5$
D	$1x10^5$	$1x10^5$	$1x10^5$	$1x10^5$	$1x10^5$	$1x10^5$	$1x10^5$	$1x10^5$	$1x10^5$	$1x10^5$	$1x10^5$	$1x10^5$
E	$1x10^5$	$1x10^5$	$1x10^5$	$1x10^5$	$1x10^5$	$1x10^5$	$1x10^5$	$1x10^5$	$1x10^5$	$1x10^5$		
F	$1x10^5$	$1x10^5$	$1x10^5$	$1x10^5$	$1x10^5$	$1x10^5$	$1x10^5$	$1x10^5$	$1x10^5$	$1x10^5$		
G	$1x10^5$	$1x10^5$	$1x10^5$	$1x10^5$	$1x10^5$	$1x10^5$	$1x10^5$	$1x10^5$	$1x10^5$	$1x10^5$		
H	$1x10^5$	$1x10^5$	$1x10^5$	$1x10^5$	$1x10^5$	$1x10^5$	$1x10^5$	$1x10^5$	$1x10^5$	$1x10^5$		

Table 4.4.

a. A colour coded layout of the compound plate used to serially dilute both *H.mad* and *H.mye* venom. Rows A and B were dedicated to *H.mad* whilst rows D and E were dedicated to *H.mye*. Column 1 contained 240µl of 500µg/ml *H.mad* and *H.mye* venom whilst columns 2 to 10 contained 120µl of PBS. The venom was diluted by 1:2 across the plate according to Section 3.3.3.1. Column 11 and 12 contained the positive (26.92µg/ml *N.nig* crude venom) and negative (PBS) control respectively. Definitively, columns 1 to 9, 11 and 12 (rows a, b, d and e) contained a final volume of 120µl, column 10 (rows a, b, d and e) contained a final volume of 240µl.

		1	2	3	4	5	6	7	8	9	10	11	12
H.mad	A												
	B												
	C												
H.mye	D												
	E												
	F												
	G												
	H												

b. The colour coded key corresponding to the compound plate (table 5.4.a.) representing the concentration of venom in each column. Starting with the highest concentration of 500µg/ml in column 1 and diluting this by half resulting in the lowest concentration of 0.977µg/ml in column 10.

KEY	
	500.00µg/ml
	250.00µg/ml
	125.00µg/ml
	62.50µg/ml
	31.25µg/ml
	15.63µg/ml
	7.81µg/ml
	3.91µg/ml
	1.95µg/ml
	0.98µg/ml
	N.nig 26.92µg/ml
	Cells and PBS only

4.3.3. Dosing with Venom Fractions

Dosing the cells with a panel of venom fractions was utilised to identify not only significant species which reduced SK-OV-3 cell metabolism, but also find particular fractions from those species which significantly impacted cell metabolism. Species involved in the venom fraction assay included *N.nig*, *A.cpi, P.reg* and *P.cav*.

As per standard set up, $1x10^5$ number of SK-OV-3 cells were plated across 3 identical 96 well plates to create 3 replicates for each venom fraction. All 3 plates were returned to the incubator overnight allowing the cells to adhere. On day 2, the compound plate and resazurin concentrations were prepared before application to the cells. A readymade compound plate was provided by Venomtech (Venomtech Ltd, UK) with a plate layout established in Table 4.5. Venomtech fractioned the venoms and prepared the plate. Venoms were fractioned by reverse phase HPLC and were quantified using UV microspectrophotometry and standardised at 6µg per well, using a DS11, in a v-bottom, low protein binding 96 well plate. Using antistatic matting in the flow hood (to prevent loss of protein) venom fractions were resuspended in 200µl of PBS and left at room temperature for 5min; this was done to ensure complete rehydration of the venom. As there was 6µg of protein per well and with the addition of 200µl of PBS, the final concentration of each venom fraction was 30µg/ml ($\frac{6\mu g}{200\mu l}\ x\ 1000 = 30\mu g/ml$). 26.92µg/ml *N.nig* (positive control) and PBS (negative control) were applied to the last 4 wells of column 12 of the compound plate also.

Once the venom fractions were rehydrated, all media was removed and discarded from the 3 test plates before transferring 50µl of the contents in the compound plate to the corresponding wells of the 3 test plates. All test plates were then returned to the incubator for 2 hours. After 2 hours, all contents from the 3 plates were removed and replaced with 160µM resazurin before the plates were analysed and data collected.

Table 4.5. The layout of the readymade compound plate supplied by Venomtech Ltd. Each well contained a volume of 200µl at a concentration of 30µg/ml. 50µl of each well was transferred to 3 tests plates with the exact same layout. 200µl of the positive control (26.92µg/ml crude *N.nig;* column 12, row E and F) and negative control (PBS; column 12, row G and H) were applied to the plate also.

	1	2	3	4	5	6	7	8	9	10	11	12
A	*N.nig r1*	*N.nig r9*	*N.nig r17*	*A.cpi r2*	*A.cpi r14*	*A.cpi r22*	*P.reg r1*	*P.reg r16*	*P.reg r25*	*P.cav r9*	*P.cav r22*	*P.cav r31*
B	*N.nig r2*	*N.nig r10*	*N.nig r18*	*A.cpi r4*	*A.cpi r15*	*A.cpi r23*	*P.reg r4*	*P.reg r17*	*P.reg r28*	*P.cav r10*	*P.cav r24*	*P.cav r32*
C	*N.nig r3*	*N.nig r11*	*N.nig r19*	*A.cpi r7*	*A.cpi r16*	*A.cpi r24*	*P.reg r5*	*P.reg r18*	*P.cav r1*	*P.cav r11*	*P.cav r25*	*P.cav r33*
D	*N.nig r4*	*N.nig r12*	*N.nig r20*	*A.cpi r9*	*A.cpi r17*	*A.cpi r26*	*P.reg r6*	*P.reg r20*	*P.cav r2*	*P.cav r14*	*P.cav r26*	*P.cav r34*
E	*N.nig r5*	*N.nig r13*	*N.nig r21*	*A.cpi r10*	*A.cpi r18*	*A.cpi r27*	*P.reg r11*	*P.reg r21*	*P.cav r3*	*P.cav r15*	*P.cav r27*	Pos Cont
F	*N.nig r6*	*N.nig r14*	*N.nig r22*	*A.cpi r11*	*A.cpi r19*	*A.cpi r28*	*P.reg r12*	*P.reg r22*	*P.cav r4*	*P.cav r16*	*P.cav r28*	Pos Cont
G	*N.nig r7*	*N.nig r15*	*N.nig r23*	*A.cpi r12*	*A.cpi r20*	*A.cpi r29*	*P.reg r13*	*P.reg r23*	*P.cav r5*	*P.cav r17*	*P.cav r29*	Neg Cont
H	*N.nig r8*	*N.nig r16*	*A.cpi r1*	*A.cpi r13*	*A.cpi r21*	*A.cpi r31*	*P.reg r15*	*P.reg r24*	*P.cav r8*	*P.cav r21*	*P.cav r30*	Neg Cont

Data was processed at the 120 min. time point in accordance with the results from the Z' assay in Section 3.3.4.2. Firstly, the percentage of inhibition was calculated for each plate individually as done in Section 3.3.3.1. Then, the average percent inhibition was calculated across all 3 plates and a graph of percent inhibition (y-axis) against venom fraction (x-axis) was plotted. Following this an arbitrary threshold of 50% was set, this meant that any fractions with percent inhibition of 50% or more were carried forward for statistical analysis using a t-test. Fractions with a p-value of 0.05 or less were considered as a significant fraction in reducing cell metabolism and were therefore explored further in induvial DR's.

4.3.4. Dose Response of *N.nig*_r11 Fraction

Following statistical analysis described in Section 4.4 (Table 4.11), it was determined that the *N.nig*_r11 fraction was of significance in reducing cell metabolism of SK-OV-3 cells. It was already identified that this fraction was of significance at a concentration of 30µg/ml, therefore a DR initiated at 200µg/ml was utilised to find the LD50 of the venom as previously done.

As previously undertaken, $1x10^5$ number of SK-OV-3 cells were plated on day 1 as shown in Table 4.7 before the plate was returned to the incubator overnight. The following day, the compound plate utilised to serially dilute the venom was set up, this is illustrated in Table 4.8 a-b. The highest concentration of the *N.nig*_r11 fraction used was 200µg/ml. Once the venom was appropriately diluted, the contents from the test plate were replaced with the respective contents in the compound plate. The test plate was returned to the incubator for 2 hours. Subsequent to this, contents from the test plate were once again replaced with 160µM resazurin and the plate was analysed as explained in Section 2.2.2.

Table 4.7. The layout of the assay plate for the DR of the *N.nig*_r11 venom fraction. Each column contained 5 replicates of $1x10^5$ SK-OV-3 cells.

	1	2	3	4	5	6	7	8	9	10	11	12
A	1x10 5	1x10 5	1x10 5	1x10 5	1x10 5	1x10 5	1x10 5	1x10 5	1x10 5	1x10 5	1x10 5	1x10 5
B	1x10 5	1x10 5	1x10 5	1x10 5	1x10 5	1x10 5	1x10 5	1x10 5	1x10 5	1x10 5	1x10 5	1x10 5
C	1x10 5	1x10 5	1x10 5	1x10 5	1x10 5	1x10 5	1x10 5	1x10 5	1x10 5	1x10 5	1x10 5	1x10 5
D	1x10 5	1x10 5	1x10 5	1x10 5	1x10 5	1x10 5	1x10 5	1x10 5	1x10 5	1x10 5	1x10 5	1x10 5
E	1x10 5	1x10 5	1x10 5	1x10 5	1x10 5	1x10 5	1x10 5	1x10 5	1x10 5	1x10 5	1x10 5	1x10 5
F												
G												
H												

Table 4.8.

a. A colour coded layout of the compound plate used to serially dilute the *N.nig*_r11 venom fraction. Column 1 contained 240µl of the highest concentration of venom starting at 200µg/ml. Columns 2 to 10 contained 120µl of PBS which was utilised to dilute the venom by 1:2 across the plate. The positive control (26.92µg/ml crude *N.nig* venom) and negative control (PBS) were dedicated to columns 11 and 12 respectively. Definitively, columns 1 to 9, 11 and 12 (rows a, b and c) contained a final volume of 120µl, whilst column 11 (rows a, b and c) contained a final volume of 240µl.

	1	2	3	4	5	6	7	8	9	10	11	12
A												
B												
C												
D												
E												
F												
G												
H												

b. The colour coded key corresponding to the compound plate (Table 4.8.a.) representing the concentration of venom in each column. Starting with the highest concentration of 200µg/ml in column 1 and diluting this by half resulting in the lowest concentration of 0.391µg/ml in column 10.

KEY	
	200.00µg/ml
	100.00µg/ml
	50.00µg/ml
	25.00µg/ml
	12.50µg/ml
	6.25µg/ml
	3.13µg/ml
	1.56µg/ml
	0.78µg/ml
	0.39µg/ml
	N.nig 26.92µg/ml
	Cells and PBS only

GraphPad Prism 5 was used to calculate the LD50 of the fraction. Using nonlinear regression analysis, dose response stimulation of log(agonist) vs. normalised response determined the concentration which inhibited 50% of cell metabolism.

4.3.5. Dose Response of *P.cav*_r28 Fraction

Like that of the previous experiment, *P.cav*_r28 fraction was considered as a significant fraction in inhibiting SK-OV-3 cell metabolism; therefore, the fraction was analysed further in the setting of a DR to determine the LD50.

In accordance to standard protocol outlined in Section 2.2, $1x10^5$ number of SK-OV-3 cells were plated on day 1 as illustrated in Table 4.9. The plate was returned to the incubator overnight allowing the cells to adhere. The following day, the compound plate was set up as illustrated in Table 4.10 a-b. Unfortunately, there were limited stocks of the *P.cav*_r28 fraction therefore the maximum concentration utilised in this experiment was 15.63µg/ml. Upon completing the compound plate, contents from the test plate were removed and replaced with the corresponding contents in the compound plate. The test plate was returned to the incubator for 2 hours before replacing the contents with 160µM resazurin and analysing the plate as per Section 2.2.2.

Table 4.9. The layout of the assay plate for the DR of the *P.cav*_r28 venom fraction. Each column contained 4 replicates of $1x10^5$ SK-OV-3 cells.

	1	2	3	4	5	6	7	8	9	10	11	12
A	1x10 5	1x10 5	1x10 5	1x10 5	1x10 5	1x10 5	1x10 5	1x10 5	1x10 5	1x10 5	1x10 5	1x10 5
B	1x10 5	1x10 5	1x10 5	1x10 5	1x10 5	1x10 5	1x10 5	1x10 5	1x10 5	1x10 5	1x10 5	1x10 5
C	1x10 5	1x10 5	1x10 5	1x10 5	1x10 5	1x10 5	1x10 5	1x10 5	1x10 5	1x10 5	1x10 5	1x10 5
D	1x10 5	1x10 5	1x10 5	1x10 5	1x10 5	1x10 5	1x10 5	1x10 5	1x10 5	1x10 5	1x10 5	1x10 5
E												
F												
G												
H												

Table 4.10

a. The colour coded layout of the compound plate used to serially dilute the *P.cav*_r28 fraction. Column 1 contained 240µl of 15.63µg/ml *P.cav*_r28 fraction whilst columns 2 to 10 contained 120µl of PBS. The venom was diluted across the plate by 1:2. Column 11 contained the positive control (26.92µg/ml crude *N.nig* venom) and column 12 contained the negative control (PBS). Definitively, columns 1 to 9, 11 and 12 (rows a and b) contained a final volume of 120µl, whilst column 10 (rows a and b) contained a final volume of 240µl.

	1	2	3	4	5	6	7	8	9	10	11	12
A												
B												
C												
D												
E												
F												
G												
H												

b. The colour coded key corresponding to the compound plate (Table 4.10.a) representing the concentration of venom in each column. Starting with the highest concentration of 15.63µg/ml in column 1 and diluting this by half resulting in the lowest concentration of 0.03µg/ml in column 10.

KEY	
	15.63µg/ml
	7.81µg/ml
	3.91µg/ml
	1.95µg/ml
	0.98µg/ml
	0.49µg/ml
	0.24µg/ml
	0.12µg/ml
	0.06µg/ml
	0.03µg/ml
	N.nig 26.92µg/ml
	Cells and PBS only

4.4. Results

The initial DR operated crude *P.tra* venom at a starting concentration of 200µg/ml. As illustrated in Figure 4.1, the venom inhibited SK-OV-3 cell metabolism by a maximum of 44.55% at the most concentrated dose of 200µg/ml. Although it is evident that the venom inhibited cell metabolism, the inhibition of significance threshold of 50% was not achieved, thus being an indication that this scorpion venom, at the specified concentration, does not significantly inhibit cell metabolism of the SK-OV-3 cell line. Furthermore, the usual sigmoidal curve achieved using logistic functions is not represented at the beginning of the DR curve and instead fluctuates between 10% and 20%; it is not until 6.25µg/ml (Log10=0.80) whereby the positive correlation between the increase in venom concentration and increase in percent inhibition is attained.

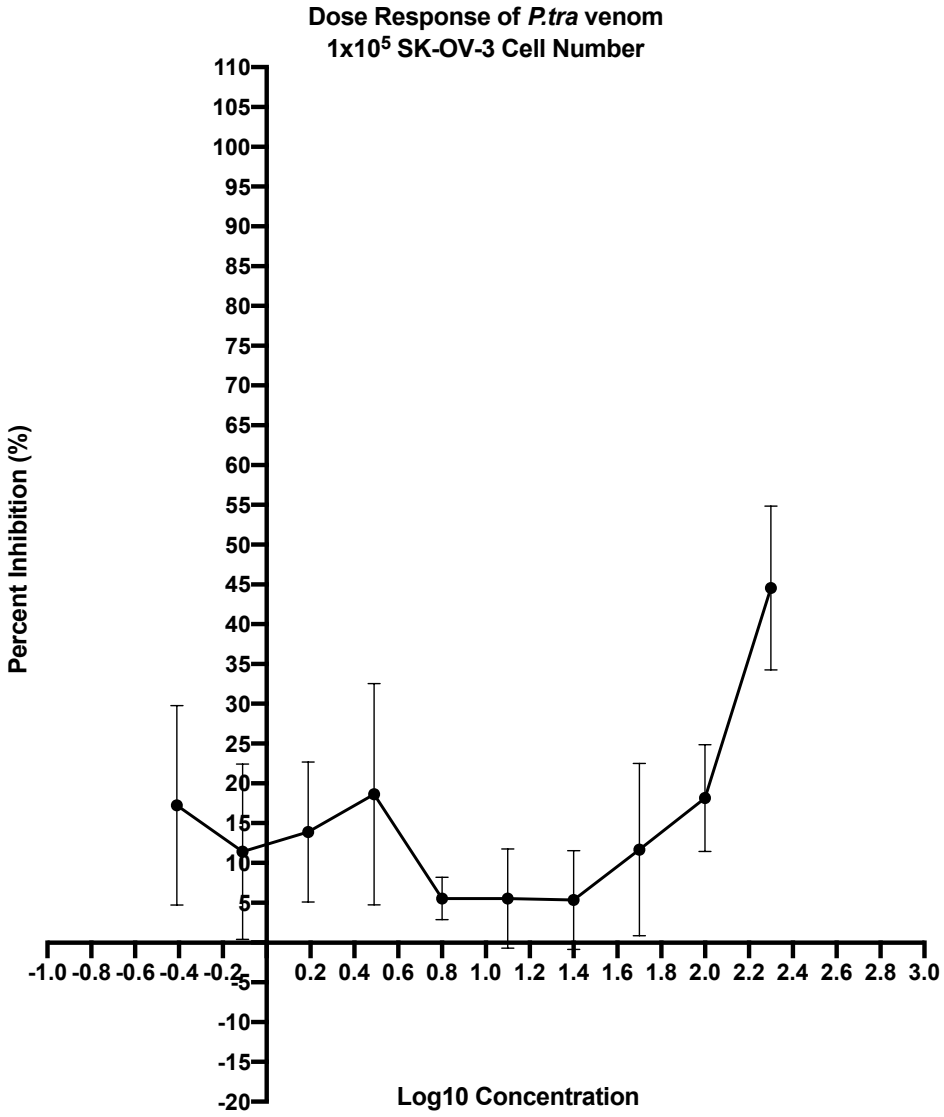

Figure 4.1. The DR curve produced for the *P.tra* venom at 120 min. Raw data was processed and averaged over a 2.5 hour period.

Following on from *P.tra* venom, the *Heterometrus* genus was investigated using crude *H.mad* and *H.mye* scorpion venom at an initial concentration of 500µg/ml. Clarified in Figures 4.2 and 4.3 respectively, both venoms did not inhibit cell metabolism of the SK-OV-3 cell line to a significant extent. *H.mad* venom, displaying considerable variation, inhibited cell metabolism by an extremity of 0.78% at the most concentrated dose of 500µg/ml (Log10=2.70). Again, no clear relationship is established between venom dosing and inhibition of cell metabolism. Similarly, *H.mye* venom inhibited 2.35% of SK-OV-3 cell metabolism at the maximal concentration of 500µg/ml whilst also exerting no positive relationship. Although *H.mye* inhibited cell metabolism to a greater extent compared to *H.mad*, the 50% threshold was not encountered by either venom which demonstrates that both venoms utilised at a concentration of 500µg/ml do not significantly inhibit cell metabolism and therefore are not considered as hits.

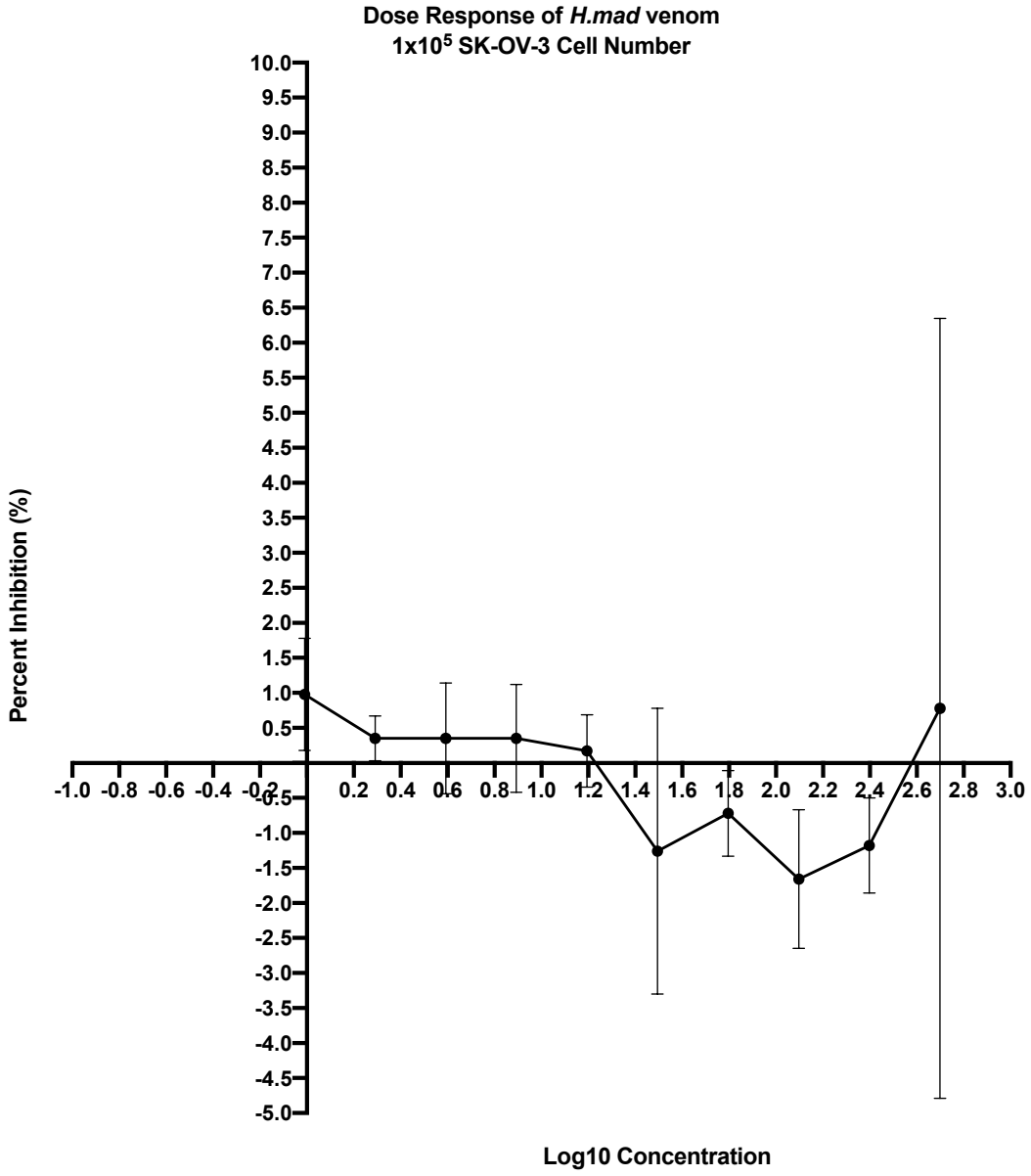

Figure 4.2. The DR curve produced for the *H.mad* venom at 120 min. Raw data was processed and averaged over a 3 hour period.

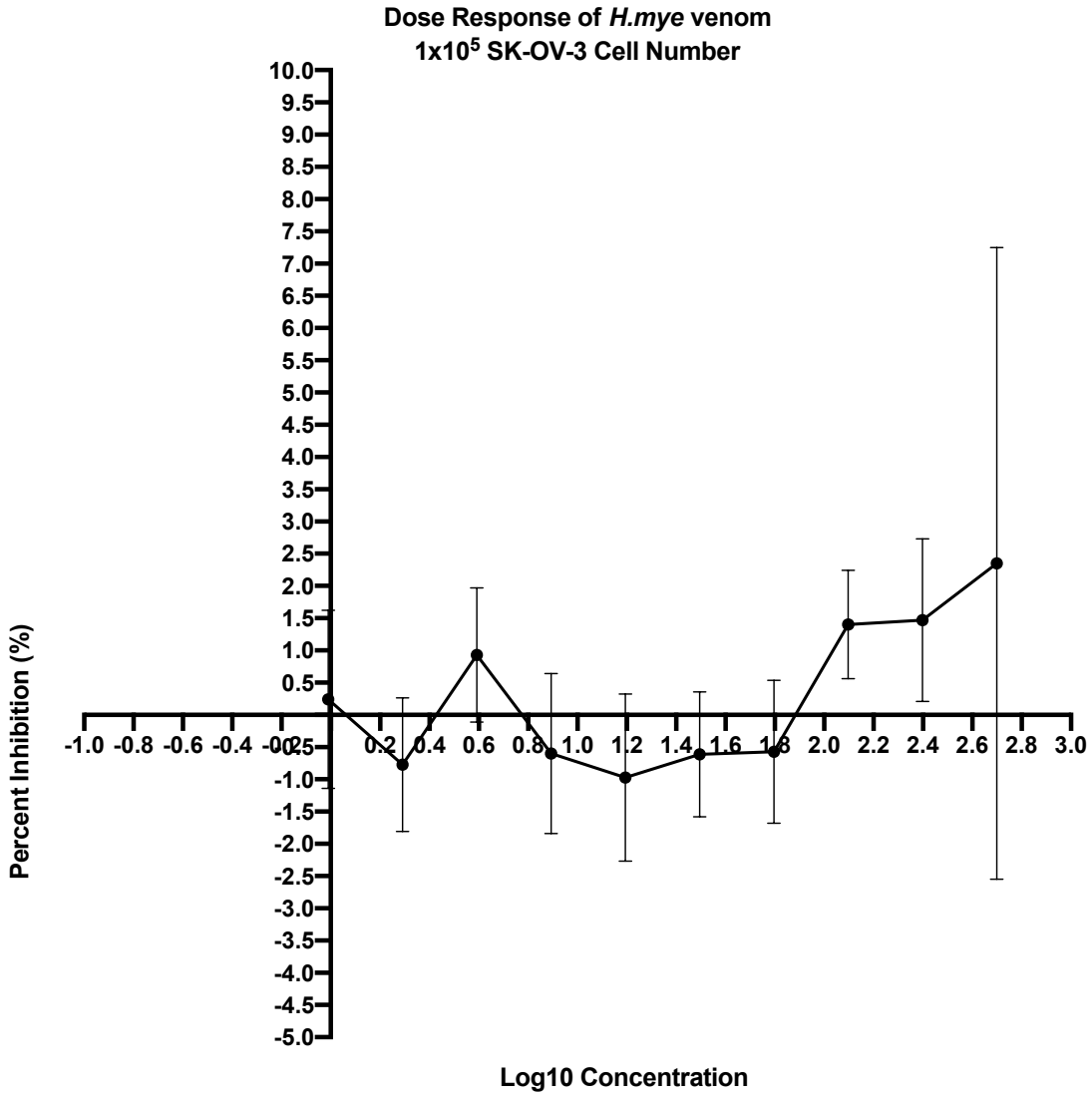

Figure 4.3. The DR curve produced for the *H.mye* venom at 120 min. Raw data was processed and averaged over a 3 hour period.

Subsequent to the crude venom assays, a panel of fractioned venoms were investigated to assess the metabolic inhibitory extent of particular venom fractions relative to the SK-OV-3 cell line. Again, fractions achieving 50% inhibition or more were considered as significant hits. Of the 92 fractions explored, 11 fractions exceeded the 50% inhibition threshold as validated in Figure 4.4. These fractions were from species *N.nig*, *P.reg* and *P.cav*. To confirm the fractions were significantly reducing SK-OV-3 cell metabolism and to ensure only statistically significant fractions were pursued, a t-test was performed demonstrated in Table 4.1. This finalised that fractions *N.nig*_r11 (p-value=0.002), *P.cav*_r28 (p-value=0.028) and *P.cav*_r30 (p-value=0.036) were statistically positive hits in significantly reducing cell metabolism. Unfortunately, there were no stocks left of the *P.cav*_r30 fraction, therefore *N.nig*_r11 and *P.cav*_r28 were carried forward only.

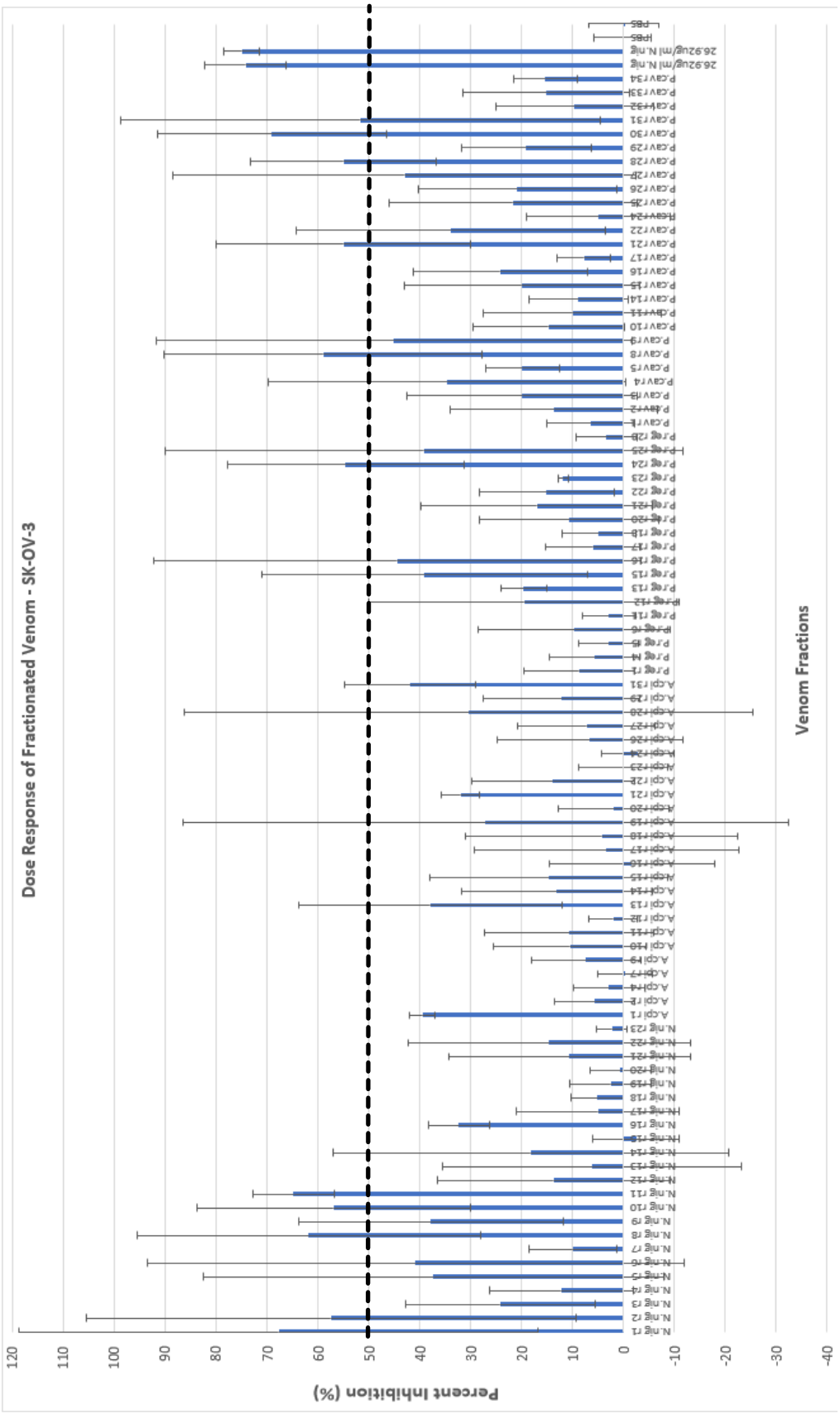

Figure 4.4. The processed results from the DR of testing various venom fractions against cell metabolism of SK-OV-3. The bar graph illustrates the percent inhibition achieved by each fraction. Due to the size of the graph, the x-axis labelling is unclear, refer to Table A.3 in the appendix for clarification. Fractions left to right on the graph correspond to ordered fractions in Table A.3.

Table 4.11. The statistical results of the t-test used to find what fractions significantly impacted the cell metabolism of SK-OV-3 cells. From the arbitrary 50% threshold put in place, the fractions listed below had a percent inhibition of 50% or greater. They were therefore carried forward and a t-test was used to highlight the fraction above 50% which significantly reduced cell metabolism. From the t-test it is clear that *N.nig*_r11, *P.cav*_r28 and *P.cav*_r30 significantly reduced cell metabolism in the SK-OV-3 cell line.

Fractions	*N.nig*_r1	*N.nig*_r2	*N.nig*_r8	*N.nig*_r10	*N.nig*_r11	*P.reg* _r24	*P.cav*_r8	*P.cav*_r21	*P.cav*_r28	*P.cav_r30*	*P.cav*_r31	PBS
P-value	0.135	0.156	0.079	0.070	0.002	0.060	0.091	0.066	0.028	0.036	0.181	0.506

Using the *N.nig*_r11 venom fraction first, a DR, starting at a maximum concentration of 200µg/ml, was performed to clarify the LD50. The processed data reflected in Figure 4.5, demonstrates that the *N.nig*_r11 fraction certainly inhibited the metabolic activity of SK-OV-3 cells. 96.44% of cell metabolism was inhibited at the maximum venom concentration of 200µg/ml whilst results also demonstrated the sigmoidal curve representing a relationship between increasing venom concentration and increase in percent inhibition. As mentioned in Section 4.3.4, GraphPad Prism 5 was used to calculate the LD50 of the fraction, as demonstrated in Table 4.12, results suggested a concentration of 37.23µg/ml (Log10=1.571) is required to inhibit cell metabolism by 50%.

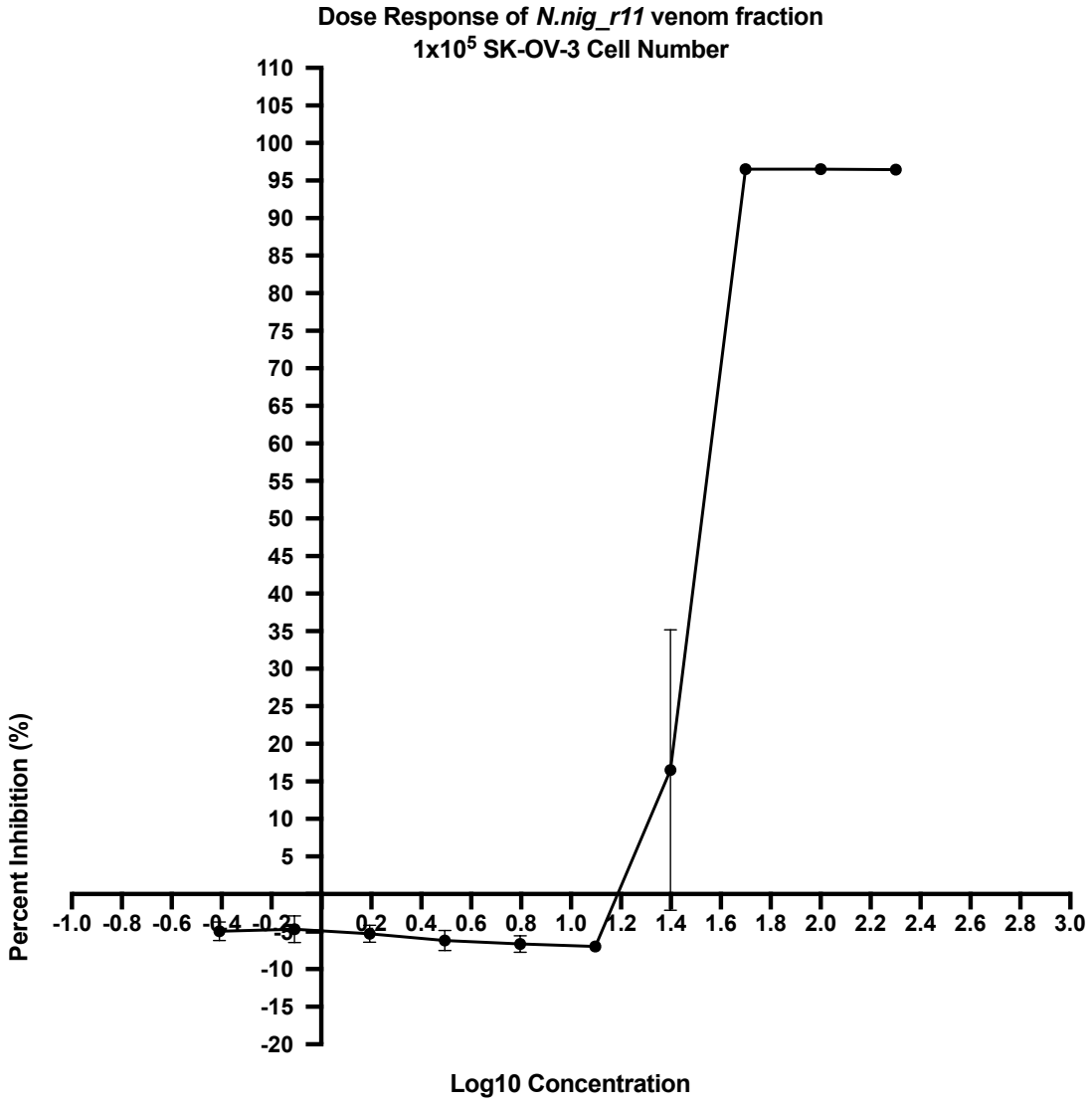

Figure 4.5. The DR curve produced by the *N.nig*_r11 venom fraction at 120 min. Raw data was processed and averaged over a 3 hour period.

Table 4.12. The calculated LD50 of the *N.nig*_r11 venom fraction using GraphPad Prism 5. The 'LOGEC50' demonstrates the Log10 concentration of the LD50 whilst 'EC50' demonstrates the LD50 in terms of µg/ml.

log(agonist) vs. normalized response	
Best-fit values	
LOGEC50	1.571
EC50	37.23
Std. Error	
LOGEC50	0.2048
95% Confidence Intervals	
LOGEC50	1.108 to 2.034
EC50	12.82 to 108.2
Goodness of Fit	
Degrees of Freedom	9
R^2	0.7796
Absolute Sum of Squares	4639
Sy.x	22.70
Number of points	
Analyzed	10

Following this, the *P.cav*_r28 fraction was investigated in the setting of a DR to also confirm the LD50. As explained in Section 4.3.5, stocks of the *P.cav*_r28 were extremely limited and could only be utilised at a maximum concentration of 15.63µg/ml. Results, represented in Figure 4.6, demonstrated that the venom inhibited an extremity of 2.54% of SK-OV-3 cell metabolism using the specified maximal concentration meaning the significant 50% inhibitory threshold was not accomplished. Ultimately, the venom starting at a concentration of 15.63µg/ml, does not reach the 50% threshold therefore the LD50 could not be considered.

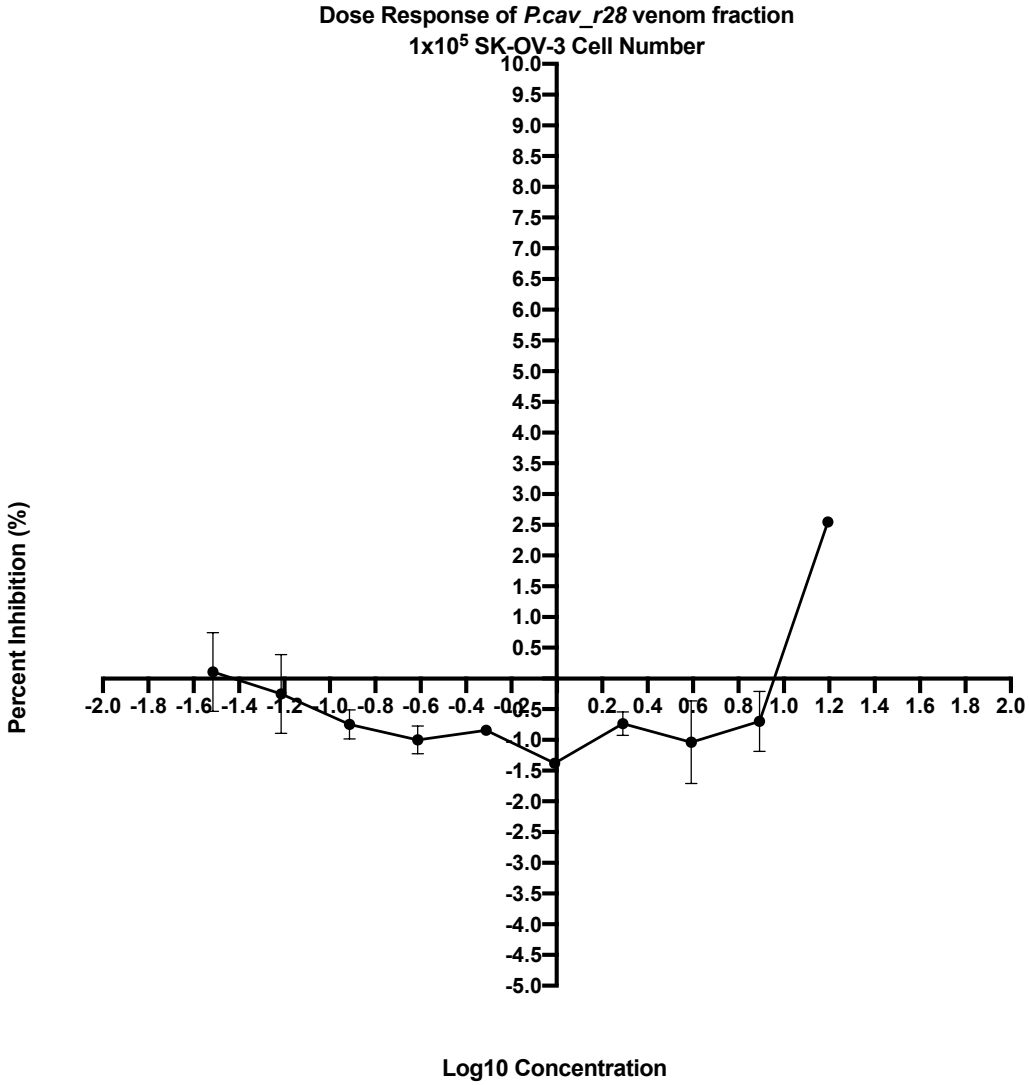

Figure 4.6. The DR curve produced for the *P.cav*_r28 venom fraction at 120 min. Raw data was processed and averaged over a 2.5 hour period.

Overall, the results suggest that the *P.tra* venom, although presenting inhibitory tendencies, did not reach the 50% threshold and can therefore not be considered as a positive hit at the specified concentration. In addition, *H.mad* and *H.mye* venom did not reach the 50% threshold even though the initial venom concentration utilised was increased to 500µg/ml. This suggests that both *Heterometrus* venoms do not present inhibitory abilities and are therefore considered as redundant. Comparing the scorpion venom, the results indicate that the *Parabuthus* venom inhibited SK-OV-3 cell metabolism more than the *Heterometrus* venom at a considerable decreased concentration. This fundamentally suggests there are specific proteins and peptides present in the *P.tra* venom which are absent from *H.mad* and *H.mye* venom that inhibit SK-OV-3 cell growth. The cytotoxic potential of the *Parabuthus* and *Heterometrus* genus' will be explored further in Section 5.1 as well as their assigned families. Likewise, from the *P.cav*_r28 assay, it is clear the venom did not significantly reduce cell metabolism, however as mentioned,

the stocks of this fraction were limited resulting in a reduced concentration of the venom being utilised in the assay. Nevertheless, the venom, when used at 30µg/ml in the fraction dosing assay, did significantly inhibit cell metabolism. The following Section will therefore explore the cytotoxic capabilities of the *Pandinus* genus and the potential proteins and peptides specific to this venom which may have attributed to its original inhibitory aptitudes. Moreover, the results indicate that the *N.nig*_r11 fraction significantly inhibited cell metabolism of SK-OV-3 cells and is therefore regarded as a positive hit warranting further investigation. Again, the distinct proteins and peptides which contribute to the *Naja* genus and Elapidae family will be discussed. Furthermore, the possible mechanisms and signalling pathways, associated with SK-OV-3 progressions, that were potentially inhibited by the aforementioned venoms will be considered in more depth.

CHAPTER FIVE – DISCUSSION

5.1. Discussion

Cancer as a whole is a major public health problem worldwide (Siegal, *et al.*, 2019); 18 million new cases of cancer were presented in 2018 on a global scale followed by 9 million deaths (Ferlay, *et al.*, 2018). Epithelial-OC is unfortunately a detrimental disease to the female population worldwide. The elusive symptoms associated with OC are commonly misdiagnosed for less serious conditions such as pre-menstrual syndrome (NHS, 2017), ultimately preventing the early diagnosis of the disease. The 5-year survival statistics in FIGO stages I and II is around 90% in comparison to 30% for stages III and IV (Sartorius, *et al*., 2018); it therefore comes as no surprise that this illness is the deadliest of gynaecologic diseases when over 75% of OC patients are diagnosed at an advanced stage (Lomnytska, *et al*., 2018).

Current standard of care for OC is surgical debulking supplemented by adjuvant chemotherapy, however, 70-80% of patients will develop chemoresistance within the first 2 years of therapy and require subsequent lines of treatment (Ventriglia, *et al*., 2018). This demonstrates that the 'one-size-fits-all' approach is failing. Although research into targeted-therapies has been amplified over recent years, OC still lacks in successful precision medicines with PARP and VEGF inhibitors being the main therapies utilised (Vetter & Hays, 2018). This highlights the need to identify more molecular-targets in OC that can be exploited for the development of targeted-therapies. With this in mind, there is a huge requirement to bridge the gap in the understanding of alternative, novel therapies which have the potential to be utilised in the treatment of OC. One area in contemporary research demonstrating a level of popularity in regards to oncology is the exploration of animal venoms and their anticancer properties. Such research, both *in vitro* and *in vivo*, has illustrated the benefits of using particular venoms to reduce cancer cell-growth and progression (Moga, *et al*., 2018).

Consequently, it was the aim of this project to identify specific venoms that reduce cell viability of OC (in particular the SK-OV-3 cell line) and thus facilitate in building foundations for future developments in regards to innovative therapeutics. This ultimately enables improvements to the ability of treating OC. The research employed intended to identify what specific venoms, crude and fractioned, reduced the cell viability of SK-OV-3 cells and to what extent, in terms of concentration, said venoms prevented at least 50% of cell metabolism. This ultimately produced

a panel of venoms that can be characterised as positive hits (i.e reduce the metabolic activity of SK-OV-3 cells) or considered as redundant (i.e do not significantly affect the metabolic activity of SK-OV-3 cells). This was achieved through the use of resazurin based-assays in the setting of a DR to identify the percent of inhibition attained by the particular venoms used.

P.tra was the initial crude venom analysed for its inhibitory effects. The results illustrated that the venom, at 200µg/ml, did not reach the 50% threshold (LD50) of inhibition in regards to metabolism of SK-OV-3 cells. Due to the venom not achieving the threshold at the specified concentration, it was characterised as redundant. Nevertheless, though the venom did not reach the threshold, inhibition at 200µg/ml reached 44.55%. This suggests *P.tra* venom does have inhibitory tendencies in relation to the SK-OV-3 cell line, however, the venom concentration used was somewhat too low. Diaz-Garcia *et al* 2013, investigated the inhibitory effects of the scorpion venom from *R.jun* against a panel of human cancer cell lines using an MTT assay. Results identified the lowest IC50 achieved by the venom was in accordance to the A549 cell line (lung carcinoma) of 630µg/ml. The highest IC50 achieved was from the Hela cell lines (cervix adenocarcinoma) reaching 1050µg/ml (Diaz-Garcia, *et al*., 2013). Unfortunately, literature regarding *P.tra* venom and cell viability assays are limited, however, the *R.jun s*corpion and *P.tra* originate from the same Buthidae family (NCBI, 2019). Furthermore, Al-Asmari *et al* 2016, using *Androctonus bicolor* venom (another Buthidae member), achieved an LD50 for the MDA-MB-231 (breast cancer) and HCT-8 (colorectal cancer) cell lines at 839µg/ml and 730µg/ml respectively (Al-Asmari, et al., 2016). Research such as this suggests venom of the Buthidae family presents cytotoxicity at considerably concentrated doses which ultimately implies increasing the concentration of *P.tra* venom would increase the cytotoxic ability and thus meet the 50% threshold. However, this does suggest the venom is less potent and would therefore be less useful as a drug; nevertheless, it is important to remember that the venom is crude and could potentially have components working antagonistically resulting in the need for an increased concentration. It is therefore a venom to still consider in characterising as a positive hit and warrants further investigation.

The Buthidae family are the largest family of scorpions and contain a number of medically valuable species (White & Meier, 1995). *P.tra* is one of the species considered as therapeutically useful (Shah, et al., 2018). Research has established that scorpion venoms contain short-chain neurotoxins (SCNs), which act on potassium (K^+) and chloride (Cl^-) channels, and long-chain neurotoxins (LCNs), which mainly act on sodium (Na^+) channels (Cologna, *et al*., 2009). Nisani *et al* 2011, using fast protein liquid chromatography and matrix-assisted laser desorption/ionisation-time of flight (MALDI-TOF) MS, identified a number of peptides present

within specific fractions of the *P.tra* venom. These included kurtoxin, parabutoxin, birtoxin, alitoxin, ikitoxin and dortoxin; such peptides have the aptitude to efficiently target Na^+, K^+, Cl^- and calcium (Ca^{2+}) channels (Nisani, *et al.*, 2012). As mentioned, *P.tra* venom used in this investigation was crude, thus meaning a cocktail of the aforementioned peptides could have been present in the venom at varying concentrations therefore suggesting any one of those peptides individually or in pairing caused the inhibition of SK-OV-3 cells through acting upon ion channels.

Kurtoxin, a 63 amino-acid peptide stabilised by 4 disulfide bonds, is known to inhibit T-type voltage-gated Ca^{2+} channels (TTVGCC); such channels have been associated with disease states such as hypertension and cancer, in particular OC. Calcium demonstrates an important role in intracellular signalling as well as controlling different cellular process such as proliferation, growth, differentiation and apoptosis (Humeau, *et al.*, 2018); the intracellular level of calcium is regulated by TTVGCC (Kim, *et al.*, 2018). Research has identified that these channels are commonly overexpressed in cancer-cells, especially OC, which in turn modulates cellular proliferation; moreover, when the channel was blocked using mibefradil or NNC 55-0396 apoptotic cell death was induced (Li, *et al*., 2011). In accordance to this, Jang *et al* 2013, identified that KYSO5090 and its derivatives (T-type Ca^{2+} inhibitors) reduced cell metabolism significantly in SK-OV-3 and A2780 cells in the form of a cell viability assay (Jang, *et al.*, 2013). Such research has established the importance of the TTVGCC in the progression of OC whilst demonstrating inhibition of this channel induces apoptosis and reduces cell viability. Considering an established TTVGCC inhibitor in *P.tra* venom, Kurtoxin, it is possible to suggest that this peptide could have been responsible for the inhibitory effects present in the venom in relation to SK-OV-3 cells.

Another peptide from *P.tra* venom of value is Parabutoxin, a 37 amino-acid peptide, that inhibits voltage-gated K^+ channels (VGPC) (Huys, *et al.*, 2002). Once again, the channel plays a key role in proliferation of many tumour cells with researchers demonstrating its overexpression in cancers of the brain, breast, lung and ovary (Bielanska, *et al.*, 2009). Of importance to this project, Asher *et al* 2010, identified that Eag (a K^+ channel substrate) was overexpressed in the SK-OV-3 cell line using immunofluorescence and IHC which was significantly associated with poor survival (p-value=0.016). Furthermore, proliferation of SK-OV-3 cells was significantly reduced when treated with VGPC inhibitors (p-vaue<0.0001) (Asher, et al., 2010). Unfortunately, there is no published research relating to the direct inhibitory effects of Parabutoxin in accordance to specific tumours including SK-OV-3; however, the research presented is an indication of potential molecular targets in the SK-OV-3 cell line as well establishing that

inhibiting such channels induces apoptosis in cancer-cells. Parabutoxin can therefore be theorised as potentially targeting VGPC and thus reducing cell metabolism of SK-OV-3 cells.

Birtoxin, alitoxin, ikitoxin and dortoxin are all toxins identified in *P.tra* venom which inhibit voltage-gated Na^+ channels (VGSC). Like TTVGCC and VGPC, VGSC have been associated with the particular processes that lead to increased tumour aggressiveness and development in many cancers, and more specifically and of great concern, OC (Rhana, *et al.*, 2017). VGSC are composed of nine members, NaV1.1 through to NaV1.9 encoded by genes SCN1A-SCN5A and SCN8A-SCN11A. Using RT-PCR, Gao *et al* 2010, identified that NaV- 1.2, 1.4, 1.5 and 1.7 were all overexpressed in the OC cell lines SK-OV-3 and Caov-3, however, NaV1.5 was expressed only in OC cells and absent from healthy cells using Western Blot analysis (Gao, *et al.*, 2010). Utilising this, Liu *et al* 2018, using patch-clamp technique and RNA interference approaches not only identified the existence of NaV1.5 channels in SK-OV-3 but also acknowledged that 15µM of eicosapentaenoic acid (EPA – inhibitor of NaV1.5) blocked 60% of NaV1.5 currents in SK-OV-3 cells whilst exemplifying a critical role in reducing SK-OV-3 cell migration and proliferation (Liu, *et al.*, 2018). However, NaV1.5 is a major cardiac sodium channel, ultimately suggesting this would not make an ideal cancer target (Belau, *et al.*, 2019). Nevertheless, the results exemplify the benefits of inhibiting certain VGSC and can be used as a framework for other investigations into the use of said toxins and the aforementioned sodium channels overexpressed in OC.

Again, specific studies involving the aforementioned *P.tra* toxins and their inhibitory efforts in tumours have not been published to date. Using the research outlined here however, sets a framework in understanding how the potential blockades of VGSC can result in the reduced cell viability of SK-OV-3 cells. By extension, utilising isolated toxins from the *P.tra* venom could potentially have the same effect of inhibiting cell viability, which would suggest VGSC inhibitors present in the crude scorpion venom could have produced the inhibitory effects of the *P.tra* species witnessed in the DR assay in this investigation.

H.mad and *H.mye* venom, unlike *P.tra,* did not exhibit inhibitory traits regardless of increasing the concentration to 500µg/ml; no more than 1% and 2.5% of inhibition was achieved in accordance to the venoms used at the specified dose. This ultimately suggested that *H.mad* and *H.mye* venoms were redundant in terms of the SK-OV-3 cell line as the 50% threshold was not achieved. To date, there are no published papers identifying specific components in the venom of *H.mad* or *H.mye* which by extension demonstrates there is no research published with an association between the antecedent venoms and their anticancer potential (PubMed, 2019). This would somewhat support the results illustrated here considering the venom did not inhibit

cell metabolism to a significant extent. Although this is the case for the specific species named, other species in the *Heterometrus* genus present more promise.

Gupta *et al* 2007, identified the anticancer properties in venom from *Heterometrus bengalensis* (*H.ben*). Using an MTT assay, it was recognised that *H.ben* venom significantly inhibited cell growth in U937 and KF62 cells (human leukemic cell lines) achieving an LD50 of 41.5µg/ml and 88.3µg/ml correspondingly. Furthermore, confocal microscopy identified chromatin condensation, margination and prominent nuclear disintegration in the dosed cells relative to untreated cells, whilst fluorescence microscopy illustrated the presence of apoptotic cells (early and late) in both cell lines when treated with venom. Finally, DNA fragmentation was significantly increased in the cell lines when dosed using a comet assay (p-value<0.05) (Gupta, *et al.*, 2007).

Subsequent to such findings, the same researchers investigated the *H.ben* venom further. Using HPLC, the specific protein responsible for the antiproliferative and apoptogenic effects was isolated and purified; this was established as Bengalin. Using the same cell lines mentioned above, an LD50 of metabolic inhibition was achieved at 3.7µg/ml and 4.1µg/ml respectively. Furthermore, inhibition of cell line proliferation transpired by apoptosis; this was evidenced by identifying extensive damage to nuclei, increase in early apoptotic cells and cell cycle arrest at the sub G1 phase. Furthermore, the Bax:Bcl2 (apoptosis regulator) ratio was elevated in the dosed cell lines. This was all achieved through fluorescence microscopy observations, flow cytometric analysis and Western Blot examination (Gupta, *et al.*, 2010).

Heterometrus laoticus (*H.lao*) is another species from the *Heterometrus* genus with medical utility. The venom from this species contains a peptide known as heteroscorpine-1 (HS-1) which possess a putative K^+ channel blocking module (Uawonggul, *et al*., 2007). As previously specified, K^+ channel inhibition is a potential mechanism specific in OC which can induce apoptosis (Comes, *et al*., 2015); thus, testing this specific compound against the SK-OV-3 cell line could present inhibitory effects.

It is evident that there are medically useful species amongst the *Heterometrus* genus, however, this does not include *H.mad* and *H.mye*. This conforms to the results produced in the projects investigation. Both *H.mad* and *H.mye* did not significantly inhibit cell metabolism, in terms of the investigation at hand, this classifies the particular venoms as redundant. The fact that that literature concerning the medical benefits of the specified species is absent, especially concerning anticancer properties, illustrates either the lack of research into the venoms or the

lack of results produced from these species. Although the outcome of the assay does not transpire to a positive hit and thus a redundant route for a targeted-therapy, the results help to eliminate this venom in the quest for potential precision medicines in OC. Furthermore, the literature above solidifies that there are not only differences in venom components between scorpion families, but the venom constituents are also species specific. This validates that different species will elicit different effects on a molecular level which ultimately reinforces the importance of this project in establishing a panel of positive hit, and redundant venoms. Moreover, considering there are around 2,000 known scorpion species to date (National Geographic, 2019), the literature available as well as this project at hand only uses a small percentage of the known species which highlights how much potential this research still has to offer. Continued investigations in this field will aid in optimising the best scorpion-cancer combination, building an initial framework for novel therapeutics.

Subsequent to the analysis of crude venoms, a number of fractioned venoms from a variety of species were investigated; this was done to establish exclusive fractions with cytotoxic propensities. Again, a 50% threshold was set and those fractions achieving 50% inhibition or more were carried forward for statistical analysis using a t-test. The results from the t-test indicated that fractions *N.nig*_r11, *P.cav*_r28 and *P.cav*_r30 were of significance in reducing SK-OV-3 cell metabolism. Unfortunately, there were no stocks left of the *P.cav*_r30 fraction and therefore could not be analysed further. *N.nig*_r11 and *P.cav*_r28 were however carried forward for additional exploration.

The *N.nig*_r11 fraction was utilised first. The results indicated that the fraction inhibited 50% of cell metabolism at a concentration of 37.23μg/ml. Literature is relatively abundant in illustrating the cytotoxic ability of snake venoms and their potential in cancer (PubMed, 2019). Research has identified various crude snake venoms as well as isolated enzymes which obtain antitumor activities; these include metalloproteases, disintegrins, L-amino acid oxidases (LAAO), C-type lectins and phospholipases A_2 (PLA_2) (Calvete, *et al*., 2007). Mode of action includes apoptosis induction (PLA_2, metalloproteases and LAAO), antiangiogenesis (disintegrins and lectins) as well as direct toxic action (PLA_2) (Calderon, *et al.*, 2014). It therefore came as no surprise that the snake venom used in this investigation significantly inhibited cell metabolism of SK-OV-3 cells.

Although research is abundant in snake venom as whole and anticancer potential, *N.nig* venom explicitly has also gained some attention regarding its cytotoxic abilities in various cancers. For example, cytotoxin P4 was isolated from crude *N.nig* venom and contained 55% of the crude cytotoxic activity with a molecular weight of 8KD (Chaim-Matyas, *et al*., 1991). Borkow *et al*

1992, utilising the cytotoxin P4 identified that cell lysis occurred in leukaemia cells, B16F10 and WEHI-3B, at concentrations of 0.8µg/ml and 1µg/ml respectively (Borkow, *et al*., 1992). Suggestions for how inhibition of growth was caused included irreversible alterations on the cells completely destroying them, alterations to cell aggregation and finally loss of cell process viability (Calderon, *et al.*, 2014). Furthermore, Chwetzoff *et al* 1989, identified a novel PLA_2 exclusive to *N.nig* that produced cytotoxic effects in epithelial FL cells. Fractioning the venom using HPLC, a specific PLA_2 was identified and named nigexine; this is a single chain of 118 amino acids. Measuring the confluency of cell growth over a 15 day period, it was determined that nigexine at a concentration of 10^{-7}M reduced cell proliferation by 70%. Moreover, cell viability of FL cells was reduced by 50% after 1 hour using a nigexine concentration of 2µM (Chwetzoff, *et al.*, 1989).

As a whole, the genus of *Naja* has shown huge potential in the field of oncology. Jokhio and Ansari 2005, validated the antimetastatic potential of *Naja naja atra* venom through decreasing the expression and activity of matrix metalloproteinase MMP-9. This was achieved through inactivating MAPK and PI3K/AKT signalling pathways which ultimately inhibited cell migration and invasion of cells initiating breast cancer (Jokhio & Ansari, 2005). In addition to this, Ebrahim *et al* 2016, using morphological analysis of HepG2 (hepatocellular carcinoma), MCF7 (breast cancer) and DU145 (prostate carcinoma) human cell lines, identified apoptosis occurred through cytoplasmic blebbing and chromatin condensation when using *Naja naja oxiana* venom. Furthermore, cell viability was inhibited by 50% at a concentration of 26.59µg/ml, 28.85µg/ml and 21.17µg/ml respectively (Ebrahim, *et al*., 2016).

With regards to *N.nig* and the SK-OV-3 cell line, research is lacking. The potential presence of either cytotoxin P4 or nigexine in the *N.nig*_r11 fraction could have elucidated the inhibitory effects this fraction had in relation to the SK-OV-3 cell line. Ultimately, as this fraction within the project is considered as a positive hit, deeper understanding of the specific constituents within the cocktail is needed to aid in not only suggesting the potential proteins responsible for the cytotoxic effects, but also propose particular mechanisms in which the venom interacts with to cause the reduction is cell metabolism. This is why the current project identifying particular venoms with beneficial properties in reducing cell viability builds the framework in developing future explorations.

The final DR utilised the *P.cav*_r28 fraction. Stocks of this venom were extremely limited therefore the maximum dose used in the assay was 15.63µg/ml which inhibited cell metabolism by 2.54%. This resulted in the characterisation of the venom being redundant as the 50%

threshold was not achieved. However, as demonstrated in the fraction dosing assay, this particular fraction achieved the 50% threshold at a concentration of 30µg/ml and therefore demonstrates inhibitory inclinations. The results of the DR, to an extent, do support this notion; a correlation between increasing venom concentration and increase in percent of inhibition begins at 3.91µg/ml. Percent of inhibition is low, however the reduced concentration utilised accounts for this. This suggests the venom is less potent but still active. Ultimately the venom cannot solely be classified as redundant and further investigations into this venom using a more concentrated dose is required.

Available research regarding *P.tra* venom is extremely limited, especially considering this particular species is considered as medically useful; however restricted, contemporary research has started to demonstrate the anticancer and antimicrobial properties of scorpion venoms arousing interest (Estrada-Gomez, *et al*., 2017). Diego-Garcia *et al* 2012, fractioned crude *P.cav* venom using HPLC and identified a number of fractions that significantly inhibited VGPC activity using electrophysiological analysis. Results identified that fractions 49, 50 and 54 inhibited ion currents through the KV1.3 channel at 50µg of protein, whilst various other fractions blocked KV1.1 and KV1.2 channels also (Diego-Garcia, *et al.*, 2012). Unfortunately, the molecular identity of the components in the fractions could not be determined. As mentioned previously, VGPC play an influencing role in tumorogenesis affecting cell proliferation, the cell cycle and differentiation elements associated with hallmarks of cancer. VGPC have been identified in various tumours, most appropriately, the KV1.3 channel has been identified in OC cell lines A2780 and SK-OV-3. Zhanping *et al* 2007, using MTT and flow cytometry identified the presence of the KV1.3 channel in A2780 cells which when blocked with 4-Aminopyridine (4-AP) inhibited cell proliferation. Furthermore, there was a significant increase in the percentage of cells present in the G0/G1 phase (p-value<0.05) whilst the percentage of cells in the S and G2/M phase significantly decreased (P-value<0.05), this suggests less cells are in the replication phase of the cell cycle explaining reduced cell growth (Zhanping, *et al.*, 2007). Asher *et al* 2010, supported Zhanping's findings; using the KV1.3 inhibitor 4-AP, cell proliferation of SK-OV-3 cells was significantly inhibited (p-value<0.001) (Asher, *et al*., 2010).

Both researchers demonstrate the importance of the KV1.3 channel in the progression of OC whilst Diego-Garcia explicitly identifies particular *P.cav* fractions which significantly inhibited the channel. In regards to the results of the DR in this investigation, the concentration was too low to elicit a significant effect on cell metabolism, however when utilised at double the concentration, an LD50 is achieved. As the molecular components in the scorpion venom which stimulated the inhibition of VGPC were not identified, it cannot be explicitly said what proteins

were in the *P.cav*_r28 fraction, however it can be theorised that the fraction potentially contained a VGPC inhibitor similar to that investigated by Diego-Garcia. With the lack of research invested into the *P.cav* species, it is hard to determine the molecular mechanisms targeted by the species and therefore cannot unequivocally hypothesise the protein profile of the venom in this investigation without further analysis.

With this in mind, it is important to consider further analyses; this includes what else could have been achieved in this project alone as well as future analyses which have the potential to build on from the foundations set within this investigation.

First and foremost, re-running of DRs using increased concentrations of specific venoms would be beneficial in distinctly categorising the venoms into positive hits or redundant. As mentioned, the *P.tra* venom did evoke inhibition of the SK-OV-3 cell line, however, due to the arbitrary 50% threshold set throughout the project, at 200µg/ml, the venom could only generate a maximum inhibition of 44.55%. Although this did not reach the threshold, simply increasing the concentration to 1mg/ml and following the 1:2 dilution could prompt the venom in reaching the 50% threshold and thus contribute to a positive hit provoking further investigation. The *P.cav*_r28 fraction would also benefit from this. As the stocks of this venom were low and there was not enough time to fraction more crude venom, 15.63µg/ml was the most concentrated dose utilised which did not reach the 50% threshold and was considered as redundant. However, when cells were dosed with this fraction at 30µg/ml, 50% inhibition of SK-OV-3 cell metabolism was exceeded. An additional DR using a higher concentration would once again solidify whether this venom warrants further investigation. Moreover, the project would benefit from investigating the inhibitory potential of the *P.cav*_r30 fraction also. Determining the LD50 of this fraction and comparing this to the *P.cav*_r28 fraction would assist in identifying if there are certain proteins specific to each fraction which, although both reduce cell viability, target separate mechanisms in the cancer.

Further analysis could also involve reducing the arbitrary 50% threshold to 40% or 30% during the venom fraction dosing assay to identify more potentially significant fractions; nevertheless, it is important to consider that these fractions would be less potent. As illustrated in Table A.3 of the appendix, fractions highlighted in purple achieved the 40% threshold, whilst fractions highlighted in blue reached the 30% threshold. When carrying such fractions forward for statistical analysis using a t-test, results determined that fraction *A.cpi*_r31 is significant at 40% (p-value=0.027) in reducing SK-OV-3 cell metabolism represented in Table A.4, whilst fractions *N.nig*_r16, *A.cpi*_r1 and *A.cpi*_r21 are significant at 30% (p-value=0.011, 0.040 and 0.018

respectively) in reducing cell metabolism demonstrated in Table A.5. This would offer additional species and fractions to investigate broadening the research capabilities.

Alternative methods of analysis could also be utilised to enhance the investigation. Fractioning the venom of positive hits further would separate the venom into their individual protein constituents which could be additionally analysed for significance against the SK-OV-3 cell line. Those of significance could then be analysed using MS which would aid in the identification of the specific proteins responsible for the prevention of SK-OV-3 cell metabolism. This is a vital step when thinking about the drug discovery aspects of the project. Identifying the protein sequence and structure would not only help in understanding the interaction between the protein and molecular mechanisms within the cell line, but will also allow for the structure to be synthesised into a drug.

Furthermore, Human Phospho-Kinase Antibody Arrays (Kinome Blots) could be used to identify exactly how the venoms, once fractioned, affect the phosphorylation profile of kinases and their protein substrates before and after dosing with the venom. This will identify if activity of certain receptors are being inhibited or knocked down ultimately affecting downstream signalling of said receptors that promote proliferation for instance and therefore reducing cell metabolism. An investigation such as this would also assist in identifying a certain molecular mechanism in the cell line which could be a target in other cancer types. For example, if the venom reduced the expression of EGFR in the SK-OV-3 cell line, it is known that non-small cell lung cancer also overexpresses this receptor and therefore could potentially procure the benefits of the specific venom used (Jurisic, *et al.*, 2018). Moreover, using additional cell lines of the same and alternative cancer types would further enhance the understanding in determining if the benefits of the venom are cell line and/or cell type specific. Again, this would contribute to the development of a panel of venoms with anticancer properties regarding certain cancer cell lines. In addition to researching the anticancer benefits of certain venom components, it would also be advantageous to investigate the effects of such components in regards to normal, healthy cells. This would not only identify the selectivity of the venom for cancer-cells, but could also describe the interaction with normal cells demonstrating potential side effects, another important aspect of drug discovery.

To date, contemporary research is lacking in the investigations into specific anticancer properties of certain venoms in relation to specific cancer types. In this investigation, the results revealed that several animal venoms contain anticancer properties concerning the SK-OV-3 cell line through inhibiting cell metabolism. Although this is only a first step of many into the

therapeutics community, the aforementioned analyses have allowed the framework to be constructed. Identifying the specific venoms which positively hit the cell line as well as those that do not, underpins the basic knowledge for further investigations. With this in mind, the foundations set here moves the identification and production of novel therapies regarding OC in the right direction.

REFERENCES

Abdelmoez, A. *et al*., 2017. Screening and identification of molecular targets for cancer therapy. *Cancer Letters ,* 28(387), pp. 3-9.

Al-Asmari, A. *et al*., 2016. Scorpion (Androctonus bicolor) venom exhibits cytotoxicity and induces cell cycle arrest and apoptosis in breast and colorectal cancer cell lines. *Indian Journal of Pharmacology ,* 48(5), pp. 537-543.

American Cancer Society , 2019. *Cancer Facts and Figures 2019,* Atlanta : American Cancer Society .

Asare-Werehene, M., Shieh, D.-B., Song, Y. & Tsang, B., 2019. Chapter 35 - Molecular and cellular basis of chemoresistance in ovarian cancer. *The Ovary ,* Issue 3, pp. 575-593.

Asher, V. *et al*., 2010. The Eag potassium channel as a new prognostic marker in ovarian cancer. *Diagnostic Pathology ,* 5(78), pp. 1-8.

ATCC, 2016. *SK-OV-3.* [Online]
Available at: https://www.lgcstandards-atcc.org/products/all/HTB-77.aspx#generalinformation
[Accessed 29 March 2019].

ATCC, 2019. *SK-OV-3.* [Online]
Available at: https://www.atcc.org/products/all/HTB-77.aspx#culturemethod
[Accessed 29 July 2019].

Athauda, A., Segelov, E., Ali, Z. & Chau, I., 2019. Integrative molecular analysis of colorectal cancer and gastric cancer: What have we learnt. *Cancer Treatment Reviews ,* 73(1), pp. 31-40.

Audeh, M. *et al*., 2010. Oral poly(ADP-ribose) polymerase inhibitor olaparib in patients with BRCA1 or BRCA2 mutations and recurrent ovarian cancer: a proof-of-concept trial. *The Lancet,* 376(9737), pp. 245-251.

Baumgartner, U. *et al*., 2018. miR-19b Enhances Proliferation and Apoptosis Resistance via the EGFR Signaling Pathway by Targeting PP2A and BIM in Non-Small Cell Lung Cancer. *Molecular Cancer ,* 17(44), pp. 1-15.

Belau, F. *et al*., 2019. DPP10 is a new regulator of NaV1.5 channels in human heart. *International Journal of Cardiology,* 284(1), pp. 68-73.

Benedito, R. *et al*., 2012. Notch-dependent VEGFR3 upregulation allows angiogenesis without VEGF-VEGFR2 signalling. *Nature: International Journal of Science ,* 484(1), pp. 110-114.

Bielanska, J. *et al*., 2009. Voltage-dependent potassium channels Kv1.3 and Kv1.5 in human cancer. *Current Cancer Drug Targets,* 9(8), pp. 904-914.

Blass, B., 2015. *Basic principles of drug discovery and development.* 1st ed. Philadelphia: Elsevier.

Bloom, D., Burnett, J. & Alderslade, P., 1998. Partial purification of box jellyfish (Chironex fleckeri) nematocyst venom isolated at the beachside. *Toxicon ,* 36(8), pp. 1075-1085.

BMJ, 1991. Advanced ovarian cancer trialists group. *BMJ,* 303(1), pp. 884-893.

Bookman, M. *et al*., 2009. Evaluation of New Platinum-Based Treatment Regimens in Advanced-Stage Ovarian Cancer: A Phase III Trial of the Gynecologic Cancer InterGroup. *Journal of Clinical Oncology ,* March, 27(9), pp. 1419-1425.

Borkow, G., Chaim-Matyas, A. & Ovadia, M., 1992. Binding of cytotoxin P4 from naja nigricollis nigricollis to B16F10 melenoma and WEHI-3B leukemia cells. *FEMS Microbiology Immunology ,* 5(1-3), pp. 139-145.

Boveia, V., Ambroz, K. & Olive, D., 2009. *Using the Z'-factor coefficient to monitor quality of near-infrared fluorescent cell-based assays ,* Lincoln: LI-COR Biosciences .

Bray, F. *et al*., 2018. Global Cancer Statistics 2018: GLOBOCAN Estimates of Incidence and Mortality Worldwide for 36 Cancers in 185 Countries. *A Cancer Journal for Clinicians ,* September , 68(6), pp. 394-423.

Bukowska, B., Gajek, A. & Marczak, A., 2015. Two drugs are better than one. A short history of combined therapy of ovarian cancer. *Contemporary Oncology ,* 19(5), pp. 350-353.

Calderon, L. *et al*., 2014. Antitumoral activity of snake venom proteins: new trends in cancer therapy. *BioMed Research International ,* 2014(1), pp. 1-19.

Calvete, J., Juarez, P. & Sanz, L., 2007. Snake venomics. Strategy and applications. *Journal of Mass Spectrometry ,* 42(11), pp. 1405-1414.

Campbell, J. & Cohall, D., 2017. Chapter 26 - Pharmacodynamics - A pharmacognosy perspective. *Pharmacognosy ,* 1(1), pp. 513-525.

Cancer Research UK, 2018. *Ovarian Cancer Statistics.* [Online]
Available at: https://www.cancerresearchuk.org/health-professional/cancer-statistics/statistics-by-cancer-type/ovarian-cancer#heading-Zero
[Accessed 17 January 2019].

Cancer Research UK, 2018. *Types of Ovarian Cancer.* [Online]
Available at: https://www.cancerresearchuk.org/about-cancer/ovarian-cancer/types
[Accessed 28 March 2019].

Casewell, N. *et al*., 2013. Complex cocktails: The evolutionary novelty of venoms. *Trends in Ecology & Evolution,* 28(4), pp. 219-229.

Chabner, B. & Roberts Jr, T., 2005. Chemotherapy and the war on cancer. *Nature Reviews: Cancer ,* 5(1), pp. 65-72.

Chaim-Matyas, A., Borkow, G. & Ovadia, M., 1991. Isolation and characterization of a cytotoxin P4 from the venom of Naja nigricollis nigricollis preferentially active on tumour cells. *Biochemistry International ,* 24(3), pp. 415-421.

Chaisakul, J., Hodgson, W., Kuruppu, S. & Prasongsook, N., 2016. Effects of Animal Venoms and Toxins on Hallmarks of Cancer. *Journal of Cancer ,* 7(11), pp. 1571-1578.

Chandna, A., 2019. Olaparib: Transcending mutational barriers. *Indian Journal of Urology,* 35(1), pp. 85-86.

Chang, L.-C.*et al*., 2018. Prognostic Factors in Epithelial Ovarian Cancer: A Population-based Study. *PLoS ONE,* 13(3), pp. 1-11.

Chaytor, J. *et al*., 2012. Inhibiting ice recrystallization and optimization of cell viability after cryopreservation. *GlycoBiology ,* 22(1), pp. 123-133.

Cheng, W. *et al*., 2005. Lineage Infidelity of Epithelial Ovarian Cancers is Controlled by HOX Genes That Specify Regional Identity in the Reproductive Tract. *Nature Medicine ,* Volume 11, pp. 531-537.

Chiu, C. *et al*., 2009. Effects of cardiotoxin III on NF-kappaB function, proliferation, and apoptosis in human breast MCF-7 cancer cells.. *Oncology Research,* 17(7), pp. 311-321.

Chwetzoff, S., Tsunasawa, S., Sakiyama, F. & Menez, A., 1989. Nigexine, a phospholipase A2 from cobra venom with cytotoxic properties not related to esterase activity. *The Journal of Biological Chemistry,* 264(22), pp. 13289-13297.

Cole, A. *et al*., 2016. *Assessing Mutant p53 in Primary High-Grade Serous Ovarian Cancer Using Immunohistochemistry and Massively Parallel Sequencing ,* s.l.: Nature .

Cologna, C. *et al*., 2009. Tityus serrulatus scorpion venom and toxins: an overview. *Protein and Peptide Letters ,* 16(8), pp. 920-932.

Comes, N. *et al*., 2015. Involvement of potassium channels in the progression of cancer to a more malignant phenotype. *Biomembranes ,* 1848(10), pp. 2477-2492.

Cortez, A., Tudrej, P., Kujawa, K. & Lisowska, K., 2018. Advances in ovarian cancer therapy. *Cancer Chemotherapy and Pharmacology,* 81(1), pp. 17-38.

Coward, J., Middleton, K. & Murphy, F., 2015. New Perspectives on Targeted Therapy in Ovarian Cancer. *International Journal of Women's Health ,* February , 7(1), pp. 189-203.

Cragg, G. & Newman, D., 2005. Biodiversity: A continuing source of novel drug leads. *Pure and Applied Chemistry,* 77(1), pp. 7-24.

Czekanska, E., 2011. Assessment of cell proliferation with resazurin-based fluorescent dye. *Methods in Molecular Biology,* 40(1), pp. 27-32.

Dar, R., Shahnawaz, M., Rasool, S. & Qazi, P., 2017. Natural product medicines: A literature update. *The Journal of Phytopharmocology,* 6(6), pp. 340-342.

Dasari, S. & Tchounwou, P., 2014 . Cisplatin in cancer therapy: molecular mechanisms of action. *European Journal of Pharmacology ,* 0(0), pp. 364-378.

Desai, A. *et al*., 2008. Medicinal plants and cancer chemoprevention. *Current Drug Metabolism,* 9(7), pp. 581-591.

Dias, D., Urban, S. & Roessner, U., 2012. A history overview of natural products in drug discovery. *Metabolites,* 2(2), pp. 303-336.

Diaz-Garcia, A. *et al*., 2013. In vitro anticancer effect of venom from Cuban scorpion Rhopalurus junceus against a panel of human cancer cell lines. *Journal of Venom Research,* 4(1), pp. 5-12.

Diaz-Garcia, A. *et al*., 2013. In vitro effect of venom from cuban scorpion Rhopalurus junceus against a panel of human cancer cell lines. *Journal of Venom Research ,* 4(1), pp. 5-12.

Diego-Garcia, E. *et al*., 2012. Molecular diversity of the telson and venom components from Pandinus cavimanus (Scorpionidae Latreille 1802): transcriptome, venomics and function. *Proteomics,* 12(1), pp. 313-328.

Doherty, A. *et al*., 2011. A rapid, semi-automated method for scoring micronuclei in mononucleated mouse lymphoma cells. *Mutation Research/Genetic Toxicology and Environmental Mutagenesis ,* 726(1), pp. 36-41.

Du, L. *et al*., 2015. Screening the molecular targets of ovarian cancer based on bioinformatics analysis. *Tumori ,* 101(4), pp. 384-389.

Ebell, M., Culp, M. & Radke, T., 2016. A systematic review of symptoms for the diagnosis of ovarian cancer. *American Journal of Preventive Medicine ,* 50(3), pp. 384-394.

Ebell, M., Culp, M. & Radke, T., 2016. A Systematic Review of Symptoms for the Diagnosis of Ovarian Cancer. *American Journal of Preventive Medicine ,* March, 50(3), pp. 384-394.

Ebrahim, K. *et al*., 2016. Anticancer activity a of caspian cobra (Naja naja oxiana) snake venom in human cancer cell lines via induction of apoptosis. *Iranian Journal of Pharmaceutical Research,* 15(Special), pp. 101-112.

Eisenkop, S. & Spirtos, N., 2001. What are the current surgical objectives, stategies, and technical capabilities of gynecologic oncologists treating advanced epithelial ovarian cancer. *Gynecologic Oncology ,* 82(3), pp. 489-497.

Estrada-Gomez, S., Gomez-Rave, L., Vargas-Munoz, L. & van der Meijden, A., 2017. Characterizing the biological and biochemical profile of six different scorpion venoms from the Buthidae and Scorpionidae family. *Toxicon,* 130(1), pp. 104-115.

Ferguson, K., 2008. A Structure-Based View of Epidermal Growth Factor Receptor Regulation. *Annual Review of Biophysics ,* 37(1), pp. 353-373.

Ferlay, J. *et al*., 2018. Estimating the Global Cancer Incidence and Mortality in 2018: GLOBOCAN Sources and Methods. *International Journal of Cancer ,* October, 0(0), pp. 1-13.

FIGO, 2015. FIGO's staging classification for cancer of the ovary, fallopian tube, and peritoneum: abridged republication. *Journal of Gynecologic Oncology ,* 26(2), pp. 87-89.

Florea, A. & Busselberg, D., 2011. Cisplatin as an anti-tumour drug: cellular mechanisms of activity, drug resistance and induced side effects. *Cancers,* 3(1), pp. 1351-1371.

Forstner, R., Meissnitzer, M. & Cunha, T., 2016. Update on Imaging of Ovarian Cancer. *Current Radiology Reports ,* 4(31), pp. 1-11.

Freed, D. *et al*., 2017. EGFR Ligands Differentially Stabilize Receptor Dimers to Specify Signalling Kinetics. *Cell Press,* 171(3), pp. 683-695.

Frezza, A., Stacchiotti, S. & Gronchi, A., 2017. Systemic treatment in advanced soft tissue sarcoma: what is standard, what is new. *BMS Medicine ,* 15(109), pp. 1-12.

Gajiwala, K., 2013. EGFR: tale of the C-terminal tail. *Protein Science ,* 22(7), pp. 995-999.

Gao, R. *et al*., 2010. Expression of voltage-gated sodium channel alpha subunit in human ovarian cancer. *Oncology Reports ,* 23(1), pp. 1293-1299.

Garziera, M. *et al*., 2018. Identification of Novel Somatic TP53 Mutations in Patients with High-Grade Serous Ovarian Cancer (HGSOC) Using Next-Generation Sequencing (NGS). *Internation Journal of Molecular Sciences ,* 9(5), pp. 1510-1529.

Gilks, B. & Kommoss, 2016. *Ovarian Carcinoma Histotypes: Their Emergence as Important Prognostic and Predictive Markers ,* New York : Oncology.

Giovannini, C. *et al*., 2017. Venom from Cuban blue scorpion has tumour activating effect in hepatocellular carcinoma.. *Scientific Reports ,* 7(44685), pp. 1-11.

Giugni, T., Chen, K. & Cohen, S., 1988. Activation of a Cytosolic Serine Protein Kinase by Epidermal Growth Factor. *The Journal of Biological Chemistry,* 263(35), pp. 18988-18995.

Goel, H. & Mercurio, A., 2013. VEGF targets the tumour cell. *Nature Reviews Cancer ,* 13(12), pp. 871-882.

Granados, M., Hudson, L. & Samudio-Ruiz, S.-L., 2015. Contributions of the epidermal growth factor receptor to acquisition of platinum resistance in ovarian cancer cells. *PLoS one ,* 1(1), pp. 1-17.

Granados, M., Hudson, L. & Samudio-Ruiz, S., 2015. Contributions of the epidermal growth factor receptor to aquisition of platinum resistance in ovarian cancer cells. *PLoS One ,* 10(9), pp. 1-17.

GraphPad, 2010. *Calculating a Z-factor to assess the qaulity of a screening assay.* [Online] Available at: https://www.graphpad.com/support/faq/calculating-a-z-factor-to-assess-the-quality-of-a-screening-assay/ [Accessed 10 08 2019].

Gullick, W., Venter, D., Kumar, S. & Tuzi, N., 1987. Overexpression of the c-erbB-2 oncoprotein in human breast carcinomas: immunohistological assessment correlates with gene amplification. *The Lancet,* 330(8550), pp. 69-72.

Guo, G. *et al*., 2015. Ligand-Independent EGFR Signalling. *Cancer Research,* 75(17), pp. 3436-3441.

Gupta, S. *et al*., 2007. Indian black scorpion (Heterometrus bengalensis Koch) venom induced antiproliferative and apoptogenic activity against human leukimic cell lines U937 and K562. *Leukemia Research ,* 31(6), pp. 817-825.

Gupta, S. *et al*., 2010. Apoptosis induction in human leukemic cells by a novel protein Bengalin, isolated from Indian black scorpion venom: through mitochondrial pathway and inhibition of heat shock proteins. *Chemico-Biological Interactions ,* 183(2), pp. 293-303.

Hait, W., 2009. Targeted cancer therapeutics. *Cancer Research,* 69(4), pp. 1263-1267.

Hanahan, D. & Weinberg, R., 2011. Hallmarks of Cancer: The Next Generation. *Cell,* 144(5), pp. 647-674.

Harding, J. & Burtness, B., 2005. Cetuximab: an epidermal growth factor receptor chemeric human-murine monoclonal antibody. *Drugs Today ,* 41(2), pp. 107-127.

Harries, M. & Smith, I., 2002. The development and clinical use of trastuzumab (Herceptin). *Endocrine-Related Cancer,* 9(2), pp. 75-85.

Himilton, T., 1992. Ovarian Cancer, Part I: Biology. *Current Problems in Cancer ,* 16(1), pp. 5-57.

Hirsch, F. *et al*., 2018. Long-term saftey and survival with gefitinib in select patients with advanced non-small cell lung cancer: Results from the US IRESSA Clinical Access Program (ICAP). *Cancer,* 124(11), pp. 2407-2414.

Hsu, H.-C.*et al*., 2017. Longlitudinal Perceptions of the Side Effects of Chemotherapy in Patients with Gynecological Cancer. *Supportive Care in Cancer ,* November, 25(11), pp. 3457-3464.

Humeau, J. *et al*., 2018. Calcium signalling and cell cycle: progression or death. *Cell Calcium ,* 70(1), pp. 3-15.

Huys, I. *et al*., 2002. Purification, characterization and biosynthesis of parabutoxin 3, a component of Parabuthus transvaalicus venom. *European Journal of Biochemistry,* 269(7), pp. 1854-1865.

Israelsson, P. *et al*., 2017. Assessment of Cytokine mRNA Expression Profiles in Tumor Microenvironment and Peripheral Blood Mononuclear Cells of Patients with High-grade Serous Carcinoma of the Ovary. *Journal of Cancer Science and Therapy ,* 9(5), pp. 422-429.

Itamochi, H., 2010. Targeted therapies in epithelial ovarian cancer: Molecular mechanisms of action. *World Journal of Biological Chemistry ,* 1(7), pp. 209-220.

Iura, A. *et al*., 2018. Negative peritoneal washing cytology during interval debulking surgery predicts overall survival after neoadjuvant chemotherapy for ovarian cancer. *Journal of Gynecologic Oncology ,* 29(5), pp. 1-11.

Jang, S. *et al*., 2013. In vitro cytotoxicity on human ovarian cancer cells by T-type calcium channel blockers. *Bioorganic and Medicinal Chemistry Letters,* 23(1), pp. 6656-6662.

Javadi, S. *et al*., 2016. Ovarian Cancer, the Revised FIGO Staging System, and the Role of Imaging. *American Journal of Roentgenology,* 206(6), pp. 1351-1360.

Jokhio, R. & Ansari, A., 2005. Cobra snake venom reduces significantly tissue nucleic acid level in human breast cancer. *The Journal of the Pakistan Medical Association ,* 55(2), pp. 71-73.

Jones, P., Issa, J.-P. & Baylin, S., 2016. Targeting the cancer epigenome for therapy. *Nature Reviews: Genetics ,* 17(1), pp. 630-641.

Jurisic, V., Obradovic, J., Pavlovic, S. & Djordjevic, N., 2018. Epidermal growth factor receptor gene in non-small cell lung cancer: The importance of promoter polymorphism investigation. *Analytical Cellular Pathology,* 2018(6192187), pp. 1-9.

Kandukuri, S. & Rao, J., 2015. FIGO 2013 Staging System for Ovarian Cancer: What is New in Comparison to the 1988 Staging System?. *Current Opinion in Obstetrics and Gynecology,* 27(1), pp. 48-52.

Katsumata, N. *et al*., 2013. Long-term results of dose-dense paclitaxel and carboplatin versus conventional paclitaxel and carboplatin for treatment of advanced epithelial ovarian, fallopian tube, or primary peritoneal cancer (JGOG 3016): a randomised, controlled, open-label trial. *The Lancet: Oncology,* 14(10), pp. 1020-1026.

Katz, S., Ramchandani, P., Torigian, D. & Siegelman, E., 2019. Hydrosalpinx in patients with hysterectomy without salpingo-oophorectomy referred for pelvic magnetic resonance imaging. *Clinical Imaging ,* 55(1), pp. 95-99.

Kayl, A. & Meyers, C., 2006. Side-effects of chemotherapy and quality of life in ovarian and breast cancer patients. *Current Opinion in Obstetrics and Gynecology ,* 18(1), pp. 24-28.

Kehoe, S. *et al*., 2015. Primary chemotherapy versus primary surgery for newly diagnosed advanced ovarian cancer (CHORUS): an open-label, randomised controlled, non-inferiority trial. *The Lancet ,* 386(9990), pp. 249-257.

Ke, X. & Shen, L., 2017. Molecular targeted therapy of cancer: The progress and future prospect. *Frontiers in Laboratory Medicine ,* 1(2), pp. 69-75.

Kim, H. & Jang, S., 2017. Optimization of a resazurin-based microplate assay for large-scale compound screenings against Klebsiella pneumoniae. *3 Biotech,* 8(1), pp. 1-6.

Kim, H. & Oh, S., 2013. Noncommunicable Diseases: Current Status of Major Modifiable Risk Factors in Korea. *Journal of Prevenive Medicine and Public Health ,* July, 46(4), pp. 165-172.

Kim, J.-W.*et al*., 2018. T-type calcium channels are required to maintain viability of neural progenitor cells. *Biomolecules and Therapeutics,* 26(5), pp. 439-445.

Kim, S. *et al*., 2018. Tumor evolution and chemoresistance in ovarian cancer. *NPJ Precision Oncology,* 2(20), pp. 1-9.

Kolasa, I. *et al*., 2006. PTEN Mutation, Expression and LOH at its Locus in Ovarian Carcinoma. Relation to TP53, K-RAS and BRCA1 Mutations. *Gynecologic Oncology,* 103(2), pp. 692-697.

Koshiyama, M., Matsumura, N. & Konishi, I., 2014. Recent Concepts of Ovarian Cancinogenesis: Type I and Type II. *BioMed Research International ,* 2014(1), pp. 1-11.

Koshiyama, M., Matsumura, N. & Konishi, I., 2017. Subtypes of Ovarian Cancer and Ovarian Cancer Screening. *Diagnostics ,* 7(12), pp. 1-10.

Kurman, R. & Shih, I.-M., 2010. The Origin and Pathogenesis of Epithelial Ovarian Cancer - A Proposed Unifying Theory. *The American Journal of Surgical Pathology ,* 34(3), pp. 433-443.

Lambert, H. & Berry, R., 1985. High dose cisplatin compared with high dose cyclophosphamide in the managment of advanced epithelial ovarian cancer (FIGO stages III and IV): report from the North Thames Cooperative Group. *British Medical Journal (Clinical Research Edition) ,* 290(6472), pp. 889-893.

Ledermann, J. *et al*., 2012. Olaparib maintenance therapy in platinum-sensitive relapsed ovarian cancer. *The New England Journal of Medicine ,* 366(15), pp. 1382-1392.

Lheureux, S., Karakasis, K., Kohn, E. & Oza, A., 2015. Ovarian cancer treatment: The end of empiricism. *Cancer ,* 121(18), pp. 3203-3211.

Li, D. *et al*., 2016. Effect of the BRCA1-SIRT1-EGFR Axis on Cisplatin Sensitivity in Ovarian Cancer. *American Journal of Translational Research ,* 8(3), pp. 1601-1608.

Lin, K. & Kraus, W., 2017. PARP inhibitors for cancer therapy. *Cell,* 169(2), p. 183.

Liu, J. *et al*., 2018. Blocking the Nav1.5 channel using eicosapentaenoic acid reduces migration and proliferation of ovarian cancer cells. *Journal of Oncology,* 53(2), pp. 855-865.

Liu, M., Chan, D. & Ngan, H., 2012. Mechanisms of chemoresistance in human ovarian cancer at a glance. *Gynecology & Obstetrics,* 2(3), p. 1000e104.

Li, W. *et al*., 2011. Blockade of T-type Ca2+ channels inhibits human ovarian cancer cell proliferation. *Cellular and Molecular Biology ,* 29(5), pp. 339-346.

Lomnytska, M. *et al*., 2018. Platelet protein biomarker panel for ovarian cancer diagnosis. *Biomarker Research,* 2(2), pp. 1-14.

McConechy, M. *et al*., 2014. Ovarian and Endometrial Endometrioid Carcinomas Have Distinct CTNNB1 and PTEN Mutation Profiles. *Modern Pathology ,* 27(1), pp. 128-134.

McCullough, D. & Trim, C., 2015. Novel approaches to targeting protein tyrosine kinases. *Drug Target Review ,* Issue 2.

McGuire III, W. & Markman, M., 2003. Primary ovarian cancer chemotherapy: current standard of care. *British Journal of Cancer ,* 89(1), pp. s3-s8.

Mehner, C. *et al*., 2017. EGFR as a prognostic biomarker and therapeutic target in ovarian cancer: evaluation of patient cohort and literature review. *Genes and Cancer,* 8(5-6), pp. 589-599.

Meigs, J., 1934. *Tumors of the female pelvic organs ,* New York : The MacMillan Company .

Meyer, L. *et al*., 2016. Use and effectiveness of neoadjuvant chemotherapy for treatment of ovarian cancer. *Journal of Clinical Oncology ,* 34(32), pp. 3854-3863.

Milenic, D. *et al*., 2008. Cetuximab: Preclinical Evaluation of a Monoclonal Antibody Targeting EGFR for Radioimmunodiagnostic and Radioimmunotherapeutic Applications. *Cancer Biotherapy and Radiopharmaceuticals ,* 23(5), pp. 619-631.

Mistry, P. *et al*., 1991. The relationships between glutathione, glutathione-S-transferase and cytotoxicity of platinum drugs and melphalan in eight human ovarian carcinoma cell lines. *British Journal of Cancer ,* 64(2), pp. 215-220.

Moga, M. *et al*., 2018. Anticancer activity of toxins from bee and snake venom - an overview on ovarian cancer. *Molecules ,* 23(3), pp. 1-21.

Molina, J. & Adjei, A., 2006. The Ras/Raf/MAPK Pathway. *Journal of Thoracic Oncology,* 1(1), pp. 7-9.

Morales, J. *et al*., 2016. Review of poly (ADP-ribose) polymerase (PARP) mechanisms of action and rationale for targeting in cancer and other diseases. *Critical Reviews in Eukaryotic Gene Expression,* 24(1), pp. 15-28.

Moridikia, A. *et al*., 2018. Anticancer and Antibacterial Effects of Iranian Viper (Vipera latifii) Venom; An In-vitro Study. *Journal of Cellular Physiology,* 233(9), pp. 6790-6797.

Morrison, J., Pearn, J., Coulter, A. & Halliday, W., 1983. Immunological stability of an elapid venom, Tropidechis carinatus, and its reevance to the clinical detection of snake

venom. *The Australian Journal of Experimental Biology and Medical Science ,* 61(5), pp. 489-495.

Mutch, D. & Prat, J., 2014. 2014 FIGO Staging for Ovarian, Fallopian Tube and Peritoneal Cancer. *Gynecologic Oncology ,* 133(3), pp. 401-404.

National Cancer Institute , 2013. *Tumour Grade.* [Online]
Available at: https://www.cancer.gov/about-cancer/diagnosis-staging/prognosis/tumor-grade-fact-sheet
[Accessed 27 January 2019].

National Center for Biotechnology Information, 2019. *PubMed.* [Online]
Available at: https://www.ncbi.nlm.nih.gov/pubmed/?term=cancer+AND+targeted+therapies
[Accessed 8 07 2019].

National Geographic , 2019. *Scorpions.* [Online]
Available at: https://www.nationalgeographic.com/animals/invertebrates/group/scorpions/
[Accessed 26 August 2019].

National Health Service , 2017. *Symptoms: Ovarian Cancer.* [Online]
Available at: https://www.nhs.uk/conditions/ovarian-cancer/symptoms/#
[Accessed 06 April 2019].

National Institure for Health and Care Excellence , 2016. *Olaparib for maintenance treatment of relapsed, platinum-sensitive, BRCA mutation-positive ovarian, fallopian tube and peritoneal cancer after response to second-line or subsequent platinum-based chemotherapy.* [Online]
Available at: https://www.nice.org.uk/guidance/ta381/chapter/3-Evidence
[Accessed 10 07 2019].

NCBI, 2019. *Taxonomy Browser: Buthidae.* [Online]
Available at: https://www.ncbi.nlm.nih.gov/Taxonomy/Browser/wwwtax.cgi?mode=Info&id=419285&lvl=3&lin=f&keep=1&srchmode=1&unlock
[Accessed 16 August 2019].

Neff, R., Senter, L. & Salani, R., 2017. BRCA mutation in ovarian cancer: testing, implications and treatment considerations. *Therapeutic Advances in Medical Oncology ,* 9(8), pp. 519-531.

Neijt, J. *et al*., 2000. Exploratory phase III study of paclitaxel and cisplatin versus paclitaxel and carboplatin in advanced ovarian cancer.. *Journal of Clinical Oncology ,* 18(17), pp. 3084-3092.

Neijt, J. *et al*., 1984. Randomised trial comparing two combination chemotherapy regimens (Hexa-CAF vs CHAP-5) in advanced ovarian carcinoma. *Lancet,* 2(8403), pp. 594-600.

Ng, R., 2004. *Drugs: From discovery to approval.* 3rd ed. Singapore: Wiley Blackwell.

NHS, 2017. *Symptoms: Ovarian Cancer.* [Online]
Available at: https://www.nhs.uk/conditions/ovarian-cancer/symptoms/
[Accessed 14 August 2019].

Nielsen, J. *et al*., 2004. Prognostic significance of p53, Her-2, and EGFR overexpression in borderline and epithelial ovarian cancer. *International Journal of Gynecological Cancer ,* 14(6), pp. 1086-1096.

Nisani, Z. *et al*., 2012. Investigating the chemical profile of regenerated scorpion (Parabuthus transvaalicus) venom in relation to metabolic cost and toxicity. *Toxicon,* 60(1), pp. 315-323.

Omura, G. *et al*., 1986. A randomized trial of cyclophosphamide and doxorubicin with or without cisplatin in advanced ovarian carcinoma. A gynecologic oncology group study. *Cancer,* 57(9), pp. 1725-1730.

O'Shea, J. *et al*., 2015. The JAK-STAT Pathway: Impact on Human Disease and Therapeutic Intervention. *Annual Review of Medicine ,* 66(1), pp. 311-328.

Oza, A. *et al*., 2015. Olaparib combined with chemotherapy for recurrent platinum-sensitive ovarian cancer: a randomised phase 2 trial. *The Lancet: Oncology ,* 16(1), pp. 87-97.

Pan, S.-T.*et al*., 2016. Molecular mechanisms for tumour resistance to chemotherapy. *Clinical and Experimental Pharmacology and Phsiology ,* 43(8), pp. 723-737.

Paramee, S. *et al*., 2018. Anti-cancer effects of Kaempferia parviflora on ovarian cancer SKOV3 cells. *BMS Complementary & Alternative Medicine ,* 18(178), pp. 1-13.

Park, J.-Y.*et al*., 2015. Outcomes of Pediatric and Adolescent Girls with Malignant Ovarian Germ Cell Tumors. *Genecologic Oncology ,* 137(3), pp. 418-422.

Patil, C. *et al*., 2019. Phase 1 study, pharmacokinetics, and fluorescence imaging study of tozuleristide (BLZ-100) in adults with newly diagnosed or recurrent gliomas. *Neurosurgery,* p. nyz125.

Pennington, M., Czerwinski, A. & Norton, R., 2018. Peptide therapeutics from venom: current status and potential. *Bioorganic & Medicinal Chemistry ,* 26(10), pp. 2738-2758.

Perez-Herrero, E. & Fernandez-Medarde, A., 2015. Advanced targeted therapies in cancer: Drug nanocarriers, the future of chemotherapy. *European Journal of Pharamaceutics and Biopharmaceutics ,* 93(1), pp. 52-79.

Phyoe-Battaglia, T., Bartels, C., Nulsen, J. & Grow, D., 2018. In Vitro Fertilization with Granulosa Cell Tumor: A Report of Two Cases. *Journal of Assisted Reproduction and Genetics ,* 35(10), pp. 1919-1921.

Piccart, M. *et al*., 2000. Randomized intergroup trial of cisplatin-paclitaxel versus cisplatin-cyclophosphamide in women with advanced epithelial ovarian cancer: three-year results.. *Journal of the National Cancer Institute ,* 92(9), pp. 699-708.

Popovic, N. & Wilson, E., 2010. Cell Surface Receptors. *Comprehensive Toxicology ,* 2(2), pp. 81-91.

Porta, C., Paglino, C. & Mosca, A., 2014. Targeting PI3K/Akt/mTOR Signalling in Cancer. *Frontiers in Oncology,* 4(64), pp. 1-11.

PubMed, 2019. *heterometrus madraspatensis AND cancer.* [Online]
Available at:
https://www.ncbi.nlm.nih.gov/pubmed/?term=heterometrus+madraspatensis+AND+cancer
[Accessed 16 August 2019].

PubMed, 2019. *SnakeVenom AND Cancer.* [Online]
Available at:
https://www.ncbi.nlm.nih.gov/pubmed/?term=snake+venom+AND+cancer
[Accessed 18 August 2019].

Ray-Coquard, I. *et al*., 2018. Non-epithelial ovarian cancer: ESMO clinical practice guidelines for diagnosis, treatment and follow-up. *Animals of Oncology ,* 29(4), pp. IV1-IV18 .

Reid, B., Permuth, J. & Sellers, T., 2017. Epidemiology of Ovarian Cancer: A Review. *Cancer Biology and Medicine ,* February , 14(1), pp. 9-32.

Rhana, P. *et al*., 2017. Is there a role for voltage-gated Na+ channels in the aggressiveness of breast cancer?. *Brazilian Journal of Medical and Biological Research ,* 50(7), pp. 1-10.

Ricigliano, M. *et al*., 2017. Evaluation of a cell viability assay based on cultures of CTICs to identify treatment options in third-line pancreatic cancer. *Journal of Clinical Oncology,* 35(4), pp. 338-338.

Risi, E. *et al*., 2018. A gene expression signature of Retinoblastoma loss-of-function predicts resistance to neoadjuvant chemotherapy in ER-positive/HER2-positive breast cancer patients. *Breast Cancer Research and Treatment ,* 170(2), pp. 329-341.

Robson, M. *et al*., 2017. Olaparib for metastatic breast cancer in patients with a germline BRCA mutation. *The New England Journal of Medicine,* 377(6), pp. 523-533.

Rosenberg, B., Vancamp, L. & Krigas, T., 1965. Inhibition of cell division in Escherichia coli by electrolysis products from a platinum electrode. *Nature ,* 13(205), pp. 698-699.

Roy, R., Chun, J. & Powell, S., 2012. BRCA1 and BRCA2: different roles in a common pathway of genome protection. *Nature Reviews Cancer ,* 12(1), pp. 68-78.

Sartorius, C. *et al*., 2018. Impact of the new FIGO 2013 classification on prognosis of stage I epithelial ovarian cancer. *Cancer Management and Research,* 10(1), pp. 4709-4718.

Sartorius, C. *et al*., 2018. Impact of the New FIGO 2013 Classification on Prognosis of Stage I Epithelial Ovarian Cancers. *Cancer Management and Research,* October, 10(1), pp. 4709-4718.

Schorge, J., Bregar, A., Durfee, J. & Berkowitz, R., 2018. Meigs to modern times: The evolution of debulking surgery in advanced ovarian cancer. *Gynecologic Oncology ,* 149(3), pp. 447-454.

Schorge, J., McCann, C. & Del Carmen, M., 2010. Surgical debulking of ovarian cancer: What difference does it make?. *Obstetrics and Gynecology ,* 3(3), pp. 111-117.

Serrano-Olvera, A. *et al*., 2006. Prognostic, predictive and therapeutic implications of HER2 in invasive epithelial ovarian cancer. *Cancer Treatment Reviews,* 32(1), pp. 180-190.

Servidei, T. *et al*., 2008. Chemoresistant tumor cell lines display altered epidermal growth factor receptor and HER3 signalling and enhanced sensitivity to gefitinib. *International Journal of Cancer,* 123(12), pp. 2939-2949.

Seshacharyulu, P. *et al*., 2012. Targeting the EGFR Signalling Pathway in Cancer Therapy. *Expert Opinion on Therapeutic Targets ,* 16(1), pp. 15-31.

Shah, P. *et al*., 2018. Scorpion venom: a poison or a medicine-mini review. *Indian Journal of Geo-Marine Sciences ,* 47(4), pp. 773-778.

Shanbhag, V., 2015. Applications of snake venoms in treatment of cancer. *Asian Pacific Journal of Tropical Biomedicine ,* 5(4), pp. 275-276.

Sheng, Q. & Liu, J., 2011. The Therapeutic Potential of Targeting the EGFR Family in Epithelial Ovarian Cancer. *British Journal of Cancer ,* 104(1), pp. 1241-1245.

Shepherd, J., 1989. Revised FIGO Staging for Gynacological Cancer. *An International Jounal of Obstetrics and Gynaecology,* 96(8), pp. 889-892.

Siegal, R., Miller, K. & Jemal, A., 2019. Cancer statistics, 2019. *CA: A Cancer Journal for Clinicians ,* 69(1), pp. 7-34.

Sigismund, S., Avanzato, D. & Lanzetti, L., 2017. Emerging Functions of the EGFR in Cancer. *Molecular Oncology ,* 12(1), pp. 3-20.

Sigismund, S., Avanzato, D. & Lanzetti, L., 2018. Emerging Functions of the EGFR in Cancer. *Molecular Oncology,* 12(1), pp. 3-20.

Singer, G. *et al*., 2003. Mutations in BRAF and KRAS Charachterize the Development of Low-Grade Ovarian Serous Carcinoma. *Journal of the National Cancer Institute ,* 95(6), pp. 484-486.

Slamon, D. *et al*., 1987. Human breast cancer: correlation of relapse and survival with amplification of the HER-2/neu oncogene. *Science,* 235(4785), pp. 177-182.

Song, J. *et al*., 2012. Cell growth inhibition and induction of apoptosis by snake venom toxin in ovarian cancer cell via inactivation of nuclear factor kB and signal transducer and activator of transcription 3.. *Archives of Pharmacal Research,* 35(5), pp. 867-876.

Spannuth, W. *et al*., 2009. Functional significance of VEGFR-2 on ovarian cancer cells. *International Journal of Cancer ,* 124(5), pp. 1045-1053.

Su, J.-C.*et al*., 2010. Concomitant inactivation of the epidermal growth factor receptor, phosphatidylinositol 3-kinase/Akt and Janus tyrosine kinase 2/signal transducer and activator of transcription 3 signalling pathways in cardiotoxin III-treated A549 cells.. *Clinical and Experimental Pharmacology and Physiology ,* 37(1), pp. 833-840.

Tan, K., Bay, B. & Gopalakrishnakone, P., 2018. L-amino Acid Oxidase from Snake Venom and its Anticancer Potential. *Toxicon ,* 144(1), pp. 7-13.

Tasoulis, T. & Isbister, G., 2017. A review and database of snake venom proteomes. *Toxins,* 9(9), pp. 1-23.

The Cancer Genome Atlas Research Network , 2011. Integrated Genomic Analyses of Ovarian Carcinoma. *Nature ,* 474(7353), pp. 609-615.

Torre, L. *et al*., 2015. Global Cancer Statistics, 2012. *Cancer Journal for Clinicians ,* February, 65(2), pp. 87-108.

Trim, S. & Trim, C., 2013. Venom: the sharp end of pain therapeutics. *British Journal of Pain ,* 7(4), pp. 179-188.

Tumini, E. *et al*., 2018. The Antitumor Drugs Trabectedin and Lurbinectedin Induce Transcription-Dependent Replication Stress and Genome Instability. *Molecular Cancer Research: Genome Maintenance,* 17(3), pp. 773-782.

Uawonggul, N. *et al*., 2007. Purification and characterization of Heteroscorpine-1 (HS-1) toxin from Heterometrus laoticus scorpion venom. *Toxicon,* 49(1), pp. 19-29.

Union for International Cancer Control, 2017. *TNM Classification of Malignant Tumours.* Eighth Edition ed. West Sussex: John Wiley & Sonds, Ltd.

Utkin, Y., 2017. Modern trends in animal venom research - omics and nanomaterials. *World Journal of Biological Chemistry ,* 8(1), pp. 4-12.

Ventriglia, J. *et al*., 2018. Trabectedin in ovarian cancer: is it now a standard of care?. *Clinical Oncology ,* 30(8), pp. 498-503.

Vergote, I. *et al*., 2011. Primary surgery or neoadjuvant chemotherapy followed by interval debulking surgery in advanced ovarian cancer. *European Journal of Cancer ,* 47(33), pp. s88-s92.

Vergote, I. *et al*., 2010. Neoadjuvant chemotherapy or primary surgery in stage IIIC or IV ovarian cancer. *The New England Journal of Medicine ,* 363(1), pp. 943-953.

Vetter, M. & Hays, J., 2018. Use of targeted therapeutics in epithelial ovarian cancer: a review of current literature and future directions. *Clinical Therapeutics ,* 40(3), pp. 361-371.

Voldborg, B., Damstrup, L., Spang-Thomsen, M. & Poulsen, S., 1997. Epidermal growth factor receptor (EGFR) and EGFR mutatins, function and possible role in clinical trials. *Annals of Oncology ,* 8(1), pp. 1197-1206.

Walzl, A. *et al*., 2014. The resazurin reduction assay can dinstinguish cytotoxic from cytostatic compounds in spheroid screening assays. *Advancing Life Sciences R&D,* 19(7), pp. 1047-1059.

Wang, J. *et al*., 2015. Erlotinib is effective in pancreatic cancer with epidermal growth factor receptor mutations: a randomized, open-label, prospective trial. *Oncotarget,* 6(20), pp. 18162-18173.

Wang, K., Li, D. & Sun, L., 2016. High levels of EGFR expression in tumor stroma are associated with agressive clinical features in epithelial ovarian cancer. *Onco Targets and Therapy ,* 9(1), pp. 377-386.

Wang, K., Li, D. & Sun, L., 2016. High Levels of EGFR Expression in Tumor Stroma are Associated with Agressive Clinical Features in Epithelial Ovarian Cancer. *OncoTargets and Therapy ,* 9(1), pp. 377-386.

Wang, V. *et al*., 2005. Ovarian Cancer is a Heterogeneous Disease. *Cancer Genetics and Cytogenetics ,* 161(2), pp. 170-173.

Weaver, B., 2014. How Taxol/paclitaxel kills cancer cells. *Molecular Biology of the Cell,* 25(18), pp. 2677-2681.

Wee, P. & Wang, Z., 2017. Epidermal Growth Factor Receptor Cell Proliferation Signalling Pathways. *Cancers,* 9(5), pp. 1-45.

White, J. & Meier, J., 1995. *Handbook of clinical toxicology of animal venoms and poisons.* 1st ed. s.l.:Taylor and Francis.

Wieduwilt, M. & Moasser, M., 2008. The Epidermal Growth Factor Receptor Family: Biology Driving Targeted Therapeutics. *Cellular and Molecular Life Sciences ,* 65(10), pp. 1566-1584.

Wilken, J. *et al*., 2012. EGFR/HER-targeted therapeutics in ovarian cancer. *Future Medicinal Chemistry ,* 4(4), pp. 447-469.

Williams, H. *et al*., 2019. The urgent need to develop novel strategies for the diagnosis and treatment of snakebites. *Toxins,* 11(363), pp. 1-29.

Wilson, L. *et al*., 2018. How many cancer cases and deaths are potenitally preventable? Estimates for Australia in 2013. *International Journal of Cancer ,* 142(1), pp. 691-701.

Wilson, T., Longley, D. & Johnston, P., 2006. Chemoresistance in solid tumours. *Annals of Oncology,* 17(10), pp. 315-324.

Wiltshaw, E. & Kroner, T., 1976. Phase II study of cis-dichlorodiammineplatinum(II) (NSC-119875) in advanced adenocarcinoma of the ovary. *Cancer Treatment Review ,* 60(1), pp. 55-60.

World Health Organisation, 2013. *International Classification of Diseases for Oncology,* Malta : World Helth Organisation .

World Health Organisation, 2020. *Biodiversity.* [Online] Available at: https://www.who.int/globalchange/ecosystems/biodiversity/en/ [Accessed 28 February 2020].

Yaginuma, Y. & Westphal, H., 1992. Abnormal Structure and Expression of the p53 Gene in Human Ovarian Carcinoma Cell Lines. *Cancer Research,* 52(15), pp. 4196-4199.

Yarden, Y. & Sliwkowski, M., 2001. Untangling the ErbB Signalling Network. *Nature Reviews: Molecular Cell Biology,* 2(2), pp. 127-137.

Young, R. *et al*., 1978. Advanced ovarian adenocarcinoma. A prospective clinical trial of melphalan (L-PAM) versus combination chemotherapy. *New England Journal of Medicine ,* 299(23), pp. 1261-1266.

Young, R. *et al*., 1979. cis-Dichlorodiammineplatinum(II) for the treatment of advanced ovarian cancer. *Cancer Treatment Review ,* 63(9-10), pp. 1539-1544.

Yun, S. *et al*., 2018. Lgand-Independent Epidermal Growth Factor Receptor Overexpression Correlates with Poor Prognosis in Colorectal Cancer. *Cancer Research and Treatment,* 50(4), pp. 1351-1361.

Zein, N., Aziz, S., El-Sayed, A. & Sitohy, B., 2019. Comparative cytotoxic and anticancer effect of Taxol derived from Aspergillus terreus and Taxus brevifolia. *Bioscience Research,* 16(2), pp. 1500-1509.

Zhang, J., Chung, T. & Oldenburg, K., 1999. A simple statistical parameter for use in evaluation and validation of high throughput screening assays. *Journal of Biomolecular Screening,* 4(2), pp. 67-73.

Zhanping, W. *et al*., 2007. Voltage-gated K+ channels are associated with cell proliferation and cell cycle of ovarian cancer cell. *Gynecologic Oncology,* 104(1), pp. 455-460.

Zheng, H.-C., 2017. The molecular mechanisms of chemoresistance in cancers. *Oncotarget,* 8(35), pp. 59950-59964.

Zhu, H. *et al*., 2019. Preperation and Charachterization of Humanized Nanobodies Targeting the Dimer Interface of Epidermal Growth Factor Receptor (EGFR). *Protein Expression and Purification ,* pp. 1-26.

APPENDIX

Table A.1. The calculated Z-Factors for the optimal SK-OV-3 cell number of $1x10^5$. From the results in this table, it is clear that at all time points the Z-Factor is above 0.5 thus categorising this cell number as robust.

Z Factor	
Time	Z Factor
0	0.522
15	0.664
30	0.770
45	0.807
60	0.837
90	0.899
120	0.942
150	0.961
180	0.968
210	0.967
240	0.964
270	0.964
300	0.958

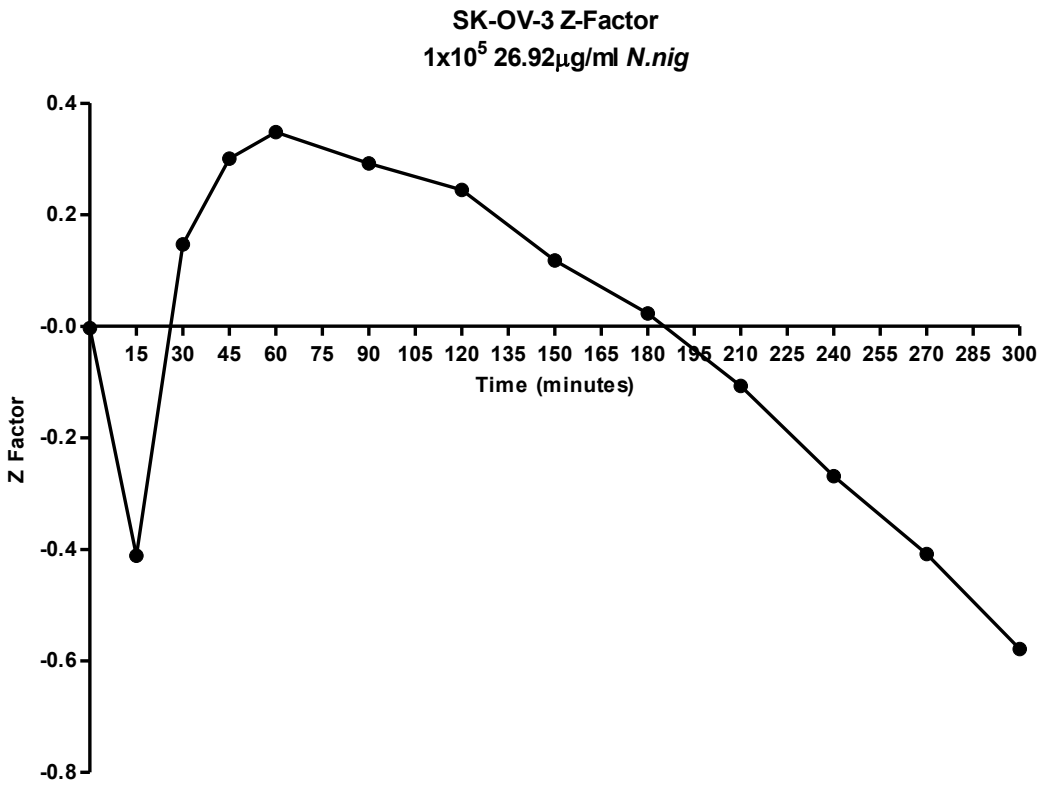

Figure A.1. The processed data of the Z' assay for the LD90 of *N.nig* crude venom. This was the first Z' assay attempt. The Z-factor is calculated every 15 min. for 1 hour and then every 30 min for the following 4 hours. A Z-factor above 0.5 is not achieved throughout the duration of the assay.

	1	2	3	4	5	6	7	8
A	39760	47800	44874	50784	98755	96402	96238	78000
B	37363	14786	45668	58104	82581	86186	85213	87990
C	20389	16307	17283	28229	91849	87812	88809	90696
D	57998	24930	32503	51135	87842	86114	84824	94643
E	93519	88630	87002	87423	60320	45878	68853	97970
F	95454	88723	89335	86711	61118	34913	35209	70522
G	91447	89943	87316	86903	56570	61262	50132	38819
H	89578	89083	92175	91160	58264	55136	61453	54457

Figure A.2. The raw data collected from the FLUOstar Omega Microplate Reader at time point 300 min for the first Z' assay. The positive controls are highlighted by green boxes to illustrate the areas of variation in the data. The calculated mean for the positive control was 46837.16 and 89323.63 for the negative control.

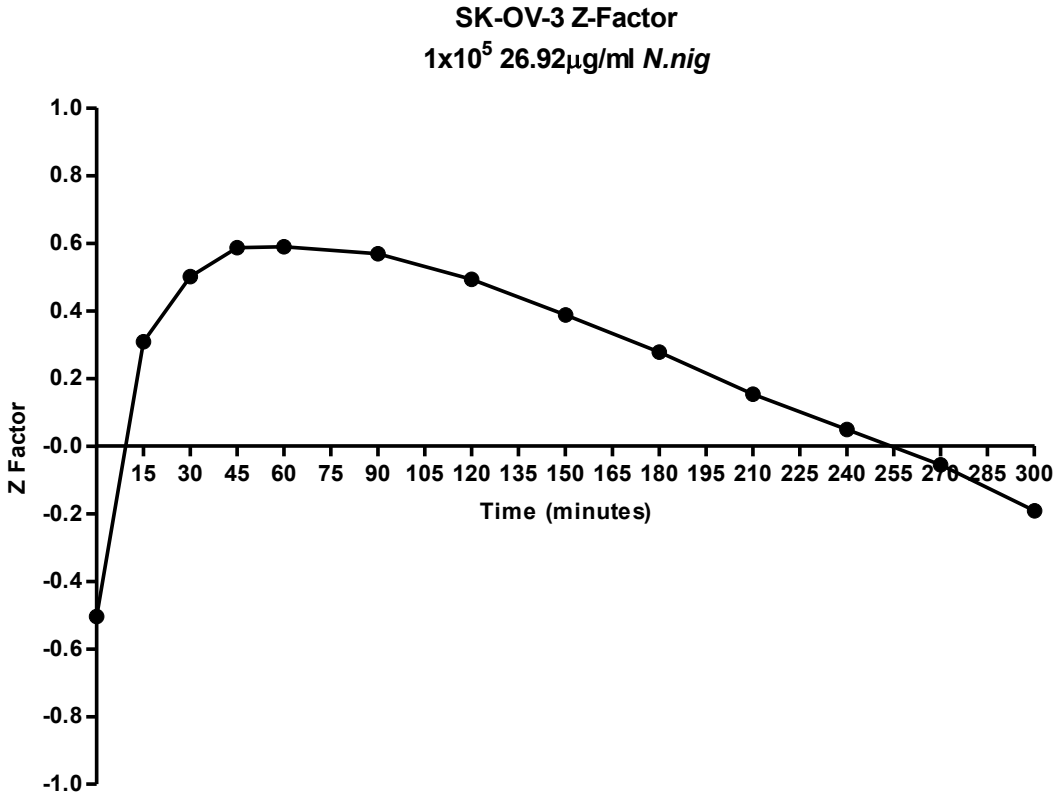

Figure A.3. The processed data of the Z' assay for the LD90 of *N.nig* crude venom. This was the second Z' assay attempt. The Z-factor is calculated every 15 min. for 1 hour and then every 30 min for the following 4 hours. A Z-factor above 0.5 is only achieved between 30 and 90 min. before returning below 0.5 and classified as a poor assay.

	1	2	3	4	5	6	7	8	9	10	11	12
A	12499	12846	28196	42287	30952	33766	124932	124792	124519	125526	125201	124105
B	36643	41533	49111	49931	41797	43716	125719	126202	126600	127312	127282	125424
C	29746	38991	61733	53513	45229	37131	126279	124241	126637	126214	125315	124638
D	52816	38468	60620	43884	42836	48306	127261	127140	127368	127648	127003	124280
E	122204	124416	124290	125412	125027	12693	104591	85762	122692	118309	126329	120100
F	123717	124900	125869	125833	125799	125006	50536	56164	44638	53924	61945	57288
G	120529	123169	124990	123322	124265	124213	72377	52215	61938	46798	53417	47689
H	115815	121048	121147	120115	120373	121167	47028	55640	51518	46982	53654	43113

Figure A.4. The raw data collected from the FLUOstar Omega Microplate Reader at time point 300 min for the second Z' assay. The positive control highlighted by the green box illustrates the areas of variation in the data. The calculated mean for the positive control was 54399.94 and 124608.30 for the negative control.

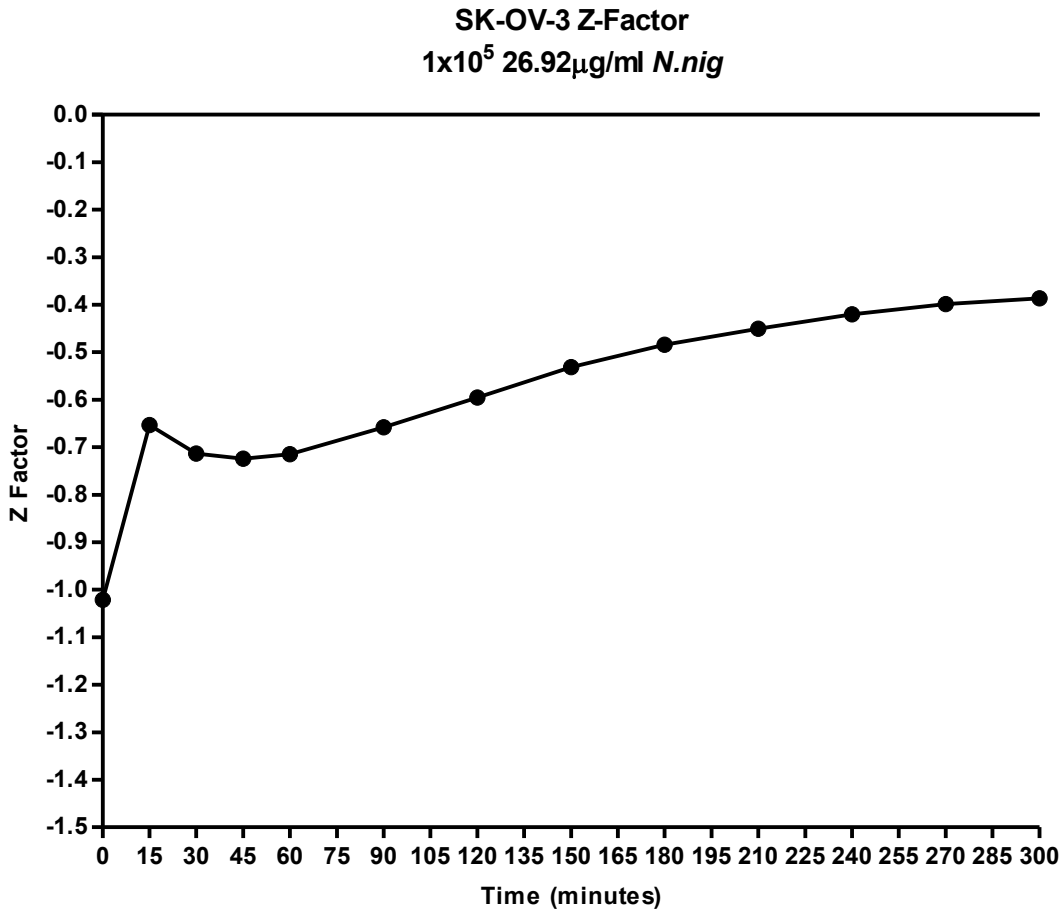

Figure A.5. The processed data of the Z' assay for the LD90 of *N.nig* crude venom. This was the third Z' assay attempt. The Z-factor is calculated every 15 min. for 1 hour and then every 30 min for the following 4 hours. A Z-factor above 0 is not achieved throughout the duration of the assay thus classified as a poor assay.

	1	2	3	4	5	6	7	8	9	10	11	12
A	5451	5518	5452	6170	5480	5881	78039	111734	5963	88657	124528	5502
B	5429	5406	5432	5387	5337	5434	125612	126111	123809	106344	126218	5550
C	5348	5391	5403	5383	5390	5451	122437	127538	128094	125881	125682	111939
D	5312	5387	5411	6653	6519	6701	126821	127117	126969	126950	127733	125870
E	110115	119980	118805	126788	126421	127682	5449	5410	5413	5428	5368	5870
F	122015	122802	126969	126940	122274	125397	5351	5293	5257	6077	5310	5546
G	119192	120425	123344	120954	6972	55154	5935	5353	7152	5718	5546	9010
H	11751	6359	86063	7070	6677	85648	6865	8510	16080	5644	6531	5981

Figure A.6. The raw data collected from the FLUOstar Omega Microplate Reader at time point 300 min for the second Z' assay. The green boxes highlight the wells amongst the negative control which produced variation. The calculated mean for the positive control was 6017.146 and 101305.40 for the negative control.

Table A.2. The calculated LD90 of crude *N.nig* venom using GraphPad. The 'ECF' calculates the LD90 to be 24.13µg/ml.

log(agonist) vs. response -- Find ECanything	
Best-fit values	
LOGECF	1.383
HILLSLOPE	6.082
F	= 90.00
BOTTOM	3.845
TOP	100.6
ECF	24.13
Span	96.73
Std. Error	
LOGECF	0.04160
HILLSLOPE	1.307
BOTTOM	0.9000
TOP	0.9767
Span	1.374
95% Confidence Intervals	
LOGECF	1.284 to 1.481
HILLSLOPE	2.991 to 9.174
BOTTOM	1.717 to 5.974
TOP	98.26 to 102.9
ECF	19.24 to 30.27
Span	93.48 to 99.98
Goodness of Fit	
Degrees of Freedom	7
R^2	0.9988
Absolute Sum of Squares	26.97
Sy.x	1.963
Constraints	
F	F = 90.00
Number of points	
Analyzed	11

Table A.3. The average fluorescence, percentage growth and inhibition as well as standard deviation of the venom fraction dosing assay. Inhibition highlighted as **GREEN** indicates those fractions which inhibited 50% or more of cell metabolism; highlighted as **PURPLE** indicates those fractions which inhibited 40% or more of cell metabolism; highlighted as **BLUE** indicates those fractions which inhibited 30% or more of cell metabolism.

Fraction	Fluorescence	%Growth	%Inhibition	StDev	StDev (%)
N.nig r1	34616.00000	32.34176	67.65824	52046.62947	51.00019
N.nig r2	44775.33333	42.64393	57.35607	48929.51461	47.94575
N.nig r3	77685.00000	75.84900	24.15100	18927.25212	18.54670
N.nig r4	89920.00000	87.76125	12.23875	14437.86234	14.14758
N.nig r5	64299.33333	62.70748	37.29252	46063.01391	45.13688
N.nig r6	60942.66667	59.19863	40.80137	53735.77425	52.65537
N.nig r7	91966.66667	90.06309	9.93691	8841.16697	8.66341
N.nig r8	39470.33333	38.25868	61.74132	34468.91432	33.77589
N.nig r9	63840.00000	62.18271	37.81729	26461.19342	25.92917
N.nig r10	43665.33333	43.10749	56.89251	27336.87272	26.78724
N.nig r11	36174.66667	35.21483	64.78517	8163.32587	7.99920
N.nig r12	88009.00000	86.33496	13.66504	23269.23684	22.80139
N.nig r13	95491.33333	93.87706	6.12294	29957.85514	29.35553
N.nig r14	83067.66667	81.74866	18.25134	39606.19765	38.80988
N.nig r15	104728.33333	102.52786	-2.52786	8703.69441	8.52870
N.nig r16	68954.00000	67.68197	32.31803	6066.02770	5.94407
N.nig r17	96989.00000	95.00551	4.99449	16350.01365	16.02128
N.nig r18	96877.66667	94.86351	5.13649	5203.59880	5.09898
N.nig r19	99428.33333	97.49187	2.50813	8077.28076	7.91488
N.nig r20	101408.66667	99.40432	0.59568	6045.05587	5.92352
N.nig r21	91195.33333	89.42394	10.57606	24199.31537	23.71277
N.nig r22	87155.66667	85.43063	14.56937	28209.31793	27.64215
N.nig r23	99662.66667	97.74905	2.25095	3058.23683	2.99675
A.cpi r1	61295.00000	60.56825	39.43175	2585.18239	2.53321
A.cpi r2	96362.00000	94.36326	5.63674	7993.54008	7.83282
A.cpi r4	99147.66667	97.12330	2.87670	7148.88777	7.00515
A.cpi r7	102329.33333	100.30616	-0.30616	5583.70248	5.47144
A.cpi r9	94513.66667	92.67673	7.32327	10946.10512	10.72602
A.cpi r10	91316.66667	89.55436	10.44564	15295.62494	14.98809
A.cpi r11	91135.33333	89.40564	10.59436	16917.50260	16.57736
A.cpi r12	99935.00000	97.98535	2.01465	4754.07152	4.65849
A.cpi r13	62276.33333	62.11057	37.88943	26338.34194	25.80879
A.cpi r14	89287.33333	86.96153	13.03847	19165.60650	18.78027
A.cpi r15	87100.00000	85.43011	14.56989	23800.24176	23.32172
A.cpi r16	103529.00000	101.67498	-1.67498	16547.07294	16.21438
A.cpi r17	98365.66667	96.65395	3.34605	26426.20929	25.89489
A.cpi r18	97469.00000	95.76458	4.23542	27292.86176	26.74412
A.cpi r19	74210.66667	72.96367	27.03633	60579.42697	59.36143
A.cpi r20	99476.00000	98.07765	1.92235	11108.30559	10.88496

A.cpi r21	69080.66667	67.99848	32.00152	3822.35089	3.74550
A.cpi r22	88280.33333	86.18482	13.81518	16376.34496	16.04709
A.cpi r23	101938.00000	99.98335	0.01665	8954.09309	8.77406
A.cpi r24	104841.00000	102.78626	-2.78626	7245.01739	7.09935
A.cpi r26	95192.00000	93.38158	6.61842	18641.79345	18.26699
A.cpi r27	94555.66667	92.76255	7.23745	13705.78864	13.43022
A.cpi r28	70786.33333	69.61719	30.38281	57068.11982	55.92072
A.cpi r29	89896.33333	87.86374	12.13626	15716.98414	15.40098
A.cpi r31	59309.33333	58.13172	41.86828	13009.17923	12.74762
P.reg r1	93276.00000	91.32206	8.67794	11173.19198	10.94855
P.reg r4	96380.33333	94.41480	5.58520	9001.74257	8.82076
P.reg r5	99156.33333	97.16701	2.83299	5985.76080	5.86541
P.reg r6	92063.00000	90.35253	9.64747	19234.59698	18.84787
P.reg r11	99075.33333	97.14214	2.85786	5352.71196	5.24509
P.reg r12	82077.66667	80.54068	19.45932	31136.11392	30.51010
P.reg r13	81854.66667	80.40943	19.59057	4543.28189	4.45194
P.reg r15	61177.00000	60.92769	39.07231	32596.41163	31.94103
P.reg r16	58585.66667	55.61491	44.38509	48887.58978	47.90467
P.reg r17	96049.00000	93.97528	6.02472	9425.03119	9.23553
P.reg r18	97150.33333	95.13700	4.86300	7359.17640	7.21121
P.reg r20	91135.33333	89.41088	10.58912	17928.22753	17.56777
P.reg r21	84465.33333	82.97269	17.02731	23117.75366	22.65295
P.reg r22	86232.66667	84.90659	15.09341	13501.12622	13.22968
P.reg r23	89778.33333	88.17917	11.82083	1020.27072	0.99976
P.reg r24	46081.33333	45.50254	54.49746	23592.17235	23.11783
P.reg r25	63888.00000	60.75569	39.24431	51851.74068	50.80922
P.reg r28	98680.00000	96.69541	3.30459	6110.40531	5.98755
P.cav r1	95552.33333	93.66307	6.33693	8797.85521	8.62097
P.cav r2	88005.33333	86.37004	13.62996	20843.60358	20.42453
P.cav r3	81605.00000	80.16405	19.83595	23036.55094	22.57338
P.cav r4	66358.66667	65.43794	34.56206	35786.73995	35.06722
P.cav r5	81372.00000	80.21547	19.78453	7437.80068	7.28826
P.cav r8	40595.66667	41.06678	58.93322	31856.79661	31.21629
P.cav r9	57853.33333	54.95711	45.04289	47597.43784	46.64045
P.cav r10	87186.66667	85.26222	14.73778	15133.54120	14.82927
P.cav r11	91789.33333	90.00092	9.99908	17868.27973	17.50902
P.cav r14	93038.66667	91.17927	8.82073	9898.96117	9.69993
P.cav r15	81354.33333	80.04260	19.95740	23509.97108	23.03728
P.cav r16	77051.66667	75.82216	24.17784	17396.38061	17.04661
P.cav r17	93733.33333	92.21208	7.78792	5328.37126	5.22124
P.cav r21	45649.66667	45.02276	54.97724	25535.44263	25.02203
P.cav r22	68351.33333	66.11769	33.88231	30992.36681	30.36924
P.cav r24	97427.00000	95.14690	4.85310	14398.09251	14.10861
P.cav r25	80242.66667	78.32828	21.67172	24820.97380	24.32193
P.cav r26	80940.66667	79.13961	20.86039	19870.67207	19.47116
P.cav r27	57966.33333	57.03571	42.96429	46387.10629	45.45446
P.cav r28	46282.00000	45.03549	54.96451	18711.78444	18.33557

P.cav r29	82177.00000	80.92288	19.07712	13000.73602	12.73935
P.cav r30	30847.33333	31.02522	68.97478	22926.40474	22.46545
P.cav r31	50135.33333	48.33664	51.66336	48062.43029	47.09610
P.cav r32	92693.00000	90.42339	9.57661	15803.12662	15.48539
P.cav r33	86762.33333	84.84149	15.15851	16571.83567	16.23865
P.cav r34	86149.33333	84.71236	15.28764	6419.98702	6.29091
26.92ug/ml N.nig	26567.66667	25.82356	74.17644	8088.19049	7.92557
26.92ug/ml N.nig	25620.66667	25.07624	74.92376	3504.81959	3.43435
PBS	101909.66667	99.88740	0.11260	5752.73364	5.63707
PBS	102194.00000	100.11260	-0.11260	6958.65425	6.81874

Table A.4. The statistical results of the t-test used to find what fractions significantly reduced cell metabolism of SK-OV-3 cells using a 40% pass threshold.

Fraction	N.nig_r6	A.cpi_r31	P.reg_r16	P.cav_r9	P.cav_r27	PBS
P-value	0.296	0.027	0.232	0.220	0.245	0.506

Table A.5. The statistical results of the t-test used to find what fractions significantly reduced cell metabolism of SK-OV-3 cells using a 30% pass threshold.

Fraction	N.nig_r5	N.nig_r16	A.cpi_r1	A.cpi_r13	A.cpi_r21	A.cpi_r28	P.reg_r15	P.reg_r25	P.cav_r4	P.cav_r22	PBS
P-value	0.276	0.011	0.040	0.151	0.018	0.448	0.197	0.297	0.241	0.156	0.528